AD

CONTRACTOR REPORT ARCCB-CR-95019

AN EXPERIMENTAL INVESTIGATION OF THE GASDYNAMIC PERFORMANCE OF GUN BORE EVACUATORS MOUNTED ON 155-MM SELF-PROPELLED HOWITZERS

H.T. NAGAMATSU, L.N. MYRABO, D.G. MESSITT
C. EKONOMIDIS, M. GREENMAN, P. YAGLE

RENSSELAER POLYTECHNIC INSTITUTE
TROY, NEW YORK

DTIC
ELECTE
NOV 14 1995
S
D
B

MARCH 1995

US ARMY ARMAMENT RESEARCH,
DEVELOPMENT AND ENGINEERING CENTER
CLOSE COMBAT ARMAMENTS CENTER
BENÉT LABORATORIES
WATERVLIET, N.Y. 12189-4050

APPROVED FOR PUBLIC RELEASE; DISTRIBUTION UNLIMITED

19951114 020

DISCLAIMER

The findings in this report are not to be construed as an official Department of the Army position unless so designated by other authorized documents.

The use of trade name(s) and/or manufacturer(s) does not constitute an official indorsement or approval.

DESTRUCTION NOTICE

For classified documents, follow the procedures in DoD 5200.22-M, Industrial Security Manual, Section II-19 or DoD 5200.1-R, Information Security Program Regulation, Chapter IX.

For unclassified, limited documents, destroy by any method that will prevent disclosure of contents or reconstruction of the document.

For unclassified, unlimited documents, destroy when the report is no longer needed. Do not return it to the originator.

REPORT DOCUMENTATION PAGE

Form Approved
OMB No. 0704-0188

Public reporting burden for this collection of information is estimated to average 1 hour per response, including the time for reviewing instructions, searching existing data sources, gathering and maintaining the data needed, and completing and reviewing the collection of information. Send comments regarding this burden estimate or any other aspect of this collection of information, including suggestions for reducing this burden, to Washington Headquarters Services, Directorate for Information Operations and Reports, 1215 Jefferson Davis Highway, Suite 1204, Arlington, VA 22202-4302, and to the Office of Management and Budget, Paperwork Reduction Project (0704-0188), Washington, DC 20503.

1. AGENCY USE ONLY (Leave blank)	2. REPORT DATE	3. REPORT TYPE AND DATES COVERED
	March 1995	Final

4. TITLE AND SUBTITLE
AN EXPERIMENTAL INVESTIGATION OF THE GASDYNAMIC PERFORMANCE OF GUN BORE EVACUATORS MOUNTED ON 155-MM SELF-PROPELLED HOWITZERS

5. FUNDING NUMBERS
Contract DAAA-C-1149

6. AUTHOR(S)
H.T. Nagamatsu, L.N. Myrabo, D.G. Messitt,
C. Ekonomidis, M. Greenman, P. Yagle

7. PERFORMING ORGANIZATION NAME(S) AND ADDRESS(ES)
Rensselaer Polytechnic Institute
Troy, NY 12180-3590

8. PERFORMING ORGANIZATION REPORT NUMBER

9. SPONSORING/MONITORING AGENCY NAME(S) AND ADDRESS(ES)
U.S. Army ARDEC
Benét Laboratories, AMSTA-AR-CCB-O
Watervliet, NY 12189-4050

10. SPONSORING/MONITORING AGENCY REPORT NUMBER
ARCCB-CR-95019

11. SUPPLEMENTARY NOTES
Charles A. Andrade: Benét Laboratories Project Engineer

12a. DISTRIBUTION/AVAILABILITY STATEMENT
Approved for public release; distribution unlimited

12b. DISTRIBUTION CODE

13. ABSTRACT *(Maximum 200 words)*

The charge and discharge cycles of the 155-mm gun bore evacuator have been investigated at the Rensselaer Polytechnic Institute (RPI) High Pressure Shock Tube and Steady-State Flow Facilities. To test the charge and discharge phases in the high pressure shock tube, a 65 percent scale model of the bore evacuator is installed on the end of the shock tube. Thin plastic diaphragms are placed over the evacuator charge and discharge ports. The pressure behind the Mach 1.89 incident shock wave is 91 psia, and the flow Mach number is 0.89. The evacuator pressure is varied to obtain ratios of the initial evacuator pressure-to-bore pressure up to 2300. The charge coefficient for the charge ports in the baseline configuration is 0.29. With no restriction at the exit of the charge ports, the charge coefficient is approximately 0.40. The charge coefficient for the angled discharge ports varies from 0.51 at a P_B/P_e of 4 to 0.58 at a P_B/P_e of 1570. During the charge phase with high pressure ratios across the evacuator ports, shock waves with high temperatures behind the waves are present in the evacuator. The discharge coefficient for the ejector ports is approximately 0.72 for an evacuator pressure range of 50 to 195 psia. A 33 percent scale model of the 155-mm gun bore evacuator is installed in the RPI Steady-State Flow Facility, and the performance of a model with six staggered ejector ports is compared to the baseline configuration. The staggered ejector configuration results in a gain of approximately 20 percent in the mass flow augmentation ratio over test pressures from 1 to 84 psig. The discharge coefficients for the baseline and staggered ejectors are nearly constant at approximately 0.80 for evacuator pressures greater than 26 psig, and the coefficient drops off rapidly at pressures lower than 16 psig.

14. SUBJECT TERMS
155-mm Self-Propelled Howitzer, Gas Dynamics, Model Bore Evacuator Performance, Staggered Ejector Nozzles, Shock Tube, Reservoir Charge-Up, Quasi-Steady-State Discharge Coefficient, Mass Flow Augmentation Ratio, Velocity, Mach Number Distribution, Thin-Film Platinum Heat Gauge

15. NUMBER OF PAGES
74

16. PRICE CODE

17. SECURITY CLASSIFICATION OF REPORT	18. SECURITY CLASSIFICATION OF THIS PAGE	19. SECURITY CLASSIFICATION OF ABSTRACT	20. LIMITATION OF ABSTRACT
UNCLASSIFIED	UNCLASSIFIED	UNCLASSIFIED	UL

GENERAL INSTRUCTIONS FOR COMPLETING SF 298

The Report Documentation Page (RDP) is used in announcing and cataloging reports. It is important that this information be consistent with the rest of the report, particularly the cover and title page. Instructions for filling in each block of the form follow. It is important to ***stay within the lines*** to meet ***optical scanning requirements***.

Block 1. Agency Use Only *(Leave blank)*.

Block 2. Report Date. Full publication date including day, month, and year, if available (e.g. 1 Jan 88). Must cite at least the year.

Block 3. Type of Report and Dates Covered. State whether report is interim, final, etc. If applicable, enter inclusive report dates (e.g. 10 Jun 87 - 30 Jun 88).

Block 4. Title and Subtitle. A title is taken from the part of the report that provides the most meaningful and complete information. When a report is prepared in more than one volume, repeat the primary title, add volume number, and include subtitle for the specific volume. On classified documents enter the title classification in parentheses.

Block 5. Funding Numbers. To include contract and grant numbers; may include program element number(s), project number(s), task number(s), and work unit number(s). Use the following labels:

C	- Contract	PR	- Project
G	- Grant	TA	- Task
PE	- Program Element	WU	- Work Unit Accession No.

Block 6. Author(s). Name(s) of person(s) responsible for writing the report, performing the research, or credited with the content of the report. If editor or compiler, this should follow the name(s).

Block 7. Performing Organization Name(s) and Address(es). Self-explanatory.

Block 8. Performing Organization Report Number. Enter the unique alphanumeric report number(s) assigned by the organization performing the report.

Block 9. Sponsoring/Monitoring Agency Name(s) and Address(es). Self-explanatory.

Block 10. Sponsoring/Monitoring Agency Report Number. *(If known)*

Block 11. Supplementary Notes. Enter information not included elsewhere such as: Prepared in cooperation with...; Trans. of...; To be published in.... When a report is revised, include a statement whether the new report supersedes or supplements the older report.

Block 12a. Distribution/Availability Statement. Denotes public availability or limitations. Cite any availability to the public. Enter additional limitations or special markings in all capitals (e.g. NOFORN, REL, ITAR).

- **DOD** - See DoDD 5230.24, "Distribution Statements on Technical Documents."
- **DOE** - See authorities.
- **NASA** - See Handbook NHB 2200.2.
- **NTIS** - Leave blank.

Block 12b. Distribution Code.

- **DOD** - Leave blank.
- **DOE** - Enter DOE distribution categories from the Standard Distribution for Unclassified Scientific and Technical Reports.
- **NASA** - Leave blank.
- **NTIS** - Leave blank.

Block 13. Abstract. Include a brief *(Maximum 200 words)* factual summary of the most significant information contained in the report.

Block 14. Subject Terms. Keywords or phrases identifying major subjects in the report.

Block 15. Number of Pages. Enter the total number of pages.

Block 16. Price Code. Enter appropriate price code *(NTIS only)*.

Blocks 17. - 19. Security Classifications. Self-explanatory. Enter U.S. Security Classification in accordance with U.S. Security Regulations (i.e., UNCLASSIFIED). If form contains classified information, stamp classification on the top and bottom of the page.

Block 20. Limitation of Abstract. This block must be completed to assign a limitation to the abstract. Enter either UL (unlimited) or SAR (same as report). An entry in this block is necessary if the abstract is to be limited. If blank, the abstract is assumed to be unlimited.

★U.S.GPO:1991-0-293-947

TABLE OF CONTENTS

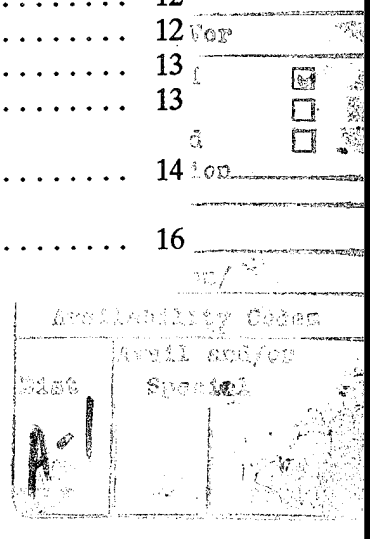

List of Illustrations

ACKNOWLEDGEMENTS

The authors wish to thank Dr. Charles Andrade and Mr. James Bendick for their guidance and enthusiastic support for the investigation of the gun bore evacuator models in the RPI High Pressure Shock Tube and Steady-State Flow Facilities. Thanks also, to Dr. John Zweig, Messrs. Russel Fiscella and Donald Jones for their continued support at Benét Laboratories. Discussions with Dr. Gary Carofano and Mr. Jeffery Haas were helpful. The authors are grateful to Messrs. F. Tesman and C. Vannier for their assistance in the construction of the models, and to K. Peterson for the CAD modelling of the Shock Tube Experiment.

NOMENCLATURE

A_c	Total Area of Charge Holes
A_{ej}	Total Area of Discharge Ejectors
a	Speed of Sound
C_d	Discharge Coefficient
h_w	Pressure in Inches of Water
i	Induced
K_c	Charge Coefficient
L	Length
M	Mach Number
m	Mass Flow Rate
P	Pressure
R	Gas Constant
T	Temperature
t	Time
u	Velocity
V	Volume
Y	Compressibility Factor
γ	Ratio of Specific Heats
ζ	Mass Flow Augmentation Ratio
ρ	Density

Superscripts

*	Sonic Condition

Subscripts

B	Bore
b	Breech
e	Conditions in Evacuator
ej	Through Ejectors
i	Ideal
o	Total
s	Shock
0	Condition Upstream of Orifice Meter
1	Shock Tube Driven Section Initial Condition
2	Condition After Passage of Normal Shock Wave
3	Condition After Passage of Expansion Wave
4	Shock Tube Driver Section Initial Condition

INTRODUCTION

After firing the M284/M185 artillery cannon with the regular charge, there is a discharge of smoke at the breech for approximately one second for all shots; however, with the charge for high velocity shots, there is no smoke at the breech. The Rensselaer Polytechnic Institute (RPI) High Pressure Shock Tube and the Steady-State Flow Facilities have been configured to investigate the performance of the cannon bore evacuator, which is designed to remove the propellant gases from the bore and prevent the discharge at the breech.

The RPI High Pressure Shock Tube (HPST) is used to simulate the flow conditions in the gun bore and evacuator for the evacuator charge and discharge cycles. Interior ballistics solutions for the 155-mm gun (ref 1) provide the flow conditions in the bore. Results from these solutions are presented in Figure 1. Figure 1a shows the pressure and temperature history in the bore until projectile exit. The initial bore-to-evacuator pressure ratio can reach 2200 immediately after the projectile passes the charge ports. The Mach number and flow velocity are shown in Figures 1b and 1c, respectively.

RPI HIGH PRESSURE SHOCK TUBE

The RPI HPST (ref 2) can be used to produce subsonic and supersonic flows behind the incident shock wave with high total pressures and total temperatures. When operated as a shock tunnel (refs 3,4), it is used to test hypersonic flows from Mach 8 to 25, with total enthalpies up to 6.5 MJ/kg (with a corresponding total temperature of 4100K) in the 24-inch diameter test section.

Description of Facility

The RPI HPST, shown in Figure 2, has a 15-foot long driver section with an internal diameter of 4 inches. This section is pressurized with room temperature air or helium at pressures up to 2000 psia. The driver is separated from the driven section by the Double Diaphragm Section (DDS), shown in Figure 3. The DDS holds two scored aluminum or stainless steel diaphragms. The region between the two diaphragms is initially pressurized to one-half the driver pressure. The test is initiated by venting the DDS gas to the atmosphere through four high pressure solenoid valves, causing the diaphragms to rupture.

The driven section of the shock tube is 55 feet long with an internal diameter of 4 inches. This section can be filled with a number of test gases. The test section is located at the end of the driven tube and exhausts into a 200 ft^3 dump tank, as shown in Figure 2. A more detailed description of the RPI shock tube can be found in Reference 2.

Shock Tube Instrumentation

The instrumentation installed in the shock tube consists primarily of piezoelectric pressure gauges and thin-film platinum heat gauges (ref 5, cf. Figure 4). Additional instrumentation, shown in Figure 5, such as an ionization gauge, photoresistor, and Schlieren system are used when the facility is operated as a shock tunnel (refs 2-4) and are not used for

these tests.

Pressure Gauges

Several pressure gauges are installed in the shock tube wall upstream of the test section. These pressure gauges are Kistler piezoelectric gauges and are connected to Model 503 charge amplifiers. The gauge located furthest upstream, as shown in Figure 5, is used to trigger the data acquisition systems. The two other Kistler gauges measure the pressure after the incident shock wave and provide a check of the shock wave speed. In addition, a mechanical Heise gauge with a 75 psia range is used to measure the initial pressure in the driven section of the shock tube (P_1).

PCB quartz pressure transducers, shown in Figure 4, are used to measure pressures in the test section. These pressure transducers are dynamically calibrated prior to the test series in the RPI Low Pressure Shock Tube (LPST), shown in Figure 2, over the range of pressure jumps experienced in the tests. A representative calibration curve is presented in Figure 6.

A Hastings Model 760 digital vacuum gauge is used to measure the initial evacuator pressure for the charge series. For the discharge series, a mechanical dial pressure gauge is used. This gauge is calibrated prior to each test series using a dead weight tester.

Heat Transfer Gauges

Two thin-film platinum heat transfer gauges are located upstream of the test section. These heat transfer gauges, shown in Figure 5, are separated by 1.5 feet and are used to determine the shock wave velocity. The gauges respond within one or two microseconds and give a very accurate measure of the shock speed.

Data Acquisition

Several data acquisition systems are used in the RPI HPST Facility. A Tektronix 2520 mainframe with 18 channels is the primary data acquisition system. This machine has six channels with high speed capability (up to 80 ns per point). A Nicolet digital oscilloscope provides an additional four channels at up to 100 ns per point. Tektronix TDS 420 and Hewlett-Packard 54501A digitizing oscilloscopes are available if added capacity is needed.

Flow Conditions in the Shock Tube

Charge Phase

Prior to initiation of the test, the driven section of the shock tube, shown in Figure 2, is filled with the room temperature test gas, typically air or nitrogen, at a pressure P_1. The driver section is then pressurized to pressure P_4 with either air or helium. The controlled bursting of the diaphragms separating the driver and driven tubes causes a shock wave to propagate down the driven tube, as shown in Figure 7. The Mach number of this shock wave is given by the following equation (ref 6):

$$\left(\frac{P_4}{P_1}\right) = \left[\frac{2\gamma_1 M_s^2 - (\gamma_1 - 1)}{\gamma_1 + 1}\right]\left[\frac{1}{1 - \frac{\gamma_4 - 1}{\gamma_1 + 1}\frac{a_1}{a_4}\left(M_s - \frac{1}{M_s}\right)}\right]^{\frac{2\gamma_4}{\gamma_4 - 1}} \tag{1}$$

where γ is the ratio of specific heats, M_s is the shock Mach number, and a is the speed of sound. The subscripts 1 and 4 refer to initial conditions in the driven and driver tubes, respectively. The theoretical driver-to-driven pressure ratio, with experimentally observed values, is plotted in Figure 8 for air and helium driver gases.

The pressure and temperature jumps across the shock wave are given by (ref 7)

$$\frac{P_2}{P_1} = \frac{2\gamma_1 M_s^2}{\gamma_1 + 1} - \frac{\gamma_1 - 1}{\gamma_1 + 1} \tag{2}$$

$$\frac{T_2}{T_1} = \frac{a_2^2}{a_1^2} = \frac{[2\gamma_1 M_s^2 - (\gamma_1 - 1)][(\gamma_1 - 1)M_s^2 + 2]}{(\gamma_1 + 1)^2 M_s^2} \tag{3}$$

and these results are presented in Figure 9.

The shock wave imparts a velocity to the driven gas, and this velocity is given by

$$u_i = u_2 = \frac{2a_1}{\gamma_1 + 1}\left(M_s - \frac{1}{M_s}\right) \tag{4}$$

And the Mach number of the gas after the shock wave is given by using Eqs. (3) and (4) as

$$M_2 = \frac{2(M_s^2 - 1)}{[(2\gamma_1 M_s^2 - (\gamma_1 - 1))((\gamma_1 - 1)M_s^2 + 2)]^{\frac{1}{2}}} \tag{5}$$

and is presented in Figure 10. The maximum induced Mach number is 1.89 for air with $\gamma = 1.4$.

For typical shock Mach numbers used in this study, the test duration is limited by the arrival of the contact surface which separates the gas that was originally on either side of the primary diaphragm, cf. Figure 7. For a given shock Mach number, the transit time of the shock wave is

$$t_s = \frac{L}{u_s} = \frac{L}{M_s a_1} \tag{6}$$

where L is the distance from the primary diaphragm. The transit time for the contact surface is

$$t_c = \frac{L}{u_2} = \frac{L}{\frac{2a_1}{\gamma_1 + 1}\left(M_s - \frac{1}{M_s}\right)} \tag{7}$$

The test time, t_t, is therefore given by

$$t_t = t_c - t_s = \frac{L}{\frac{2a_1}{\gamma_1 + 1}\left(M_s - \frac{1}{M_s}\right)} - \frac{L}{M_s a_1} \tag{8}$$

For a given shock tube length, the duration of the passage of the shock heated gas decreases with the shock velocity, as shown in Figure 10.

Discharge Phase

For the discharge phase test series, the shock tube is initially pressurized to a pressure P_4. A diaphragm placed at the muzzle exit separates the high pressure gas in the shock tube from the surrounding dump tank, which is at atmospheric pressure. After the diaphragm ruptures, a series of expansion waves propagates toward the breech end, cf. Figure 11. This expansion fan accelerates the gas initially in the driven tube. The expansion is isentropic, and

$$\frac{P_4}{\rho_4^\gamma} = \frac{P_3}{\rho_3^\gamma} \tag{9}$$

The Riemann invariant for a right-running characteristic (in Figure 11) can be used to relate the velocity and sound speed in region 3

$$u_3 = \frac{2}{\gamma - 1}(a_4 - a_3) \tag{10}$$

Combining Eqs. (9) and (10),

$$M_3 = \frac{2}{\gamma - 1}\left(\frac{P_4}{P_3}\right)^{\frac{\gamma - 1}{2\gamma}} \tag{11}$$

This relation can be used to calculate the flow Mach number in region 3 from the initial bore pressure P_4 and the measured pressure P_3.

The time to establish steady flow in region 3 after initiation of the test by the main diaphragm break is the time for the tail of the expansion to pass the test section, cf. Figure 11. The speed of the trailing expansion wave is $u_3 - a_3$ (ref 8). The flow establishment time is then

$$t_{est} = \frac{L_M}{a_4\left(\frac{2}{\gamma - 1} - \left(\frac{P_3}{P_4}\right)^{\frac{\gamma-1}{2\gamma}}\right)} \tag{12}$$

where L_M is the length of the model measured from the diaphragm.

DETERMINATION OF EVACUATOR ORIFICE COEFFICIENTS

The mass flow rate into or out of the evacuator chamber, Figure 12b, during the charge or discharge phase can be written as the product of an ideal mass flow rate and a charge or discharge coefficient, i.e.,

$$\dot{m}_e = K\dot{m}_i \tag{13}$$

The flow coefficient for a specific geometry can be determined by measuring the pressure history in the evacuator chamber.

Charge Coefficient

Using the equation of state for an ideal gas (ref 7), the mass in the evacuator can be written as

$$m_e = \frac{P_e V_e}{RT_e} \tag{14}$$

where R is the gas constant and V_e is the evacuator volume. Differentiating Eq. (14) with respect to time gives the mass flow rate into the evacuator chamber as

$$\dot{m}_e = V_e\left(\frac{\partial P_e}{\partial t}\frac{1}{RT_e} - \frac{P_e}{RT_e^2}\frac{\partial T_e}{\partial t}\right) \tag{15}$$

The energy equation, neglecting kinetic energy terms in the reservoir and heat loss to the walls, is (ref 9)

$$\frac{\partial}{\partial t}(C_v m_e T_e) = \dot{m}_e C_P T_{B_o} \tag{16}$$

where $T_{B,o}$ is the total temperature of the gas in the bore, given by

$$T_{B_o} = T_B\left(1 + \frac{\gamma - 1}{2} M_2^2\right) \tag{17}$$

Combining Eqs. (15) and (16), the mass flow rate into the evacuator chamber is

$$\dot{m}_e = \left(\frac{\partial P_e}{\partial t}\right)\frac{V_e}{\gamma R T_{B_o}} \tag{18}$$

The mass flow through the orifices can be expressed as (ref 10)

$$\dot{m}_e = K_c A_c \sqrt{P_B \rho_B} \tag{19}$$

where A_c is the total area of the orifices and the subscript B denotes conditions in the bore. K_c is the charge coefficient and depends on the orifice geometry, the ratio of specific heats in the barrel (γ_B), and the flow Mach number in the bore. Equations (18) and (19) can be combined to yield the equation for the charge coefficient

$$K_c = \left(\frac{\partial P_e}{\partial t}\right)\frac{1}{\gamma R}\frac{V_e}{A_c}\frac{1}{T_{B_o}\sqrt{P_B \rho_B}} \tag{20}$$

Discharge Coefficient

The mass flow rate out of the evacuator during the discharge phase is given by Eq. (15). Assuming constant specific entropy and a small pressure decrease in the reservoir, the mass flow rate can be expressed as

$$\dot{m}_e = \frac{1}{\gamma}\frac{V_e}{RT_e}\left(\frac{\partial P_e}{\partial t}\right) \tag{21}$$

which is equivalent to Eq. (18). These assumptions effectively limit this equation to small times after initiation of the discharge cycle (several hundred milliseconds).

The ideal mass flow rate through the ejectors is given by

$$\dot{m}_{e_i} = \left(\frac{\rho^*}{\rho_e}\right)\rho_e\left(\frac{a^*}{a_e}\right)a_e\left(\frac{A^*}{A_e}\right)A_e \tag{22}$$

where the superscript * indicates conditions at M = 1, and A_{ej} is the total area of the discharge ports. For the shock tube discharge phase experiments, the ejector flow is always choked, and $A^*/A_e = 1$. The ratios (ρ^*/ρ_e) and (a^*/a_e) can be found in Reference 7. Combining Eqs. (21) and (22), and defining C_d as (m_e/m_{ei}), the discharge coefficient is given by

$$C_d = \left(\frac{1}{\gamma}\right)^{\frac{3}{2}}\left(\frac{2}{\gamma+1}\right)^{-\frac{\gamma+1}{2(\gamma-1)}}\frac{V_e}{A_{ej}}\frac{1}{P_e\sqrt{RT_e}}\left(\frac{\partial P_e}{\partial t}\right) \tag{23}$$

SIMULATION OF 155-MM GUN FLOW DURING THE CHARGE PHASE

A 65 percent scale model of the 155-mm gun bore evacuator, Figure 12a, has been constructed and installed in the RPI HPST to determine the charge and discharge coefficients for the baseline 155-mm gun configuration.

Shock Tube Bore Evacuator Model

The bore of the model consists of a 38-inch long steel pipe with a 4-inch internal diameter, c.f. Figure 12b. The pipe has a wall thickness of 0.75 inch over the length of the evacuator, with ten charge holes and three angled discharge holes to scale with the 155-mm gun bore evacuator.

The evacuator casing is constructed of steel tubing with a 9-inch internal diameter and two 0.75-inch thick steel flanges. The model is held together by six threaded tie rods and was designed so that the evacuator length-to-diameter ratio (L/D) could be easily altered. The upstream end of the evacuator has a mahogany spacer machined to match the internal geometry of the actual 155-mm gun bore evacuator, cf. Figure 12b. A model of the experiment has been constructed using the CAD program ProEngineer, cf. Figure 12c, so that future model design changes can be easily evaluated.

Instrumentation

For tests of the charge cycle, the bore evacuator model is instrumented with four pressure gauges and four heat gauges. Figure 12b shows the location of these gauges.

Pressure Gauges

The bore evacuator model contains four piezoelectric pressure gauges. The gauge farthest upstream, PG1 in Figure 12b, is a Kistler gauge and measures the pressure after the incident shock wave. This gauge has been calibrated dynamically in the HPST.

The other pressure gauges are PCB Model 113A20 quartz pressure gauges with sensitivities of approximately 20 mv/psi. These gauges are connected to a PCB Model 494A06 power supply, and are calibrated in the RPI LPST prior to each test, cf. Figure 2. Pressure gauge PG2 is located in the side wall of the evacuator and measures the evacuator chamber pressure. Gauge PG3 is located in the evacuator casing and is angled in line with a discharge port. PG4 is mounted in the bore at the center of the model and measures the bore pressure.

Platinum Heat Gauges

Thin-film platinum heat transfer gauges, constructed by painting or sputtering a platinum film onto a pyrex substrate material, act as resistance thermometers and can be calibrated to measure heat transfer rates (ref 5). For this experiment, however, they are used only to measure shock wave speed by comparing the delay in initial response between two gauges separated by a known distance. A typical output of two gauges installed in the shock tube wall and used for this purpose (HG1 and HG2 in Figure 12b) is shown in Figure 13.

Two heat transfer gauges, HG3 and HG4, were installed in the evacuator model to demonstrate the presence of strong shock waves in the evacuator at the early stages of the charge phase, cf. Figure 12b. HG3 was placed in line with a discharge orifice and mounted to allow the distance between the gauge and the orifice to be varied. HG4 was fixed at the exit of this orifice.

Shock Tube Flow Conditions For Simulation of the Charge Phase

The 65 percent scale model of the 155-mm gun bore evacuator is installed on the end of the RPI HPST, cf. Figure 12a, to test the charge phase. Two 0.035-inch stainless steel diaphragms are scored in a cross 0.018-inch deep and placed in the DDS, Figure 3. The initial driven pressure is 22.6 psia, and air is used as the driver gas at 1100 psia. These conditions produce a shock wave Mach number of 1.89. The Mach number of the flow after the shock is 0.89, and the bore pressure is 91 psia, Figure 9.

Figure 7 depicts how the shock tube flow is used to simulate the actual gun flow. After the main diaphragm burst, a shock wave propagates down the driven tube. The pressure distribution along the entire shock tube at an early time is shown at the bottom of Figure 7. The test begins when the shock wave passes the bore evacuator model. The time history of the model pressure is shown at the right of Figure 7. A typical bore pressure trace, recorded from PG4, is shown in Figure 14 for comparison. The flow is steady for at least 10 ms for all tests.

To enable testing of high ratios of the bore pressure to the evacuator pressure, (P_B/P_e), simulating the early charge cycle, diaphragms must be p ed over the charge and discharge orifices. Thin plastic diaphragm material is placed on a 3-inch steel tube, Figure 15, which is then inserted into the model from the muzzle end. The bore evacuator reservoir is evacuated to a low pressure P_e, typically on the order of several Torr. The pressure in the bore is the initial shock tube driven pressure, P_1.

Shock Tube Charge Phase Results and Discussion

Figure 14 is a typical bore pressure trace, recorded from PG4 (Figure 12b) during the charge phase tests. The bore pressure is 91 psia and is steady for at least 10 ms.

Two thin-film platinum heat gauges are located in the evacuator chamber to measure the starting shock wave through the discharge ports. Figure 16 is a trace recorded from these gauges at an initial bore-to-evacuator pressure ratio (P_b/P_e) of 2300. The presence of strong shock waves is clearly evident.

The charge coefficient is calculated with Eq. (20), using the measured pressure change in the evacuator chamber. A sample trace, recorded from PG2, Figure 12b, is presented in Figure 17. The slope of the pressure history is linear, and the evacuator pressure only changes several psi over the 10 ms test time.

The charge coefficient for the angled discharge ports, Figure 12b, at bore-to-evacuator pressure ratios up to 2300 is presented in Figure 18. The charge ports are sealed for these tests, and all mass flow into the evacuator chamber is through the discharge ports. The charge coefficient ranges from 0.51 at low P_B/P_e to 0.58 at a P_B/P_e of 1570. Figure 18 also contains data obtained without the diaphragm sleeve, cf. Figure 15. The sleeve has little effect on the charge coefficient.

The charge coefficient for the charge ports is presented in Figure 19. The discharge ports are sealed for these tests. The charge coefficient is nearly constant at 0.29. Figure 19 also contains data obtained after removing the mahogany spacer, Figure 12b. The spacer simulates the geometry of the casing used to hold the valve ring in the actual 155-mm bore evacuator. The charge coefficient without the spacer is near 0.40, higher than the baseline by 25 percent.

SHOCK TUBE CONDITIONS FOR THE SIMULATION OF THE DISCHARGE PHASE

Testing of the bore evacuator discharge phase in the RPI HPST is done using the same model as that used in the charge phase. Slight modifications made to the model are illustrated in Figure 20. A 19-inch long extension is placed on the muzzle to simulate the correct position for the evacuator on the bore. In addition, the charge ports are sealed.

Instrumentation

The initial evacuator pressure is measured by the pressure gauge labeled P_e in Figure 20. This is a mechanical gauge and is calibrated with a dead weight tester prior to the test series. PG2 and PG3 measure the pressure history in the evacuator after initiation of the test and are the same PCB transducers used in the charge phase. PG4 is also a PCB and measures the time history of the bore pressure.

The center line static and pitot pressures are measured six inches upstream of the muzzle, cf. Figure 20. These pressures are measured by PCB pressure transducers. The center line Mach number of the flow in the bore can be determined from the ratio of these pressures. In addition, the pitot probe is used to trigger the data acquisition systems.

Shock Tube Flow Conditions For Simulation Of Discharge Phase

For the simulation of the flow in the 155-mm gun bore evacuator during the discharge phase, a scored aluminum diaphragm is placed at the end of the muzzle. The shock tube and bore evacuator model are initially pressurized to a pressure P_e determined by the thickness of the diaphragm and the depth of the score.

When the diaphragm breaks, expansion waves travel back down the shock tube toward the driver, cf. Figure 11. Behind these expansion waves the flow is steady. The test time, limited by the time constant of the pressure transducers, is approximately 100 ms. The time history of the bore pressure at the center of the model is shown in Figure 21. After the tail of the muzzle expansion fan passes, the flow through the model is steady for an extended time.

Shock Tube Discharge Phase Results and Discussion

A typical pressure history recorded from PG4, Figure 20, is shown in Figure 21. This compares well with the curve obtained from analysis of the wave diagram, cf. Figure 11. The bore pressure is constant for well over 100 msec.

The center line Mach number obtained from the pitot and static pressures measured six inches upstream of the muzzle is presented in Figure 22. The results from Eq. (11) are presented for comparison. There is a slight increase in flow Mach number from the theoretical value due to the presence of flow from the ejector ports.

A sample time history of the bore evacuator chamber pressure recorded from PG2 is presented in Figure 23. The evacuator pressure decreases linearly with time and changes only several psi over the first 30 msec after bore flow establishment. The discharge coefficient obtained from using these pressure traces in Eq. (23) is plotted in Figure 24. The discharge coefficient is approximately 0.72 over all test pressures, indicating choked flow through the ejector orifices.

QUASI-STEADY DISCHARGE PHASE

An approximately 33 percent scale model is installed in the RPI Steady-State Flow Facility (ref 11) to test quasi-steady performance of the 155-mm gun bore evacuator's discharge phase, cf. Figure 25a. The performance of the 155-mm cannon bore evacuator is tested at evacuator pressures of 1 to 84 psig. For these tests, the evacuator pressure is kept constant and the pressure and velocity distributions are measured.

33 Percent Scale Bore Evacuator Model

The approximately 33 percent scale model of the 155-mm gun bore evacuator, shown in Figure 25a, has a barrel made of 2-inch copper tubing. Ten charge holes and three discharge holes are drilled to scale with the actual gun. The charge holes are sealed for all tests.

The quasi-steady model is 78.4 inches long. The discharge holes are 16.4 inches from the muzzle, reproducing the actual length-to-diameter ratios of 31 at the breech side and 8.2 at the muzzle. A bell-mouth inlet is attached to the breech end.

The evacuator chamber has two 2.5-inch wide plexiglass spacers which, if removed, would allow testing at different evacuator length-to-diameter ratios. High pressure air is supplied to the evacuator chamber through two openings in the evacuator casing, cf. Figure 25b.

The performance of the baseline bore evacuator configuration is compared to a second configuration with staggered discharge orifices. The second model is identical to the baseline, except the three ejectors are replaced by six staggered ejectors of diameter 0.046 inch, cf. Figure 26. These six ejectors have 90.2 percent of the total hole area as the baseline, and the three downstream ejectors are at the same axial location. The second row of three ejectors is placed 1 inch upstream of the first row and offset 60 degrees radially.

Instrumentation

The pressure distribution along the barrel is measured using a Sertra Model 339-1 digital manometer. Muzzle velocity surveys, which use a pitot-static tube, also use this manometer. The calibration of the digital manometer is checked against U-tube and inclined manometers prior to the test series.

The velocity distribution at the breech end is measured using a TSI Model 1210-20 thin-film sensor. The sensor is connected to a TSI Model 1050 anemometer, and measurements are made with an HP 54501A digital oscilloscope. The sensor is calibrated at velocities up to 68 ft/sec in the RPI Low Speed Calibration Tunnel. For velocities larger than 68 ft/sec, the calibration is conducted in the model itself. These calibrations use the velocity calculated from a center line static pressure measurement. A typical calibration curve is presented in Figure 27.

The mass flow into the evacuator chamber is calculated from the measured pressure drop across a 1-inch diameter sharp-edged orifice. The mass flow is obtained through the relation (ref 12):

$$\dot{m}(slugs/\text{sec}) = \frac{0.0997}{32.2} KY\sqrt{\rho_0 h_w} \qquad (24)$$

The factor h_w is the measured pressure drop across the orifice in inches of water and can be very small at low evacuator pressures.

A simple inclined manometer is used to measure this pressure drop. The manometer, shown in Figure 25a, has a large reservoir (155 times the tube inner diameter); the tube is inclined 18.5 degrees from the horizontal. Indicating fluid with a specific gravity of 0.824 over a wide range of temperatures is used for the tests.

The evacuator pressure and the pressure upstream of the orifice are measured using mercury U-tube manometers for evacuator pressures up to 16 psig. Higher pressures are measured using bordon tube pressure gauges. These gauges are calibrated using a dead weight tester.

Orifice Meter Calibration

Because the orifice mass flow is very small, it is important to ensure no possibility of air leaking out of the model to the atmosphere. Before every test series, the muzzle is plugged, and the model configuration is altered to accurately calibrate the mass flow through the orifice with the mass flow through the breech. The modification entails installing 1/8-inch honeycomb upstream of the breech to smooth the velocity profile. The breech velocity profile is measured with a hot film anemometer from 3 to 86 psig. The sensor is calibrated for very low velocities (less than 10 ft/sec) using the calibration tunnel and fitted to a curve obtained from a correlation by Colis and Williams (ref 13).

For the mass flow calibration, the breech velocity profile is integrated numerically to obtain the mass flow rate, and this is compared to the mass flow rate obtained from the orifice meter. The mass flows from the two different methods agree to within five percent for a range of 3 to 86 psig evacuator pressure, Figure 28.

Calculation of Evacuator Performance

The mass flow rate into the breech can be expressed as

$$\dot{m}_b = \int \rho u dA \tag{25}$$

This equation is integrated numerically by Simpson's 3/8 rule using the measured velocity profile at the breech. The mass flow augmentation ratio, defined as the ratio of induced flow rate through the breech to the measured flow rate through the ejectors, is then

$$\zeta = \frac{\dot{m}_b}{\dot{m}_{ej}} = \frac{\int \rho u dA}{\dot{m}_{ej}} \tag{26}$$

The discharge coefficient is defined as the ratio of actual mass flow rate through the ejectors to the ideal mass flow rate. With the ideal mass flow rate given by Eq. (22), the discharge coefficient is

$$C_d = \frac{\dot{m}_{ej}}{\left(\frac{\rho^*}{\rho_e}\right)\rho_e\left(\frac{a^*}{a_e}\right)a_e\left(\frac{A^*}{A_e}\right)A_e} \tag{27}$$

Test Conditions

The quasi-steady discharge tests are conducted by maintaining the evacuator pressure vessel at a constant pressure. Air from a laboratory compressor is supplied through two pressure feeds in the evacuator casing, cf. Figure 25b. The constant mass flow rate of air into the model is determined from Eq. (27). This mass flow rate must necessarily be the mass flow rate out of the evacuator chamber through the ejectors.

The tests are conducted at evacuator pressures from 1 to 84 psig. At each test pressure, the barrel pressure distribution, breech and muzzle velocity profiles, and ejector mass flow rate are measured. After each test, the data is entered into a FORTRAN computer program that automatically calculates the performance characteristics such as the orifice coefficient, augmentation ratio, and breech and muzzle mass flow rates.

Quasi-Steady Discharge Phase Results and Discussion

A comparison of the discharge coefficients for the baseline and staggered configurations is presented in Figure 29. For evacuator pressures greater than 26 psig, the discharge coefficient is constant at approximately 0.79 for the baseline configuration and 0.80 for the staggered ejectors. The discharge coefficient begins to decrease at pressures lower than 26 psig. At pressures lower than 16 psig, the discharge coefficient drops rapidly toward zero. At pressures higher than approximately 16 psig, the flow through the ejectors is sonic, i.e. the flow is choked.

The barrel pressure distributions for the baseline configuration are shown in Figures 30a and 30b and for the staggered configuration in Figures 30c and 30d. For both cases there is a gradual pressure drop associated with viscous losses upstream of the ejector orifices (which are at $X = 0$ inch). The pumping action of the ejectors can be seen in the pressure rise downstream, and the pressure decreases to ambient at the muzzle exit.

The velocity profiles at the breech, measured with a hot film anemometer, are shown in Figures 31a and 31b for the baseline configuration and Figures 31c and 31d for the staggered configuration. These profiles are very nearly uniform at all evacuator pressures. Figure 32 is a comparison between the mean breech velocities for the baseline and staggered configurations. The staggered ejector orifices, shown in Figure 26, result in a gain of approximately twelve percent in breech velocity for all evacuator pressures.

The muzzle velocity profiles, measured with a pitot-static probe, for both configurations are presented in Figures 33a through 33d. The muzzle velocity profiles are much more non-uniform than the breech profiles because of the presence of the ejector orifices just upstream of the muzzle. The tests were preformed with the model oriented so that the downstream ejector was rotated 30 degrees from the vertical. The asymmetry of the ejectors is a primary cause of this asymmetry in the muzzle velocity profile.

A comparison between the mean velocities of the core muzzle flow of the staggered and baseline configurations is shown in Figure 34. The staggered ejector orifices result in a gain of approximately five percent over all evacuator pressures.

A pitot-static probe was used to measure the center line velocities at the breech and muzzle for the 155-mm cannon with room temperature air supplied to the evacuator at Benét Laboratories (ref 14), and the variation of the breech and muzzle velocities as functions of the evacuator pressure are presented in Figure 35. Also, the center line velocities for the 33 percent scale bore evacuator model are presented. Due to the lower Reynolds number for the scale model, the mean velocities are slightly lower than for the full-scale gun. Thus, the 33 percent scale model can be used to investigate various evacuator concepts before applying the promising configurations to the 155-mm gun.

The mass flow augmentation ratios for the baseline and staggered configurations are presented in Figure 36. The staggered ejectors result in a gain of approximately 20 percent over all evacuator pressures. The augmentation reaches a peak of 13 for the baseline and 16 for the staggered at an evacuator pressure of 12 psig. At pressures below this, the rapid decrease in orifice coefficient causes a decrease in augmentation. At the higher pressures, the augmentation ratio drops off slowly as evacuator pressure increases because the supersonic region with shock bottles increases. This decreases the mixing of the supersonic jets with the ambient air, as discussed in Reference 15.

During the course of one of the experiments to calibrate the orifice meter, the model was placed in a configuration with a short breech end and a muzzle L/D ratio of 34. While in this configuration, a preliminary test was done to determine whether a screen placed at the breech end would affect the mixing in the bore. A 1-inch thick, 1/8-inch honeycomb screen was placed at the breech end, and a muzzle velocity profile was obtained for several evacuator pressures. A preliminary comparison of the muzzle velocity profiles in the L/D = 34 configuration with and without the screen is presented in Figure 37. The presence of the screen at the breech produces turbulence which increases the mixing at the jets, resulting in a much more uniform muzzle velocity profile.

CONCLUSIONS

The RPI HPST and a 65 percent scale model of the 155-mm gun bore evacuator are used to simulate the flow conditions in the gun bore and evacuator for the evacuator charge and discharge cycles. Interior ballistics solutions for the 155-mm gun (ref 1) provide the flow conditions in the bore. The model is tested at a shock tube shock wave Mach number of 1.89. The Mach number of the flow after the shock is 0.89, and the bore pressure is 91 psia. To enable testing of high ratios of the bore pressure to the evacuator pressure, (P_B/P_e), simulating the early charge cycle, diaphragms must be placed over the charge and discharge orifices.

Two thin-film platinum heat gauges are located in the evacuator chamber to measure the starting shock wave through the discharge ports. The time histories of these two heat gauges reveal strong shock waves propagating from the discharge orifices during the early charge cycle.

The charge coefficient for the angled discharge ports has been evaluated at bore-to-evacuator pressure ratios up to 2300. The charge ports are sealed for these tests, and all mass flow into the evacuator chamber is through the discharge ports. The charge coefficient ranges from 0.51 at low P_B/P_e to 0.58 at a P_B/P_e of 1570. The sleeve has little effect on the charge

from 0.51 at low P_B/P_e to 0.58 at a P_B/P_e of 1570. The sleeve has little effect on the charge coefficient.

The charge coefficient for the charge ports, with the discharge ports sealed, is nearly constant at 0.29. After removing a spacer, which simulates the geometry of the casing used to hold the valve ring in the actual 155-mm bore evacuator, the charge coefficient rises to near 0.40--higher than the baseline by 25 percent.

Testing the bore evacuator discharge phase in the RPI HPST is done using the same model as used for the charge phase. The discharge coefficient is approximately 0.72 over all test pressures, indicating choked flow through the ejector orifices.

To test the quasi-steady performance of the discharge phase of the 155-mm gun bore evacuator, an approximately 33 percent scale model is installed in the RPI Steady-State Flow Facility (ref 11). The performance of the 155-mm cannon bore evacuator is tested at evacuator pressures of 1 to 84 psig. For these tests, the evacuator pressure is kept constant and the pressure and velocity distributions are measured. The performance of the baseline bore evacuator configuration is compared to a second configuration with staggered discharge orifices.

For evacuator pressures greater than 26 psig, the discharge coefficient is constant at approximately 0.79 for the baseline configuration and 0.80 for the staggered ejectors. The discharge coefficient drops off rapidly at lower pressures. At pressures higher than approximately 16 psig, the flow through the ejectors is sonic, i.e. the flow is choked.

The staggered ejector orifices, Figure 26, result in a gain of approximately ten percent in breech velocity for all evacuator pressures. The staggered ejectors result in a gain in mass flow augmentation ratio of approximately 20 percent over all evacuator pressures. The augmentation reaches a peak of 13 for the baseline and 16 for the staggered at an evacuator pressure of 12 psig. At pressures below this, the rapid decrease in orifice coefficient causes a decrease in augmentation.

A preliminary study of the effects of the presence of a screen at the breech produces turbulence which increases the mixing at the jets, resulting in a much more uniform muzzle velocity profile.

REFERENCES

1. P.M. Vottis, "Digital Computer Simulation of the Interior Ballistics Process in Gun," WVT-6515, Benét Weapons Laboratory, Watervliet, NY, October 1966.

2. M.A.S. Minucci and H.T. Nagamatsu, "An Investigation of Hypersonic Shock Tunnel Testing at an Equilibrium Interface Condition of 4100 K: Theory and Experiment," AIAA Paper 91-1707, June 1991.

3. D.G. Messitt, P.C. Dallemagne, L.N. Myrabo, and H.T. Nagamatsu, "Comparison Between Computational and Experimental Data for a Hypersonic Laser Propelled Vehicle," AIAA Paper 92-3808, July 1992.

4. M.A.S. Minucci, H.T. Nagamatsu, and S. Kim, "Investigation of a 2-D Scramjet Inlet, M_∞ = 8-25 and T_o = 800-4100 K," AIAA Paper 91-5018, December 1991.

5. R.E. Dillon, Jr. and H.T. Nagamatsu, "Heat Transfer and Transition Mechanism on a Shock Tube Wall," *AIAA Journal*, Vol. 22, November, 1984, pp. 1524-1528.

6. A. Ferri, *Fundamental Data Obtained From Shock Tube Experiments*, Pergamon Press, 1961, pp. 86-136.

7. Ames Research Staff, "Equations, Tables and Charts for Compressible Flow," NACA Rept. 1135, 1953.

8. I.I. Glass, *Shock Tubes, Part I: Theory And Performance Of Simple Shock Tubes*, UTIA Review No. 12, University of Toronto, 1958.

9. J. Haas, "Theoretical Description of the Bore Evacuator Pressure Cycle," ARDEC Technical Report, Benét Laboratories, Watervliet, NY, to be published.

10. H.T. Nagamatsu, K.Y. Choi, R.E. Duffy, and G.C. Carofano, "An Experimental and Numerical Study of the Flow Through a Vent Hole in a Perforated Muzzle Brake," *Proceedings of the Third Workshop on Launch Blast Overpressure*, U.S. Army Ballistic Research Laboratory, Aberdeen Proving Ground, Maryland, 1987, pp. 61-78.

11. C.A. Andrade, H.T. Nagamatsu, O.F. Sodergren, and G.S. Iannelli, "Cannon Bore Evacuator Flow Theory, CFD, and Experimental Validation," AIAA Paper 92-0832, January 1992.

12. A.S.M.E. Research Committee on Fluid Meters, "Fluid Meters: Their Theory And Application," A.S.M.E., Fourth Edition, 1937.

13. R. Goldstein, *Fluid Mechanics Measurements*, Hemisphere Publishing Corp., NY, 1983, p. 111.

14. J. Bendick, Private Communication, Benét Laboratories, Watervliet, NY, June 1992.

15. H.T. Nagamatsu and R.E. Sheer, Jr., "Subsonic and Supersonic Jets and Supersonic Suppressor Characteristics," *Aeroacoustics: Jet and Combustion Noise; Duct Acoustics*, Vol. 37 of Progress in Aeronautics and Astronautics Series, AIAA and MIT Press, 1975, pp. 125-152.

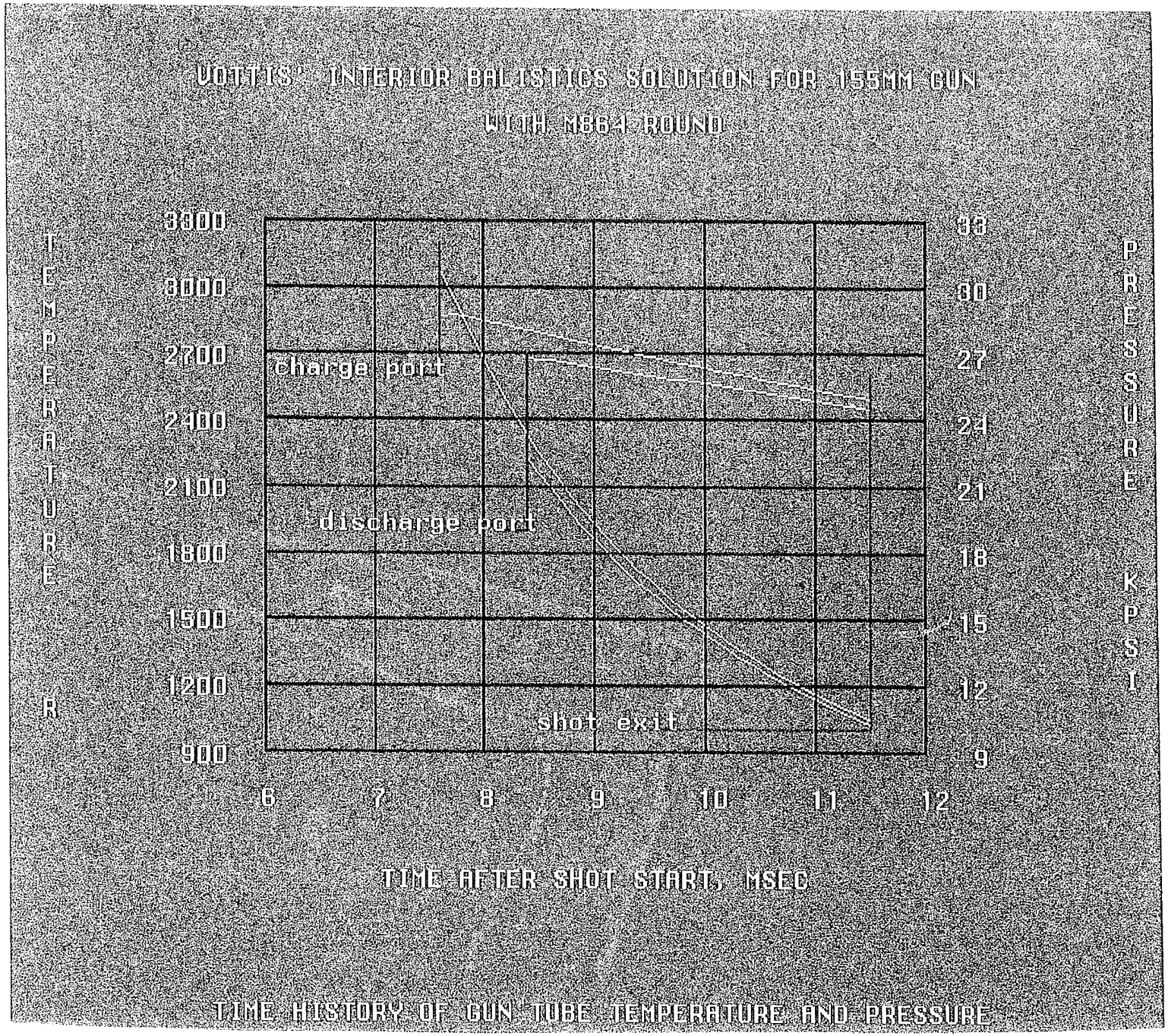

Figure 1a. Interior ballistics solution for 155-mm gun with M864 round showing pressure and temperature in the bore.

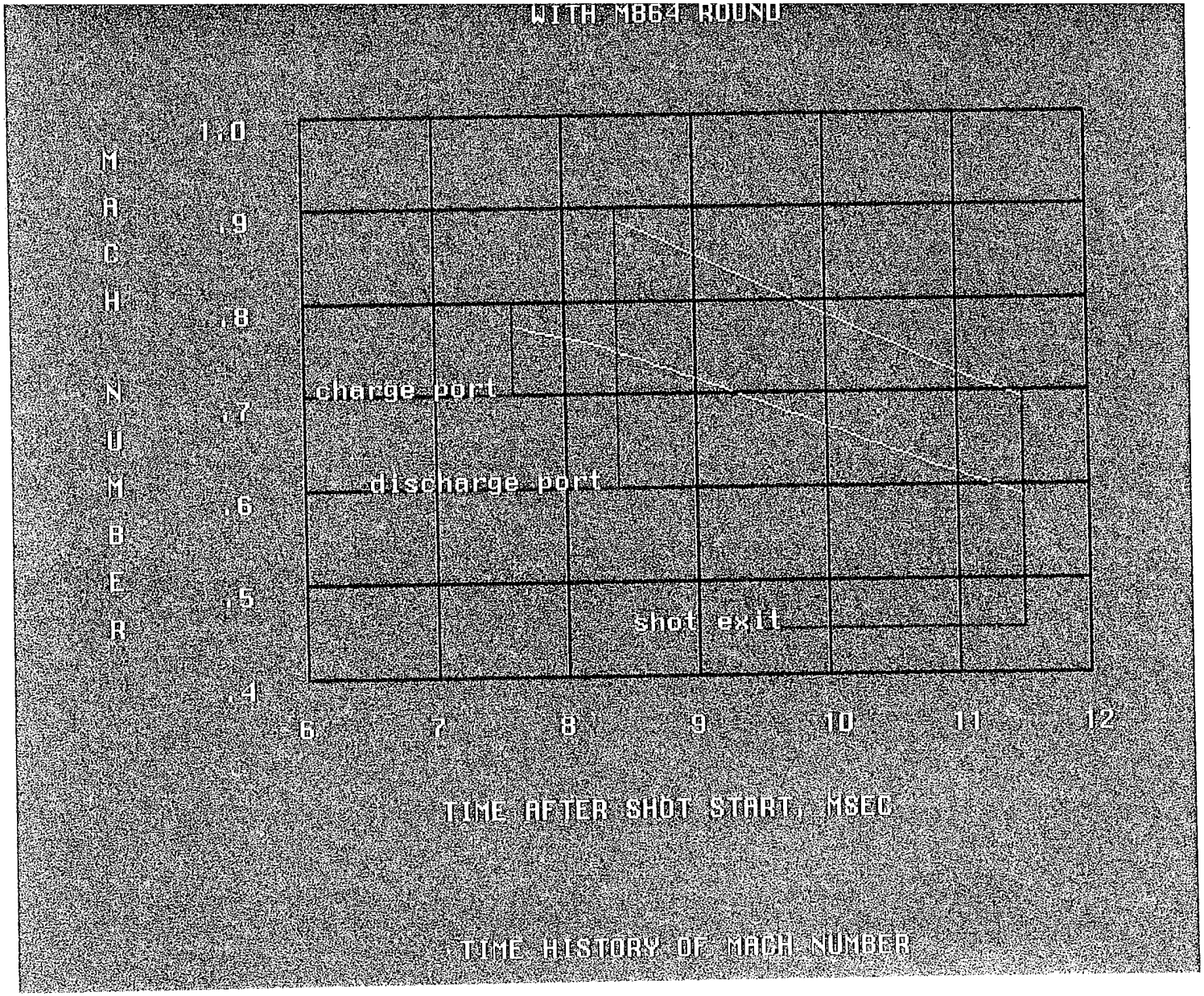

Figure 1b. Interior ballistics solution for 155-mm gun with M864 round showing the Mach number in the bore.

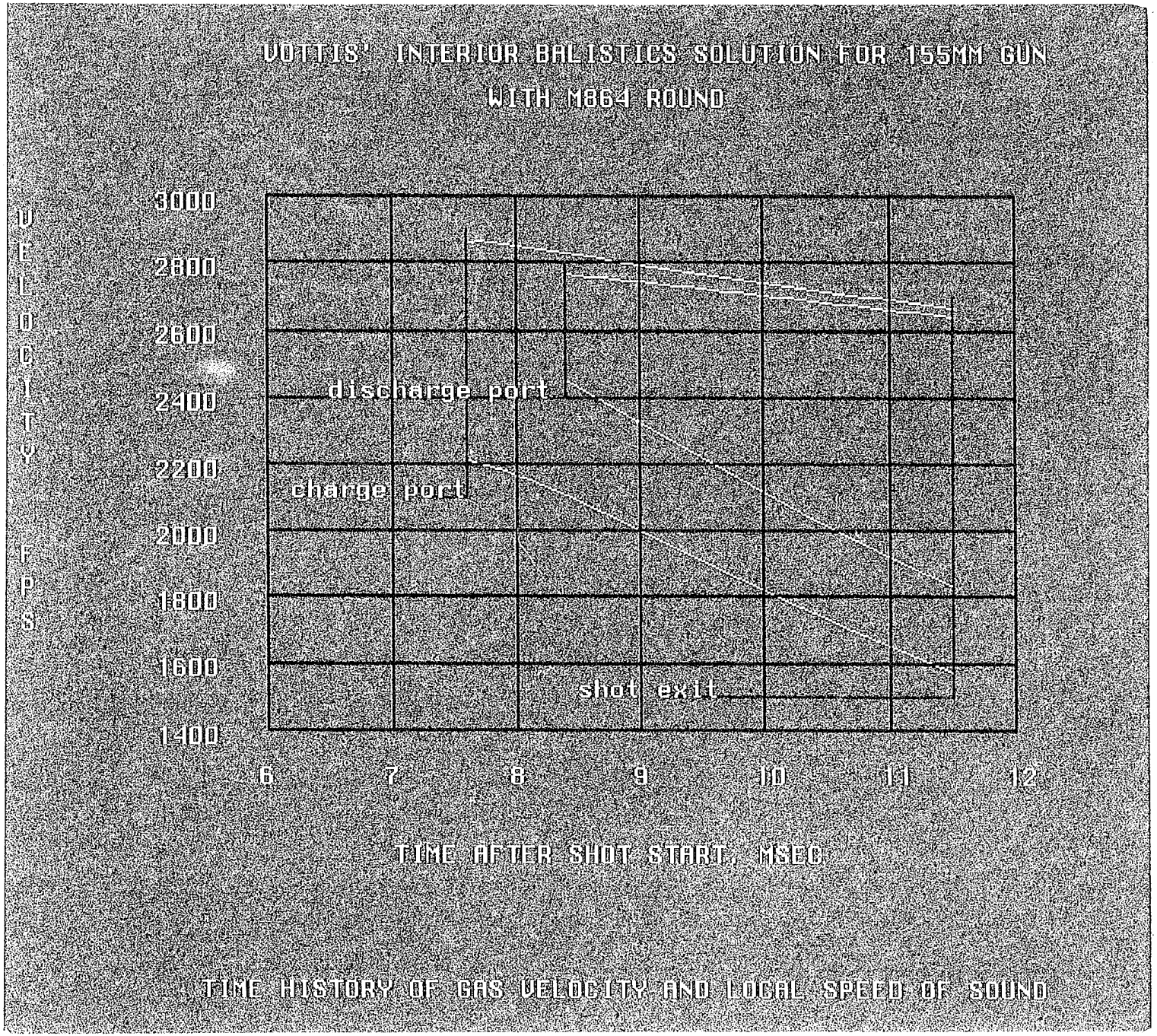

Figure 1c. Interior ballistics solution for 155-mm gun with M864 round showing velocity and sound speed in the bore.

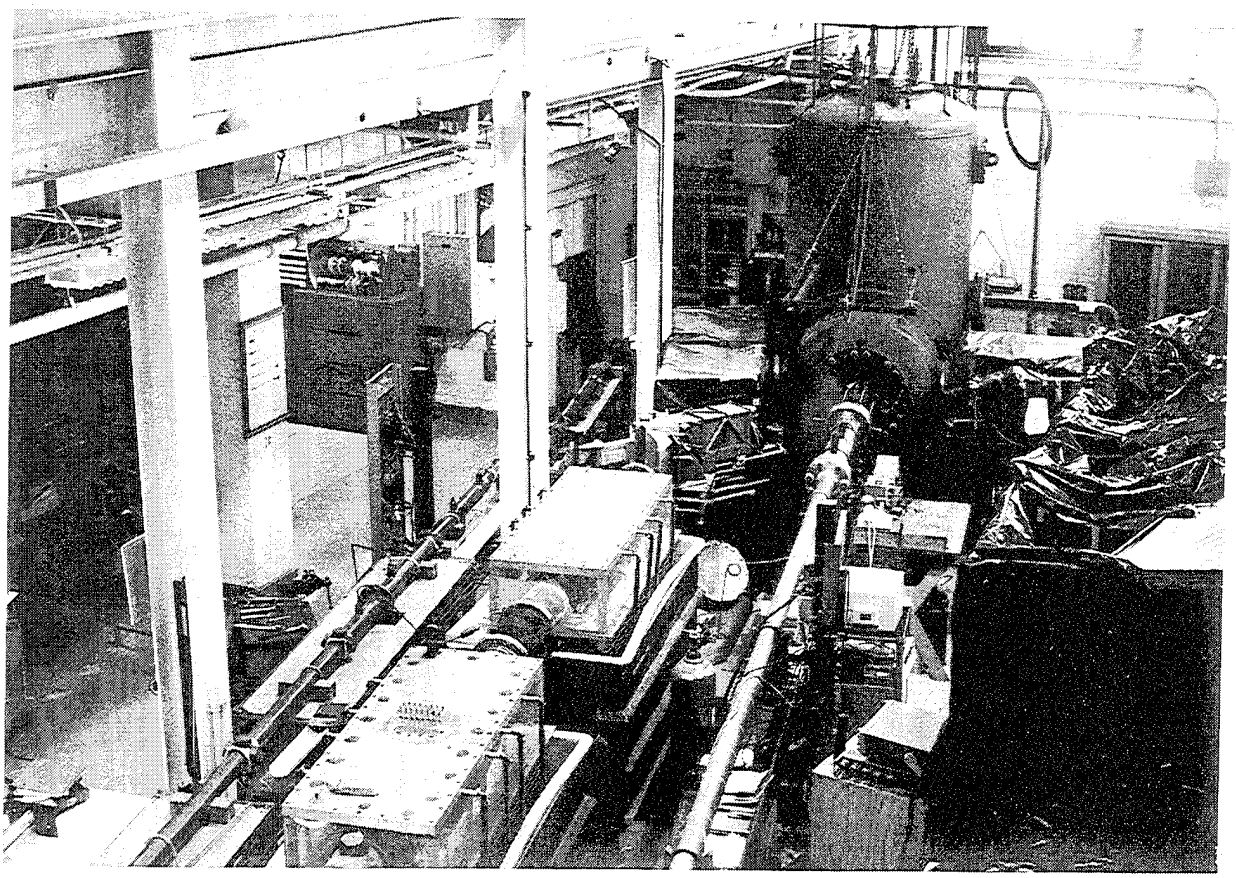

Figure 2. RPI low and high pressure shock tubes.

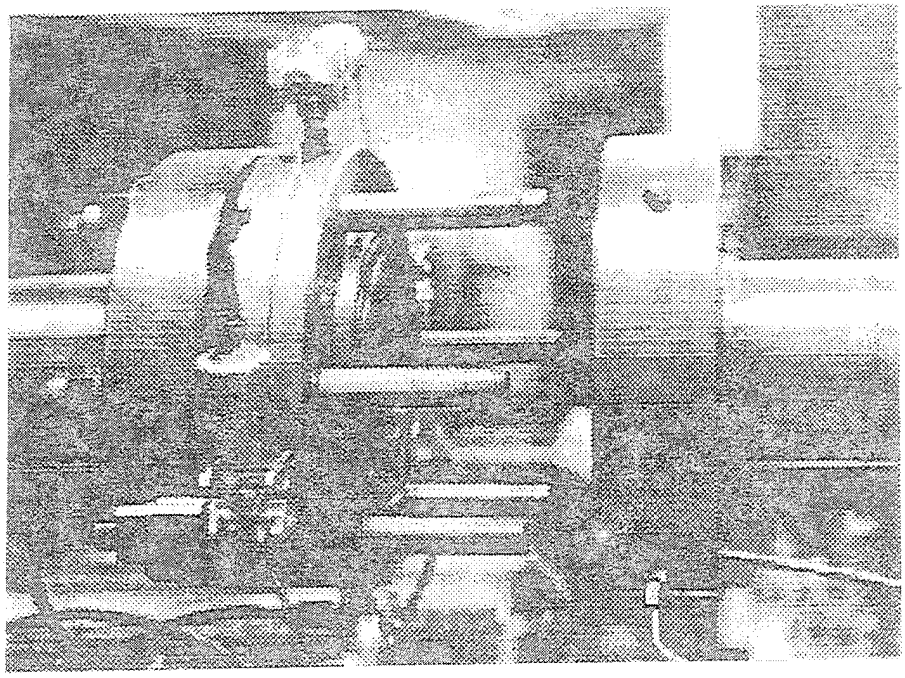

Figure 3. Double diaphragm section of RPI high pressure shock tube.

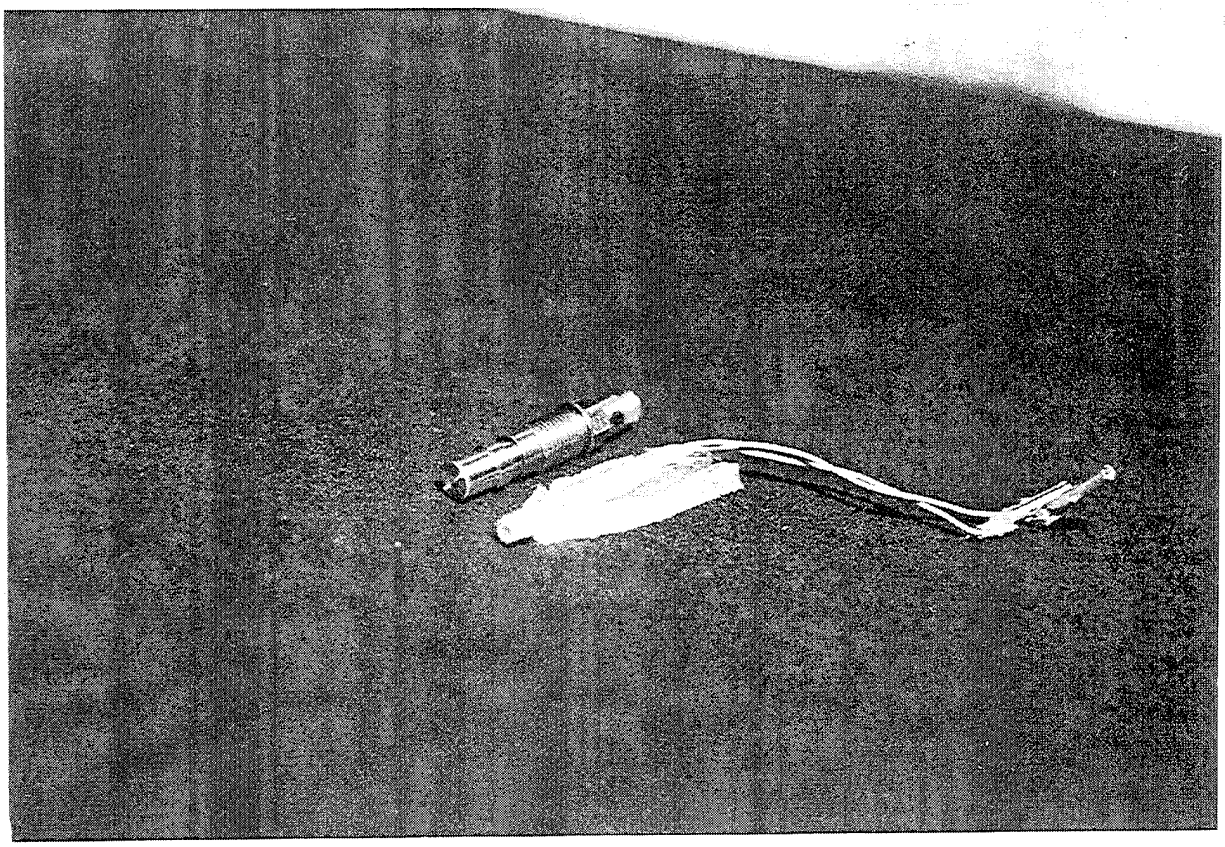

Figure 4. Thin-film platinum heat gauge and PCB pressure gauge.

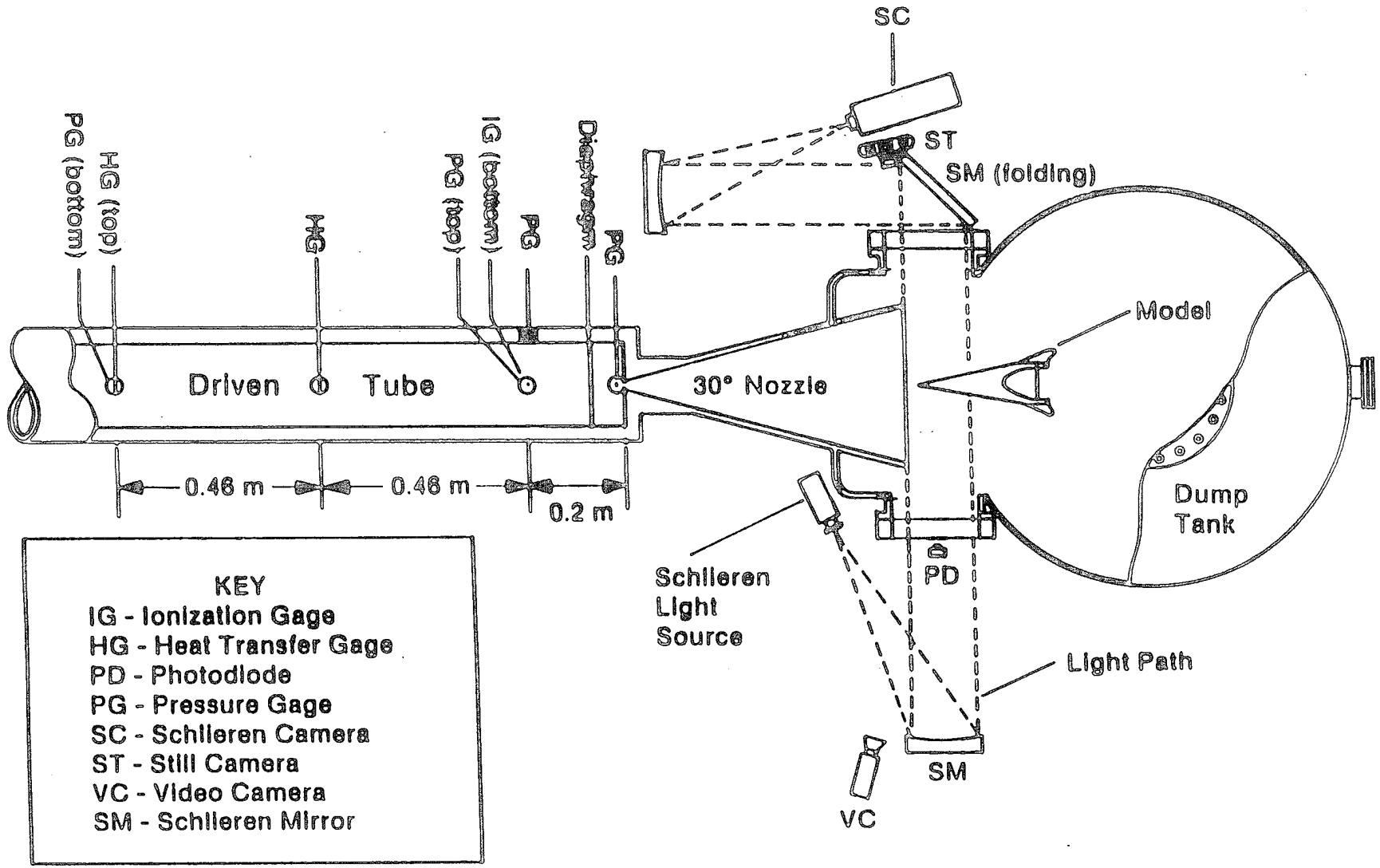

Hypersonic Shock Tunnel Instrumentation

Figure 5. Instrumentation installed in the RPI high pressure shock tube.

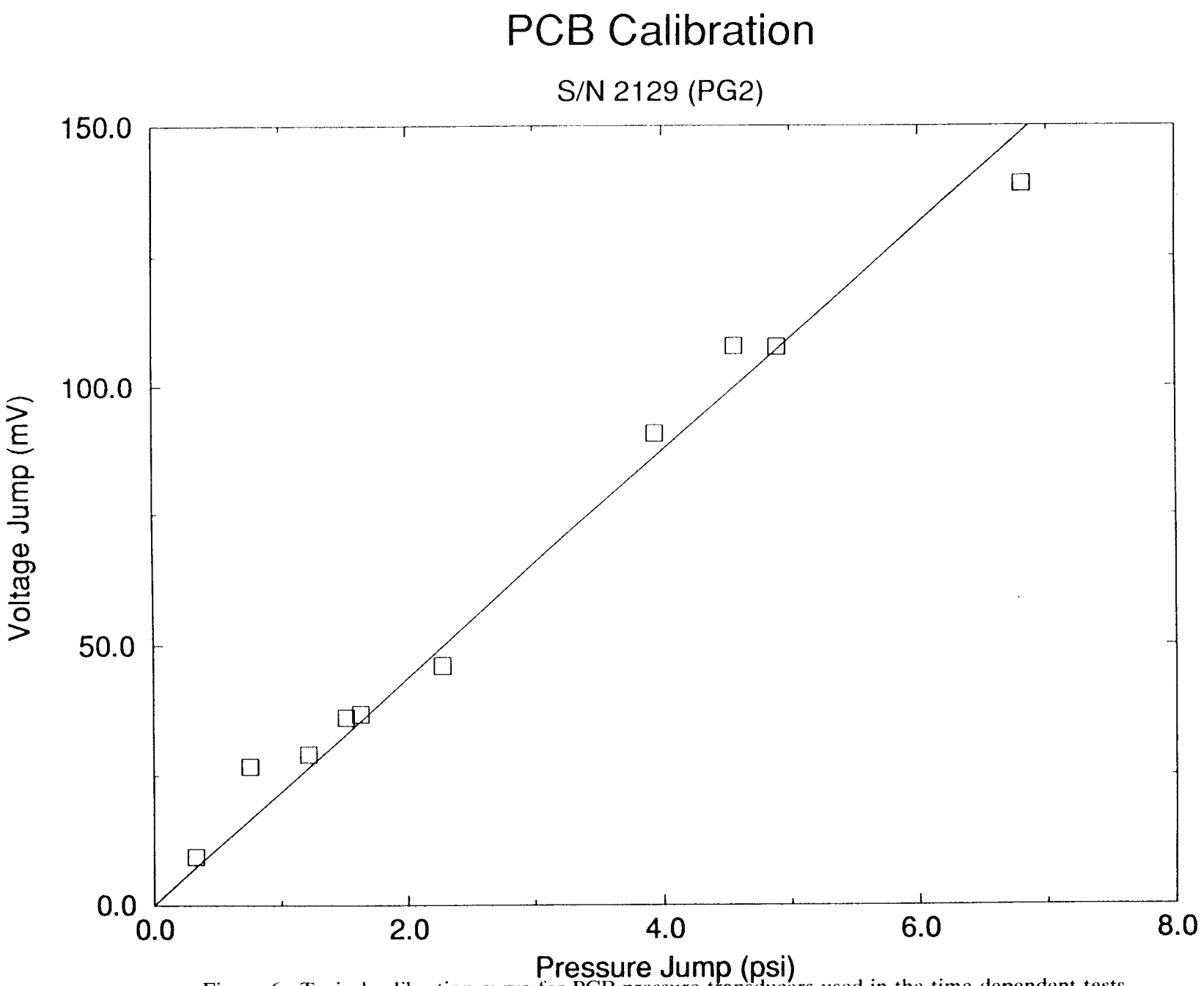

Figure 6. Typical calibration curve for PCB pressure transducers used in the time-dependent tests.

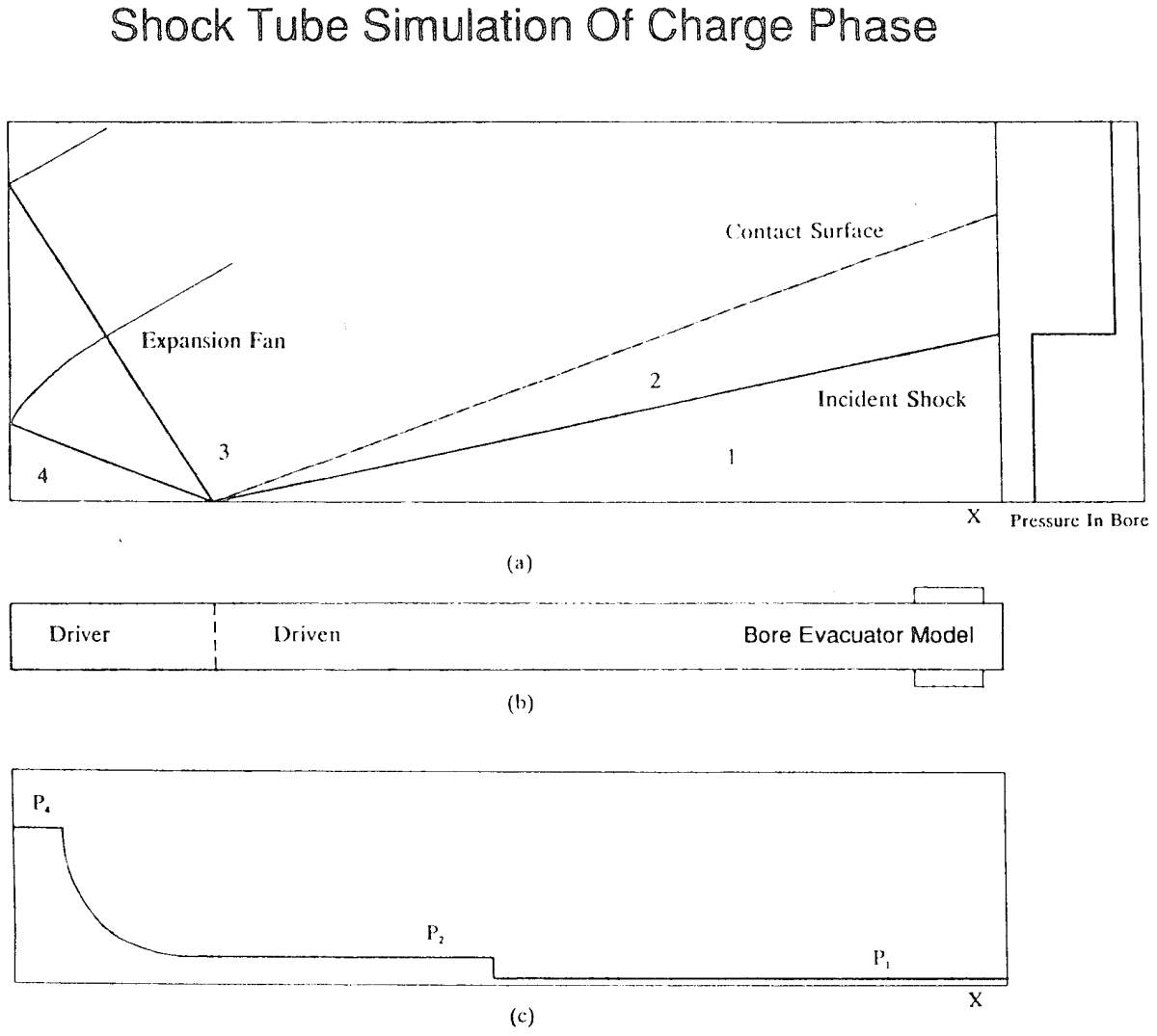

Figure 7. (a) Shock tube X-t diagram and pressure history in the model for the charge tests, (b) Shock tube configuration, and (c) Pressure distribution along shock tube at an early time.

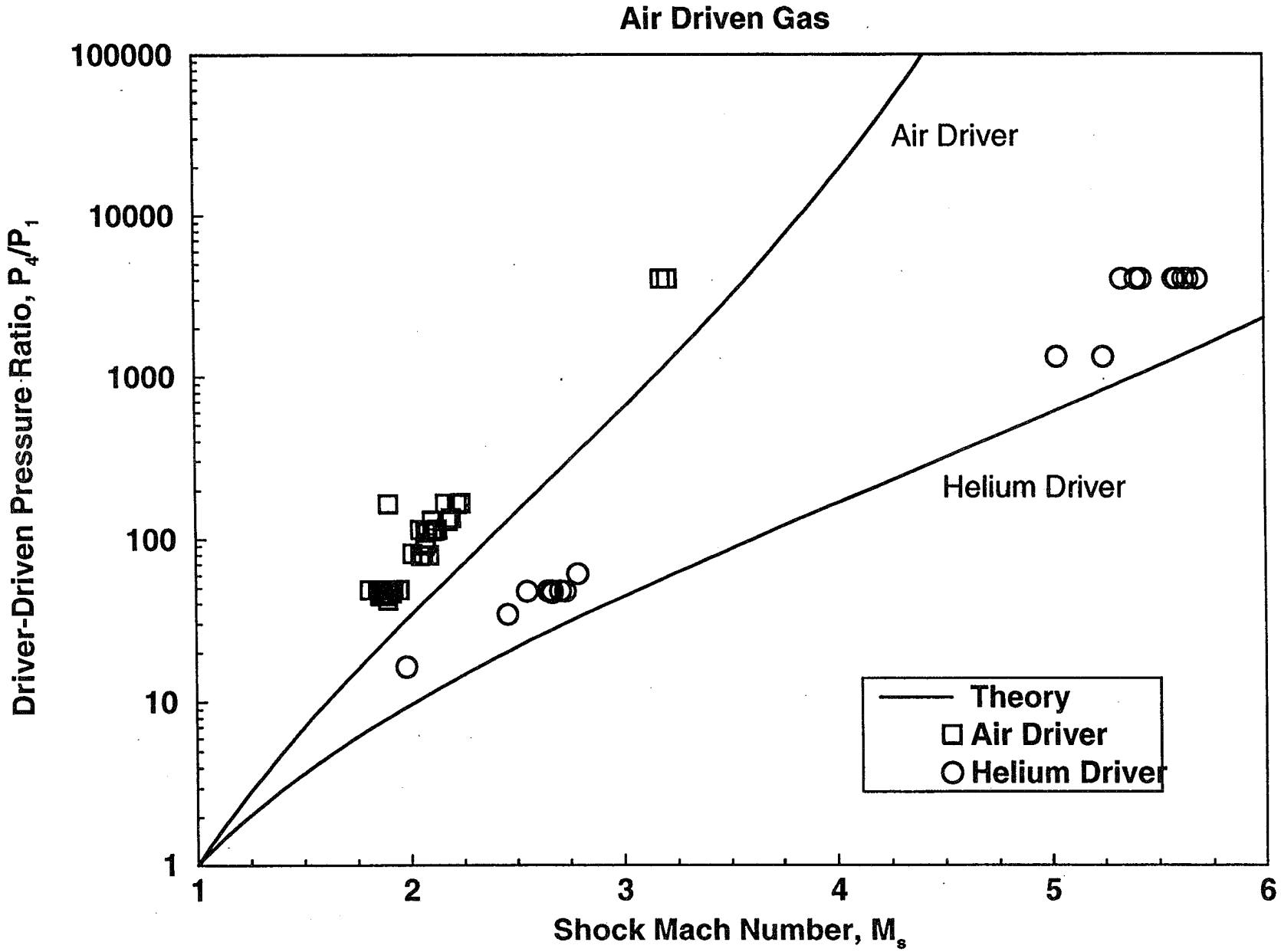

Figure 8. Driver-to-driven pressure ratio required for a given incident shock Mach number with experimental data.

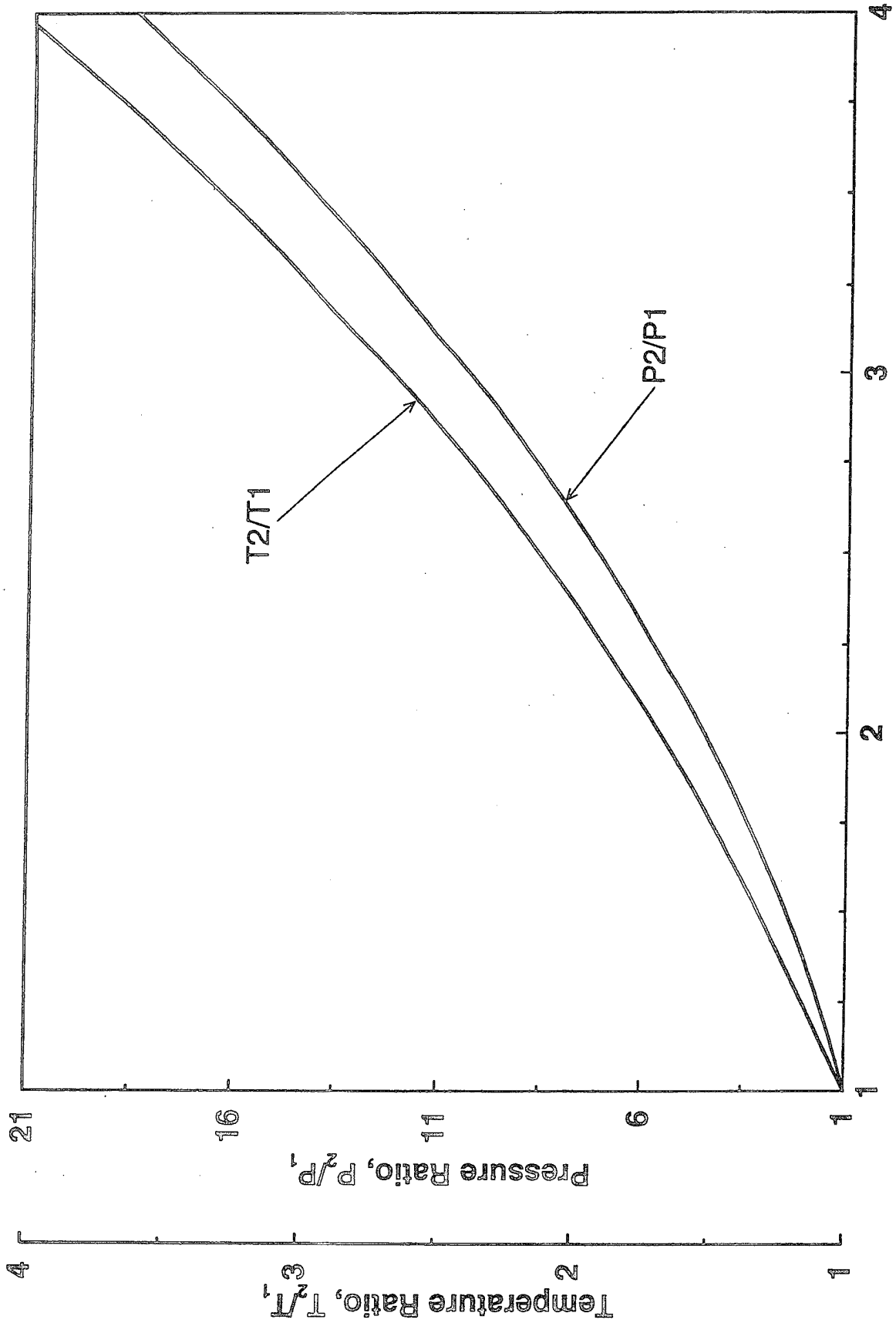

Figure 9. Pressure and temperature jumps across a shock wave.

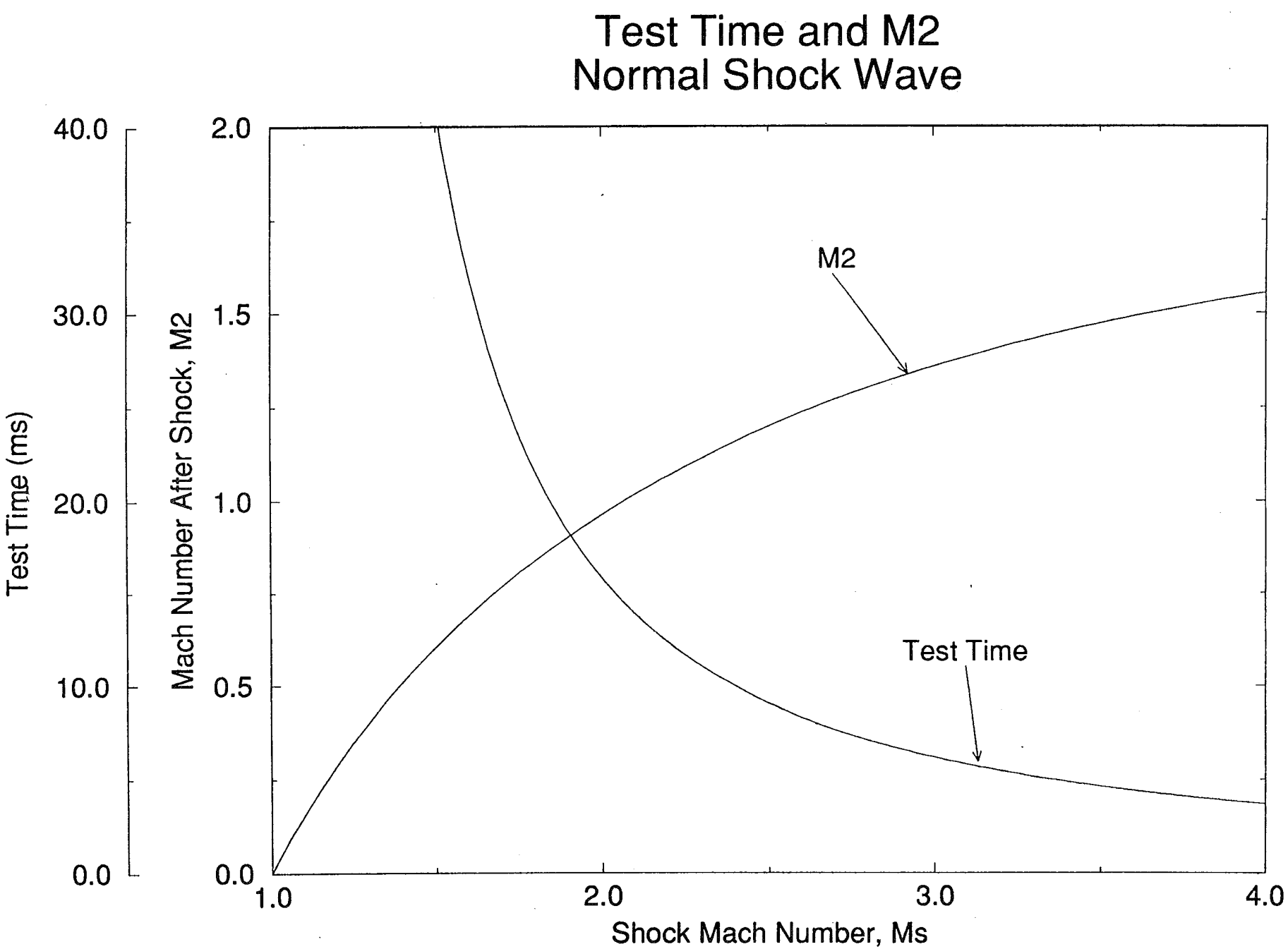

Figure 10. Flow Mach number and shock tube test time versus shock Mach number.

Shock Tube Simulation Of Discharge Phase

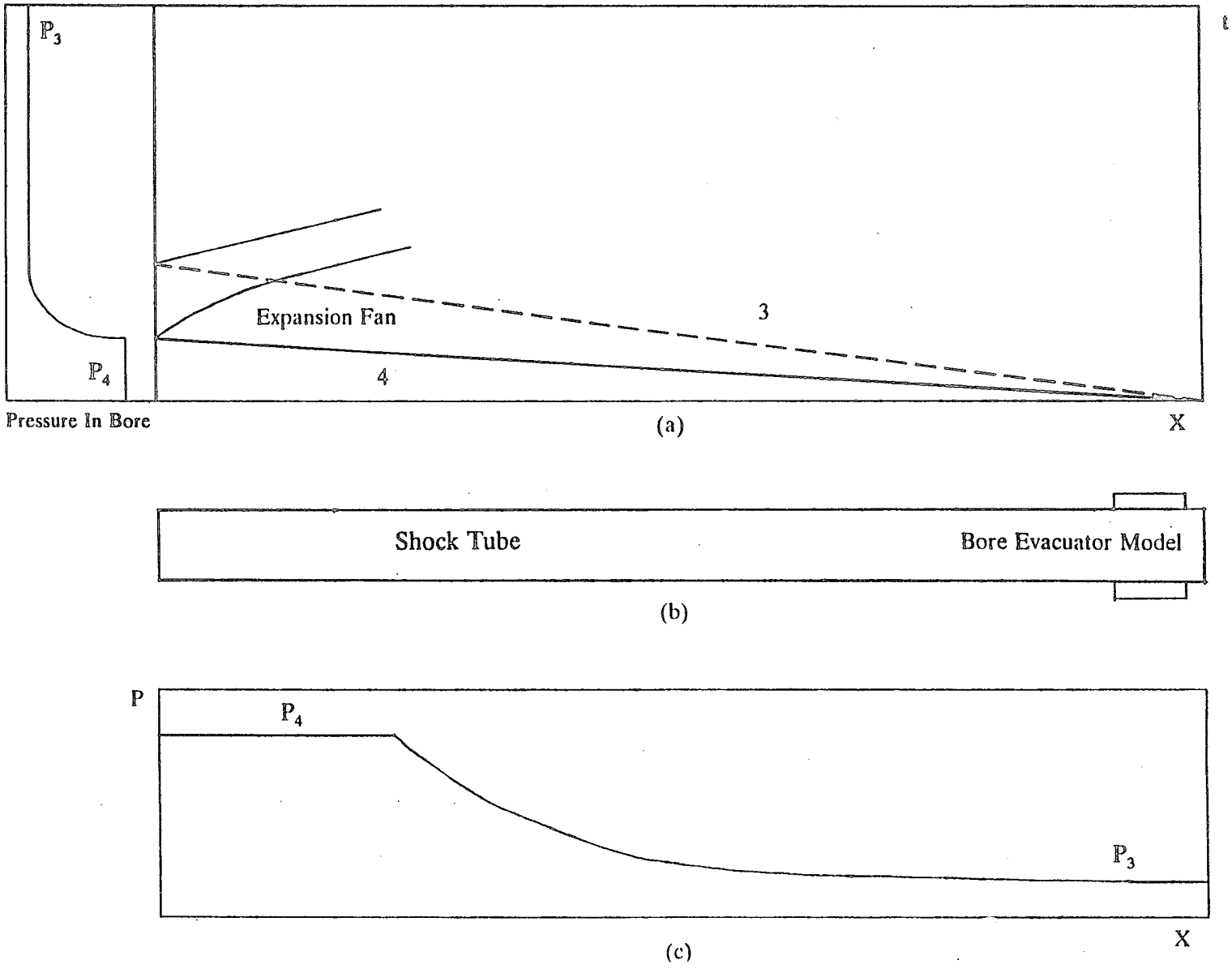

Figure 11. (a) Shock tube X-t diagram and pressure history in the model for the discharge phase tests, (b) Shock tube configuration, and (c) Pressure distribution along shock tube at an early time.

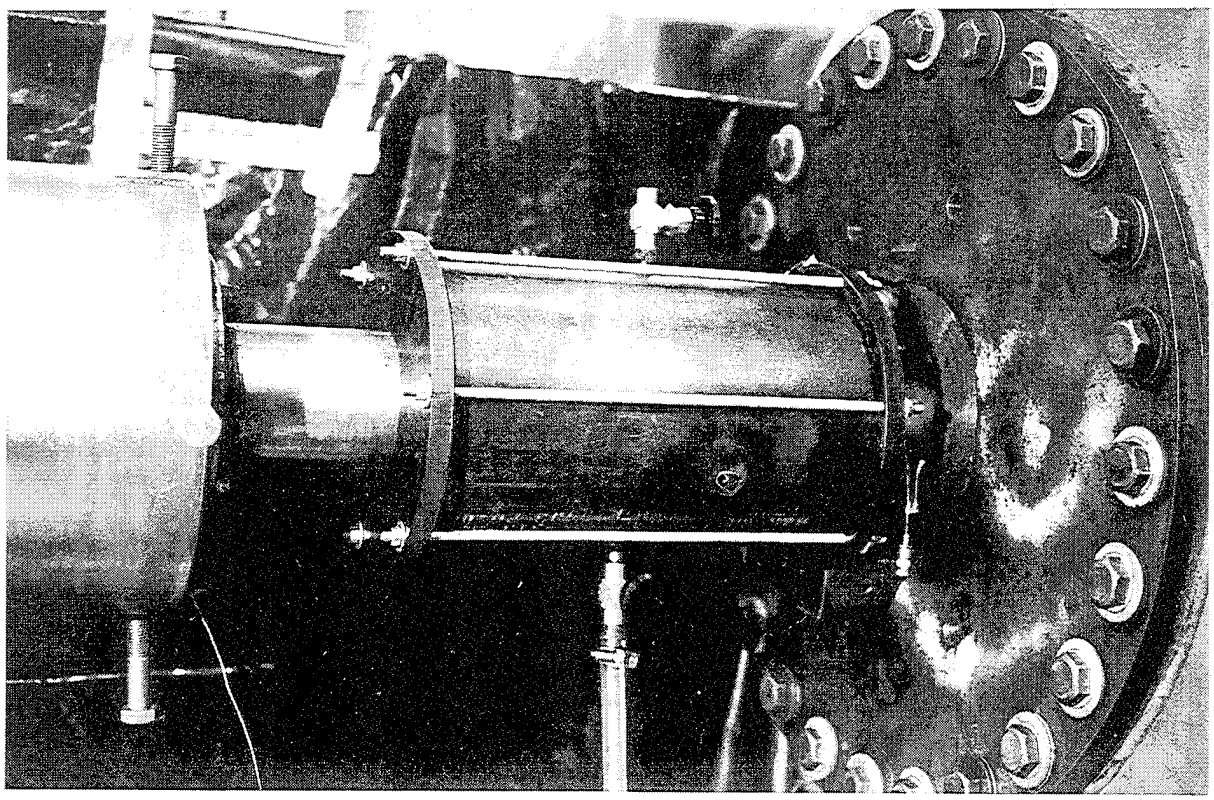

Figure 12a. Photograph of the 65 percent scale bore evacuator model installed on the RPI high pressure shock tube.

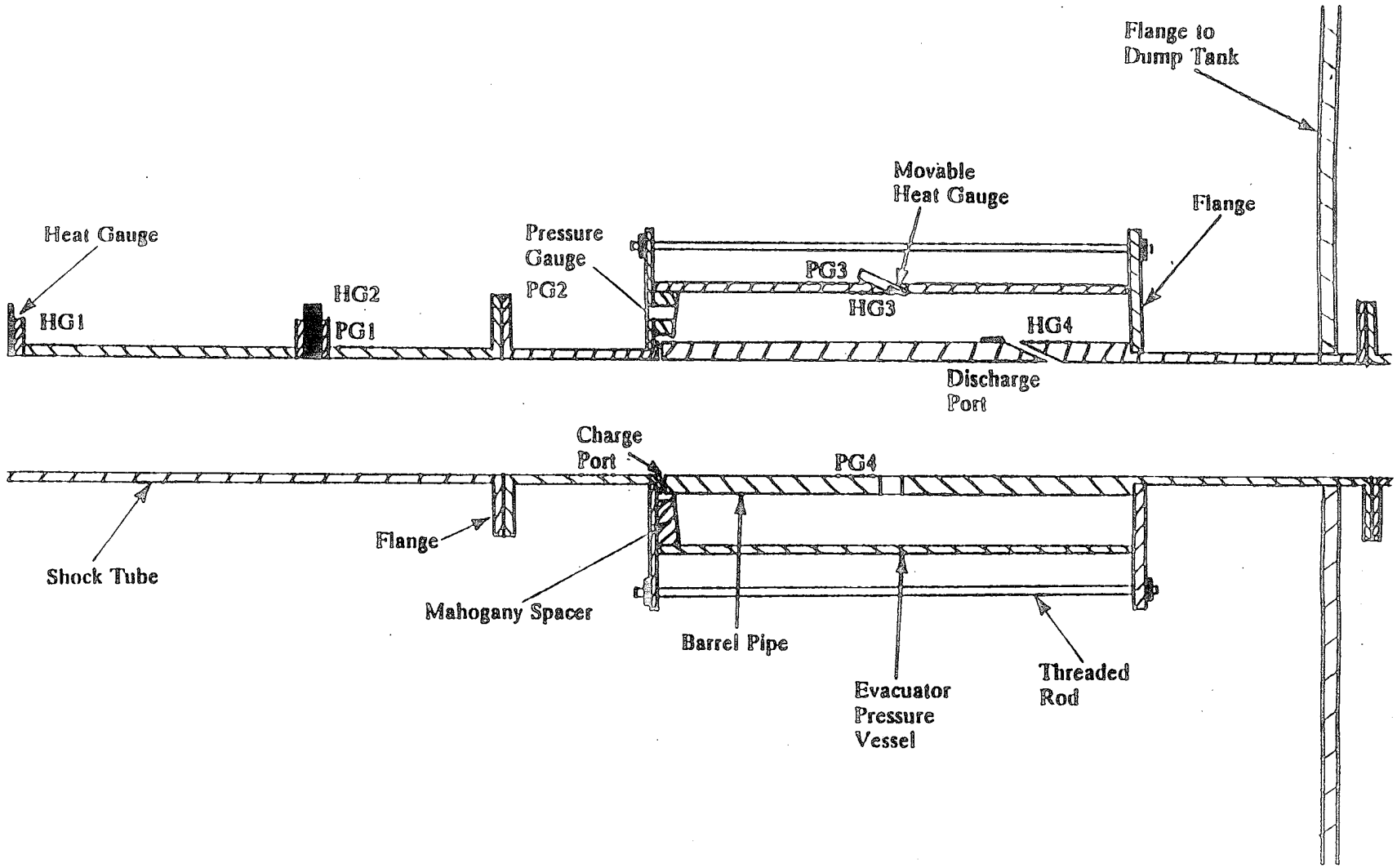

Figure 12b. Schematic of the bore evacuator model configuration for the charge phase tests.

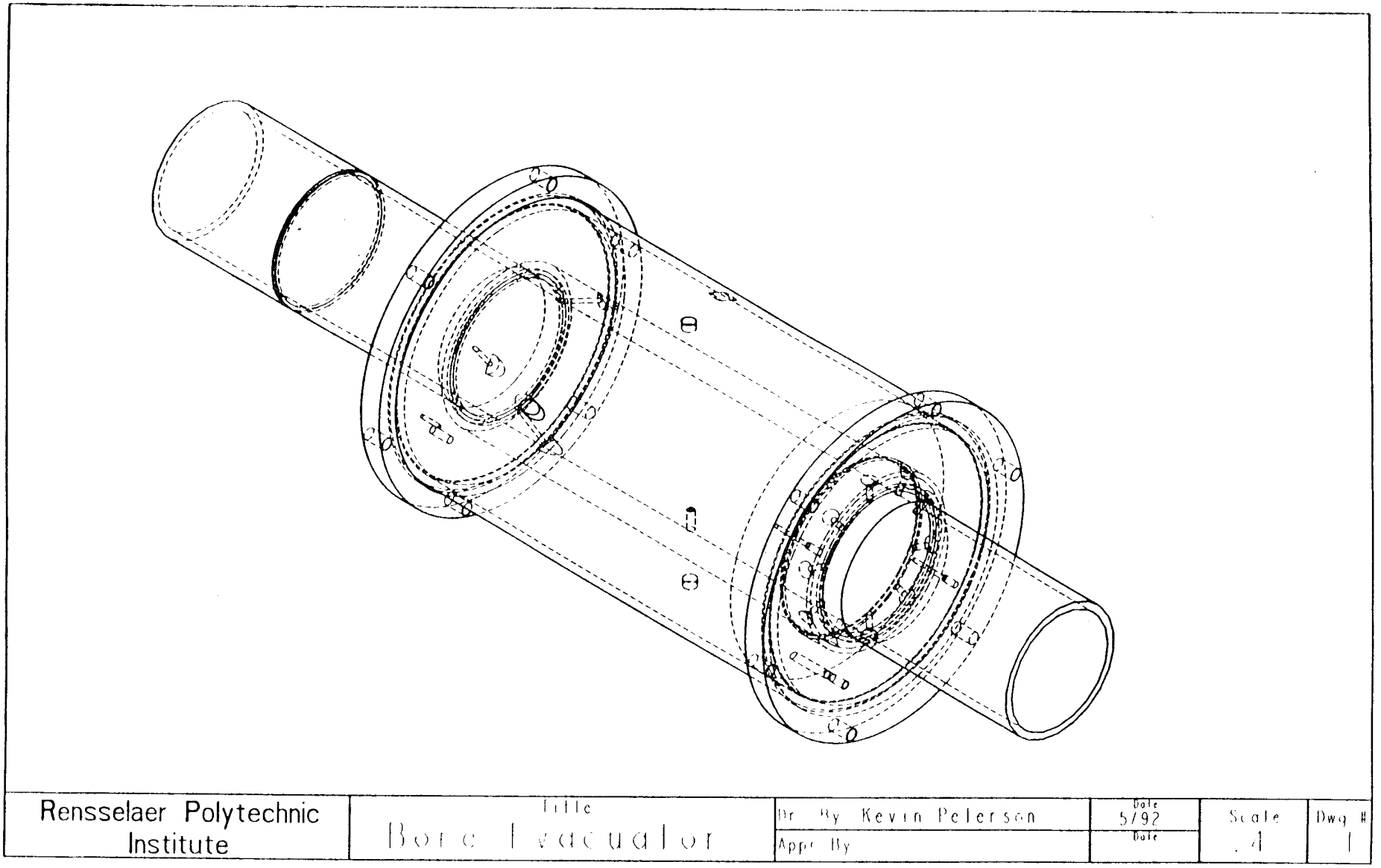

Figure 12c. ProEngineer assembly drawing of bore evacuator model.

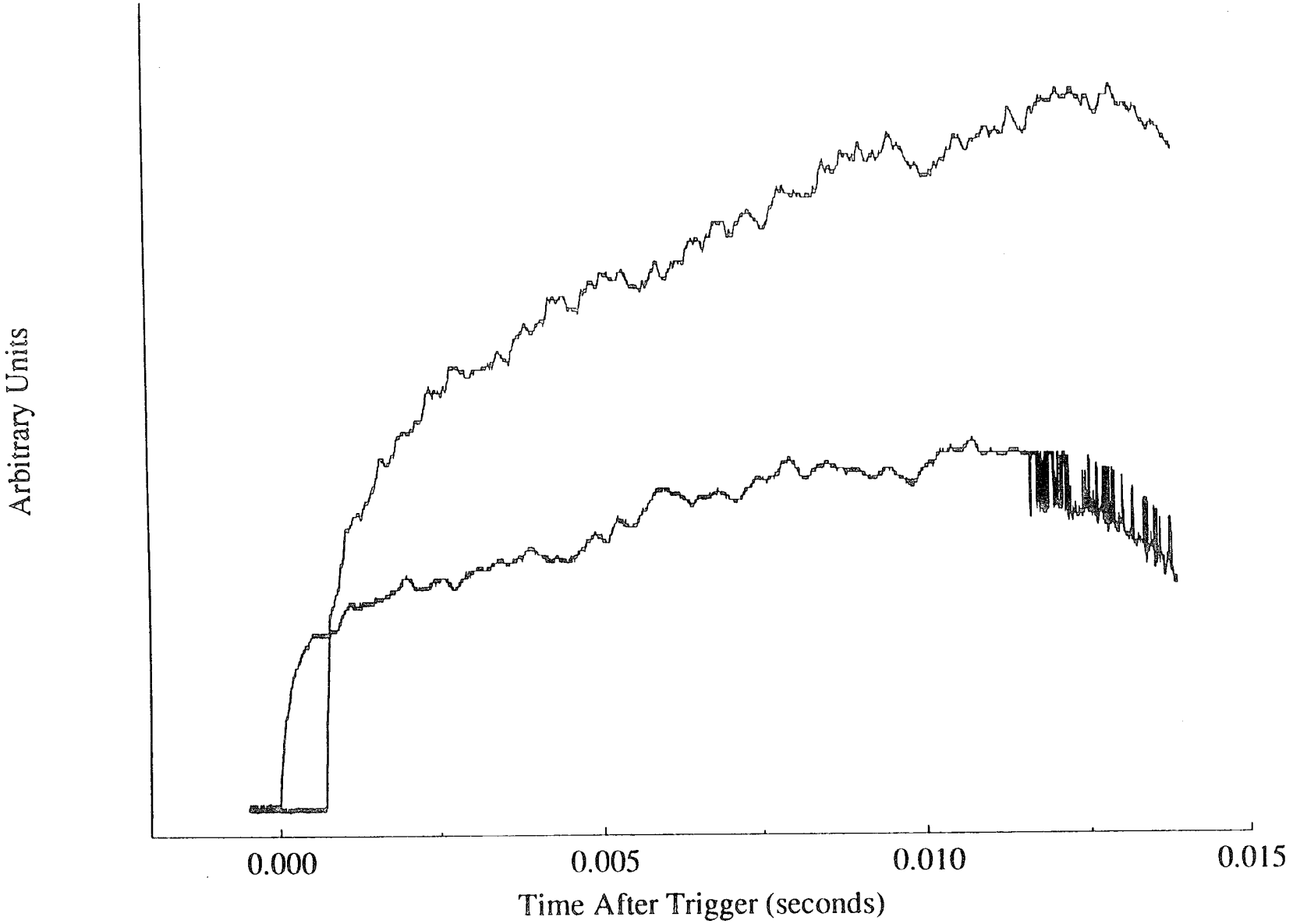

Figure 13. Typical output of heat gauges installed in RPI high pressure shock tube showing passage of the incident shock wave.

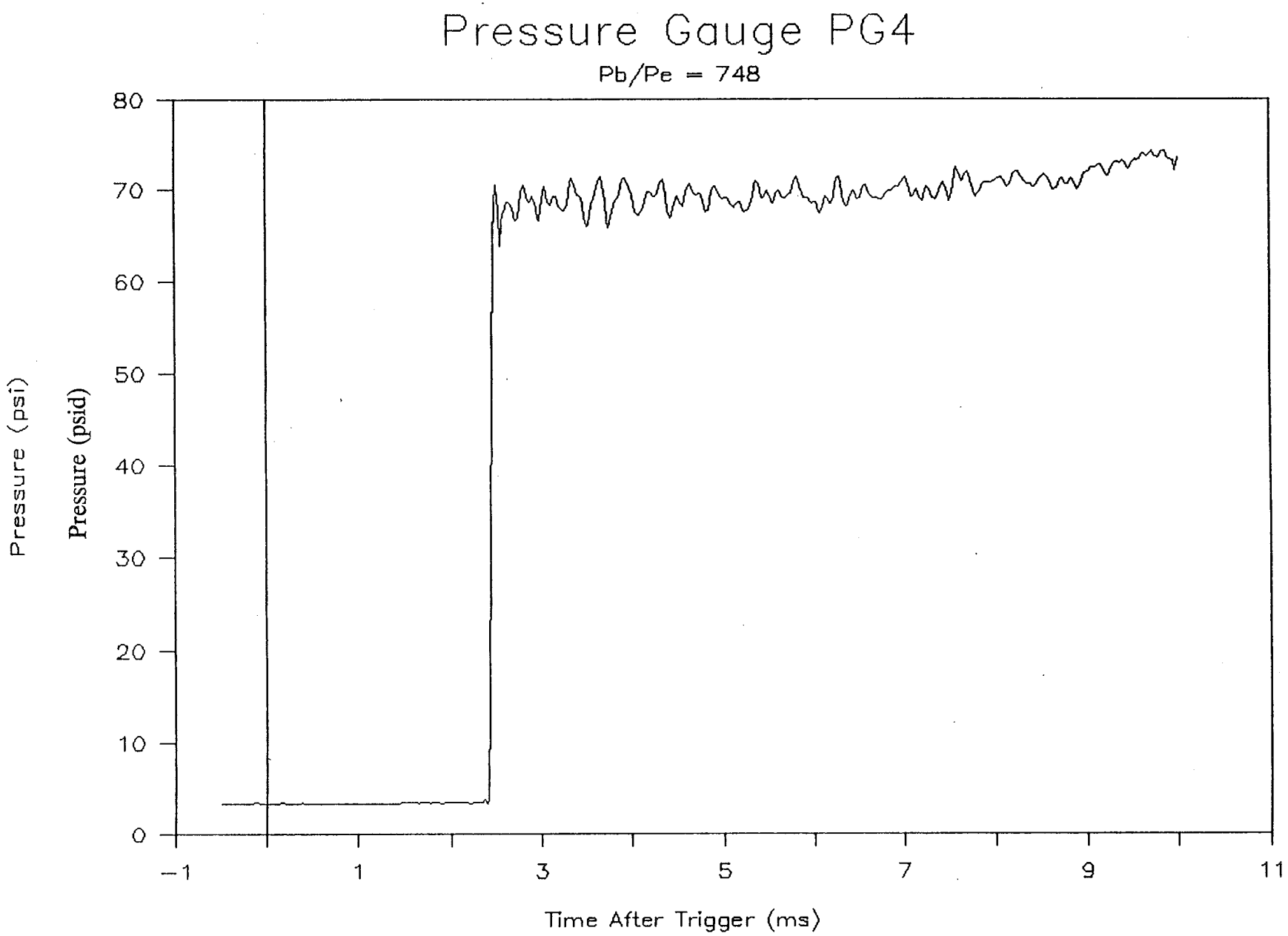

Figure 14. Typical pressure trace from PG4 showing the time history of the bore pressure.

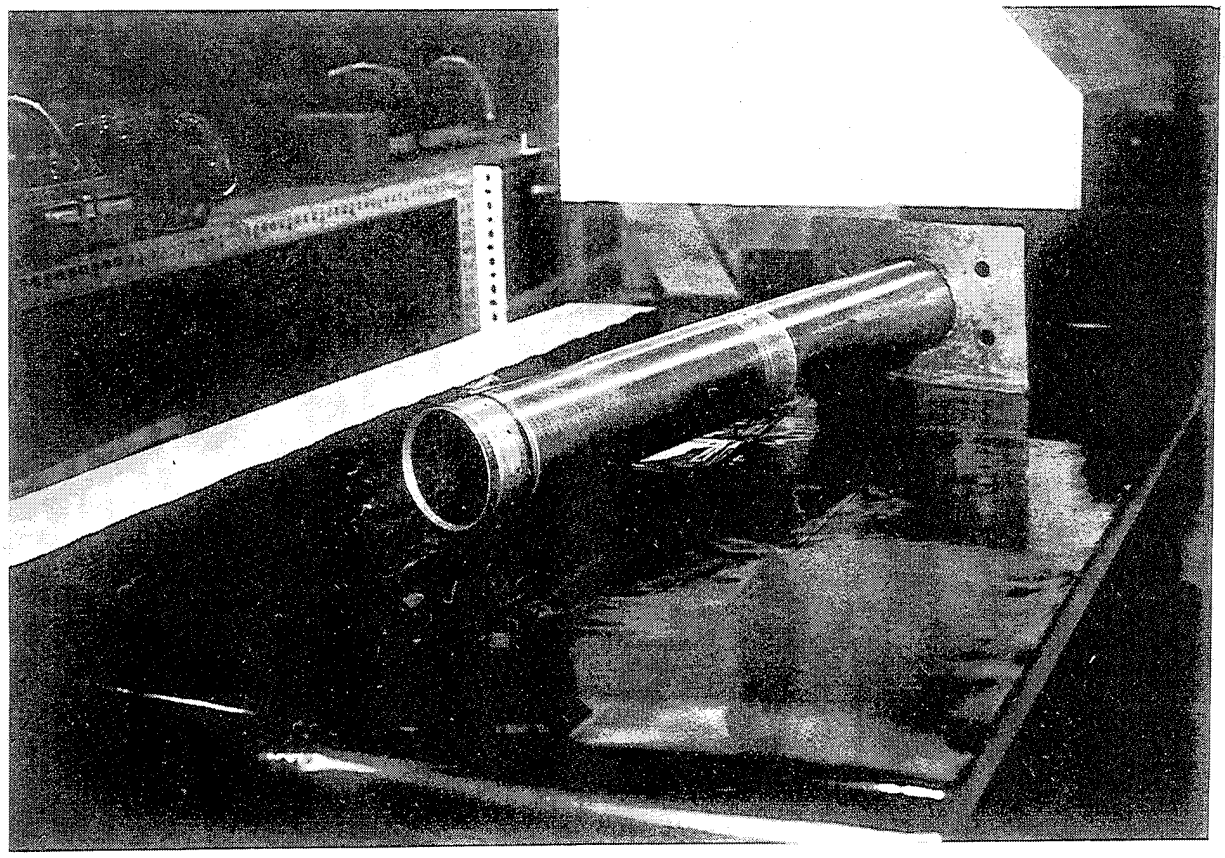

Figure 15. Photograph of 1/8-inch steel sleeve used to hold diaphragms over charge and discharge holes.

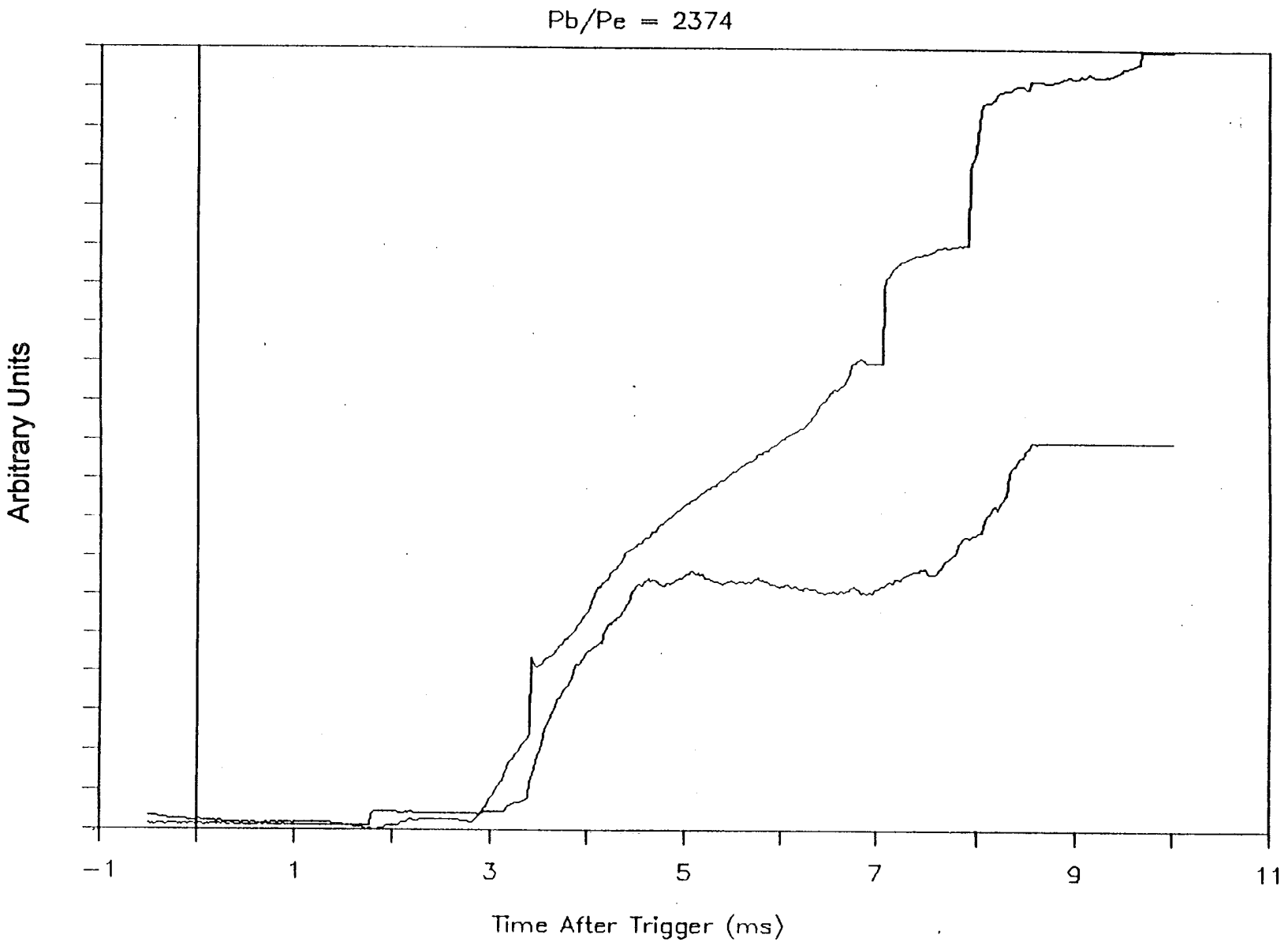

Figure 16. Output of heat transfer gauges in bore evacuator for P_b/P_e of 2300 showing presence of shock waves.

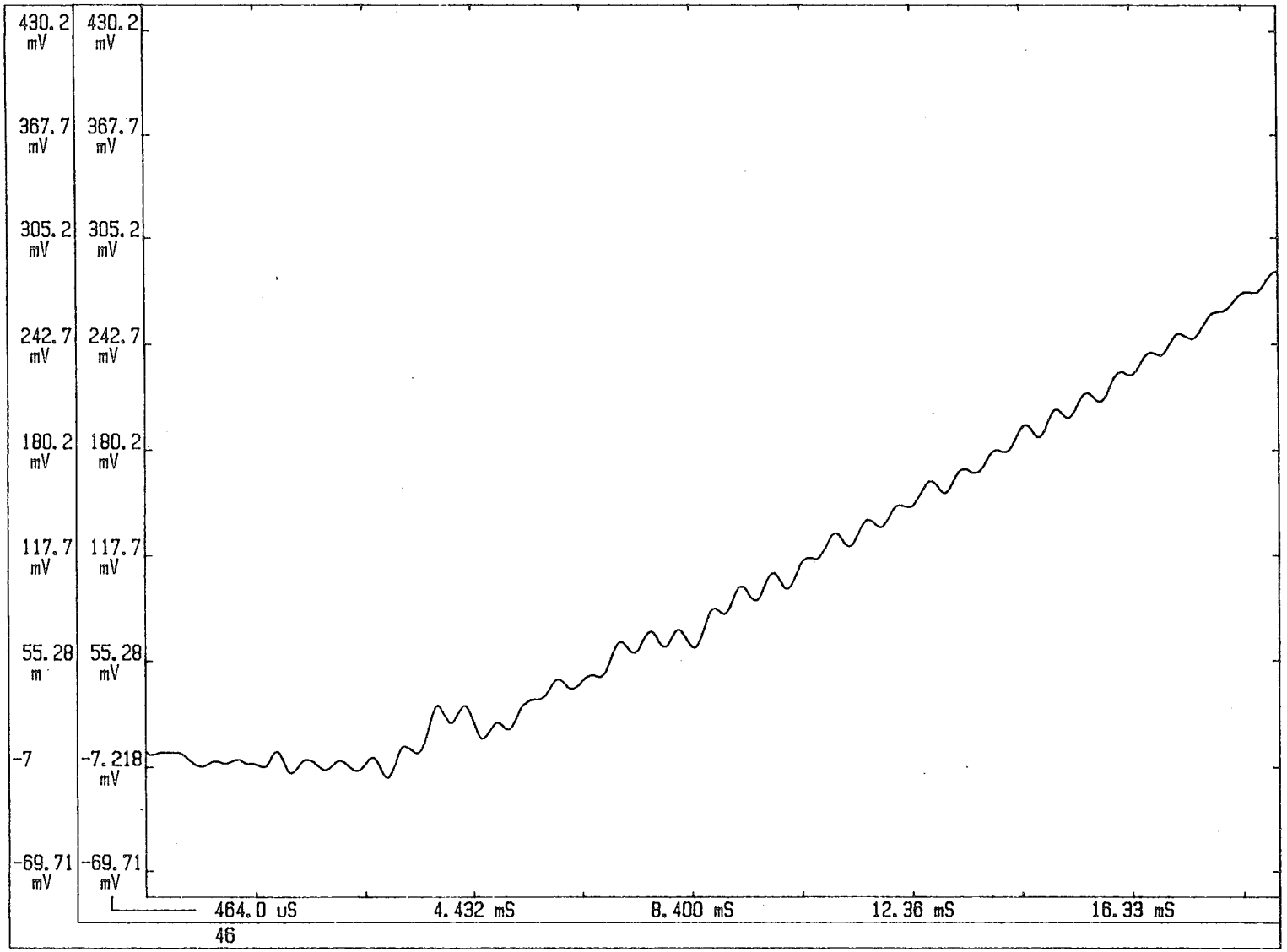

Figure 17. Typical pressure trace from PG2 during tests of the charge phase with the charge ports sealed.

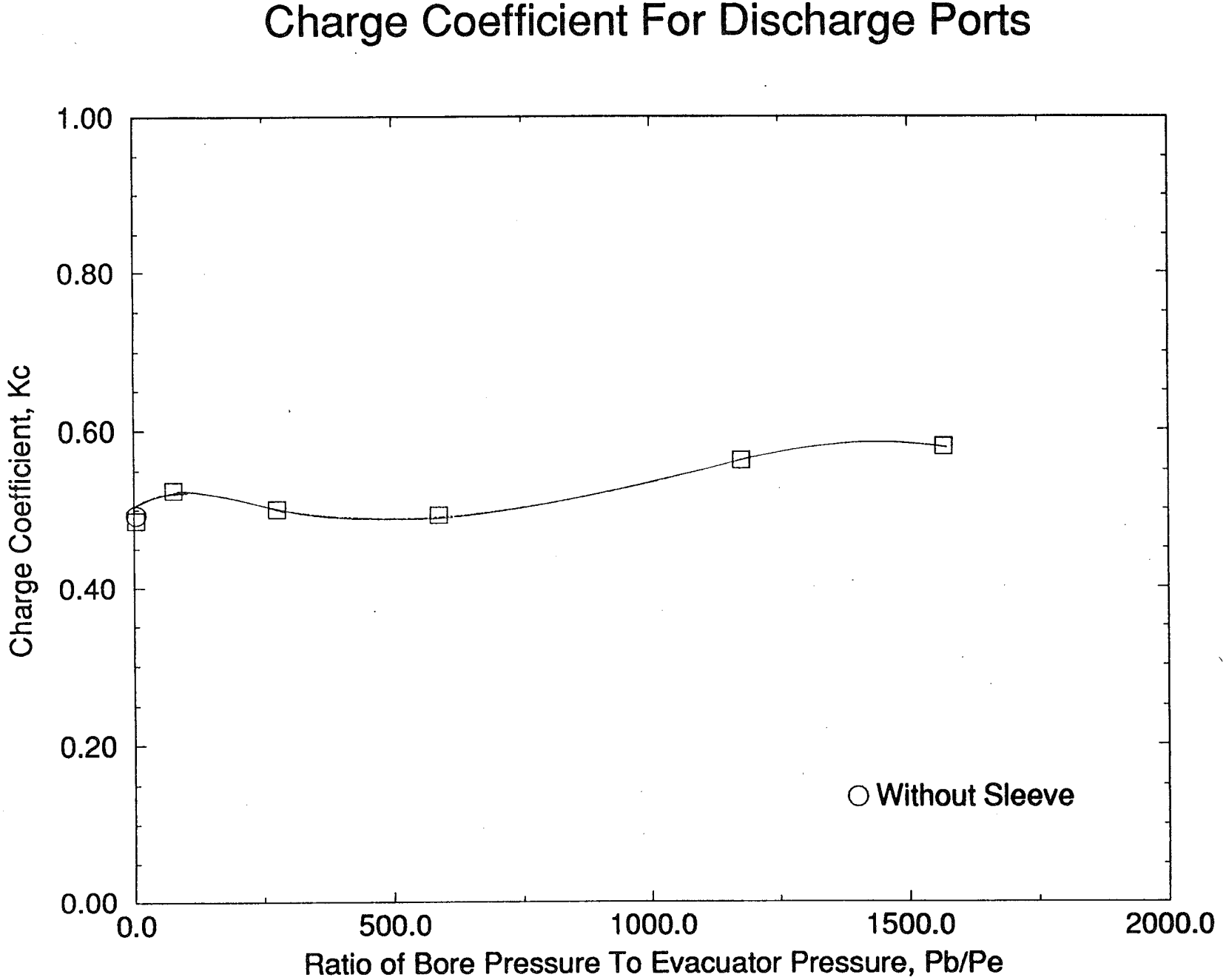

Figure 18. Variation of charge coefficient for discharge ports.

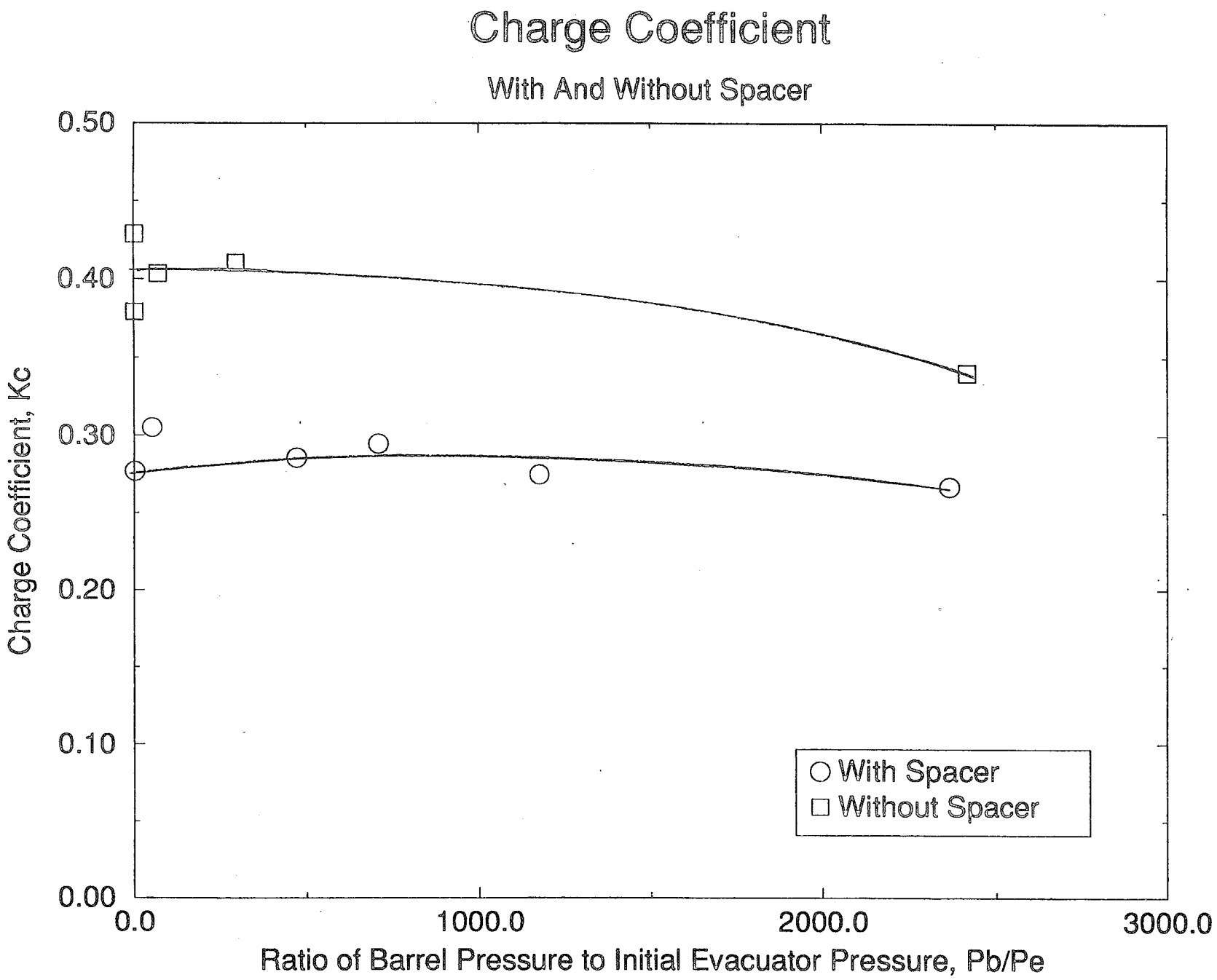

Figure 19. Variation of charge coefficient for charge ports with and without restriction.

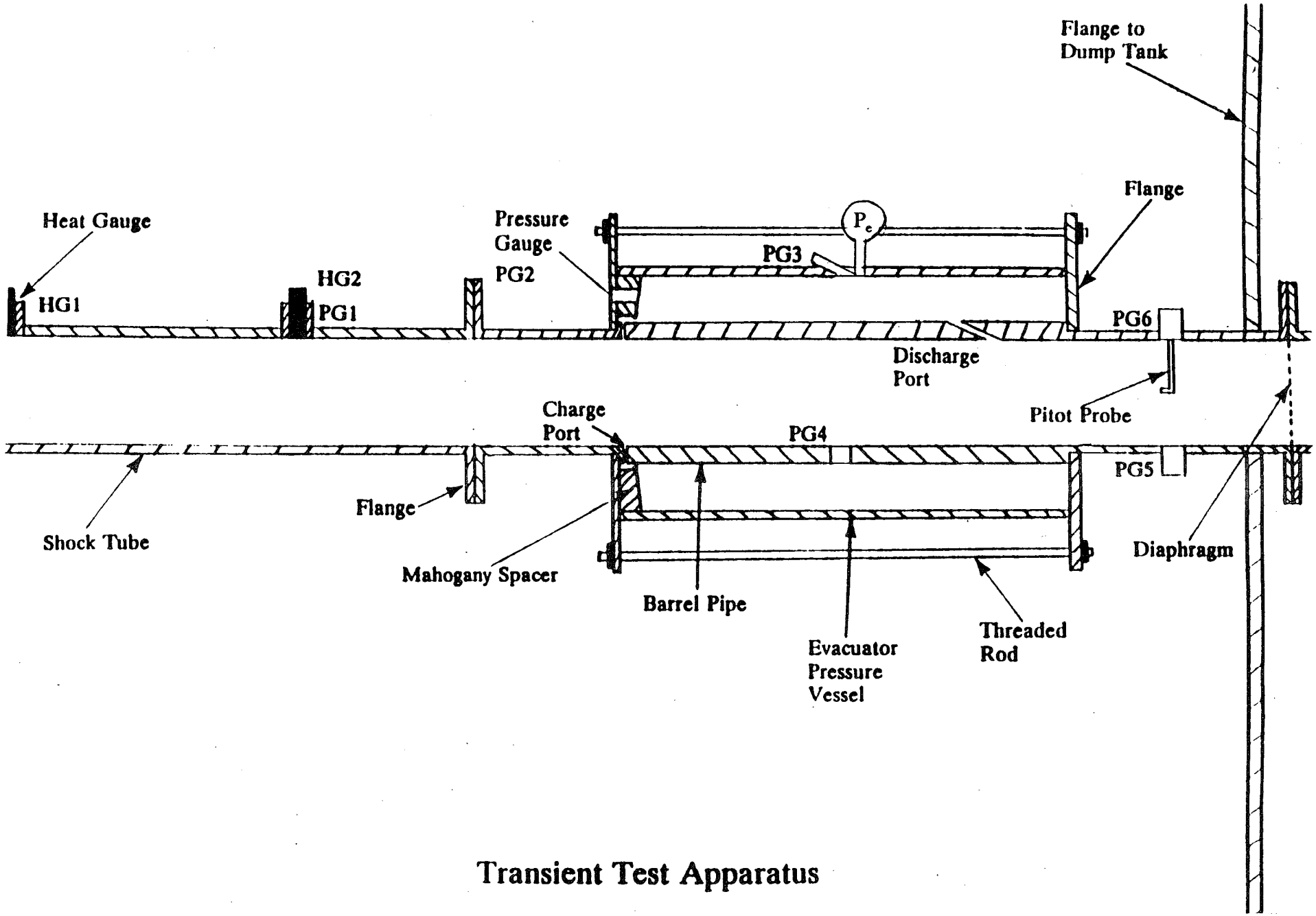

Figure 20. Schematic of the bore evacuator model configuration for the discharge phase tests.

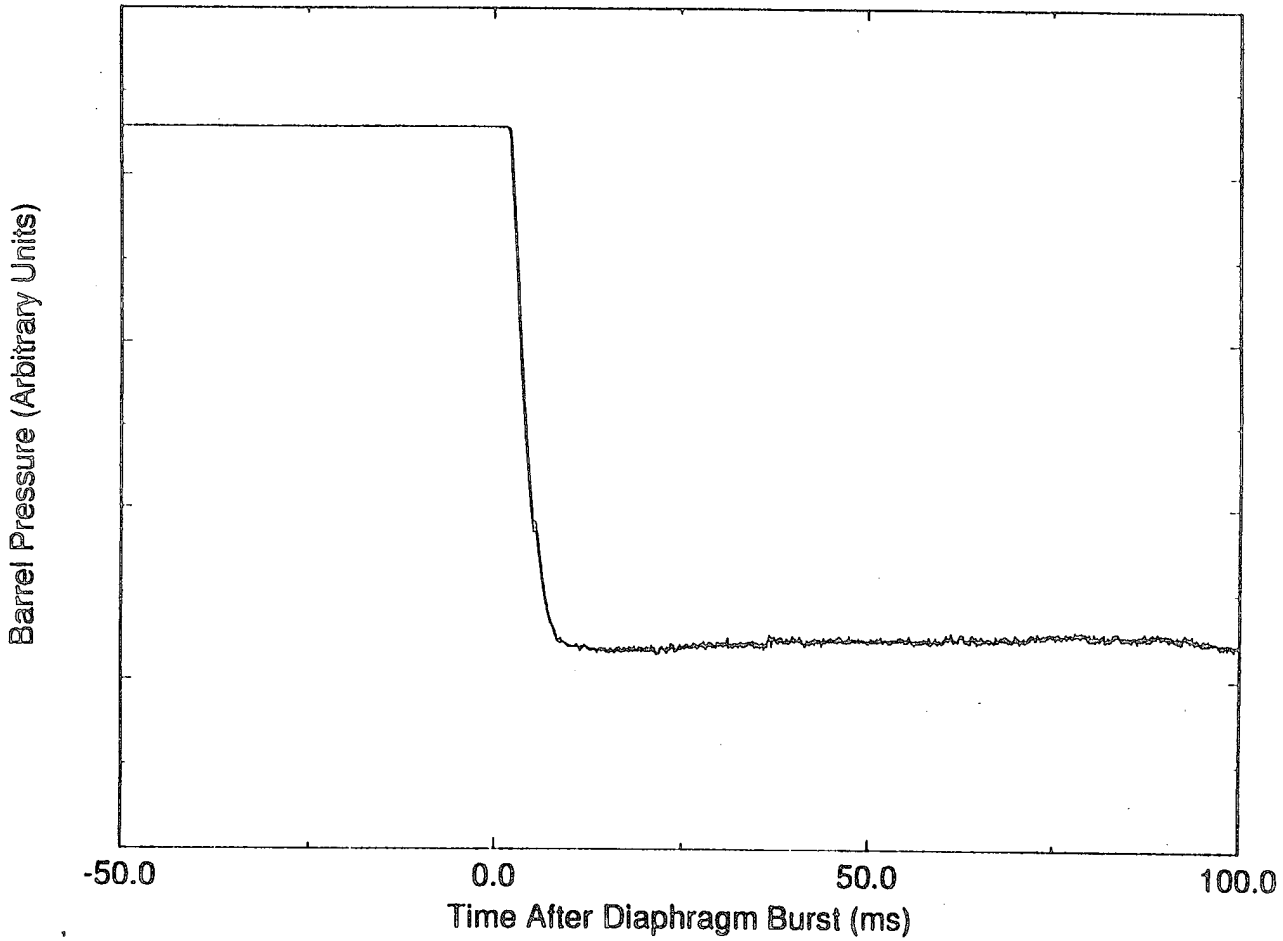

Figure 21. Typical pressure trace recorded from PG4 during the discharge phase tests showing the time history of the bore pressure.

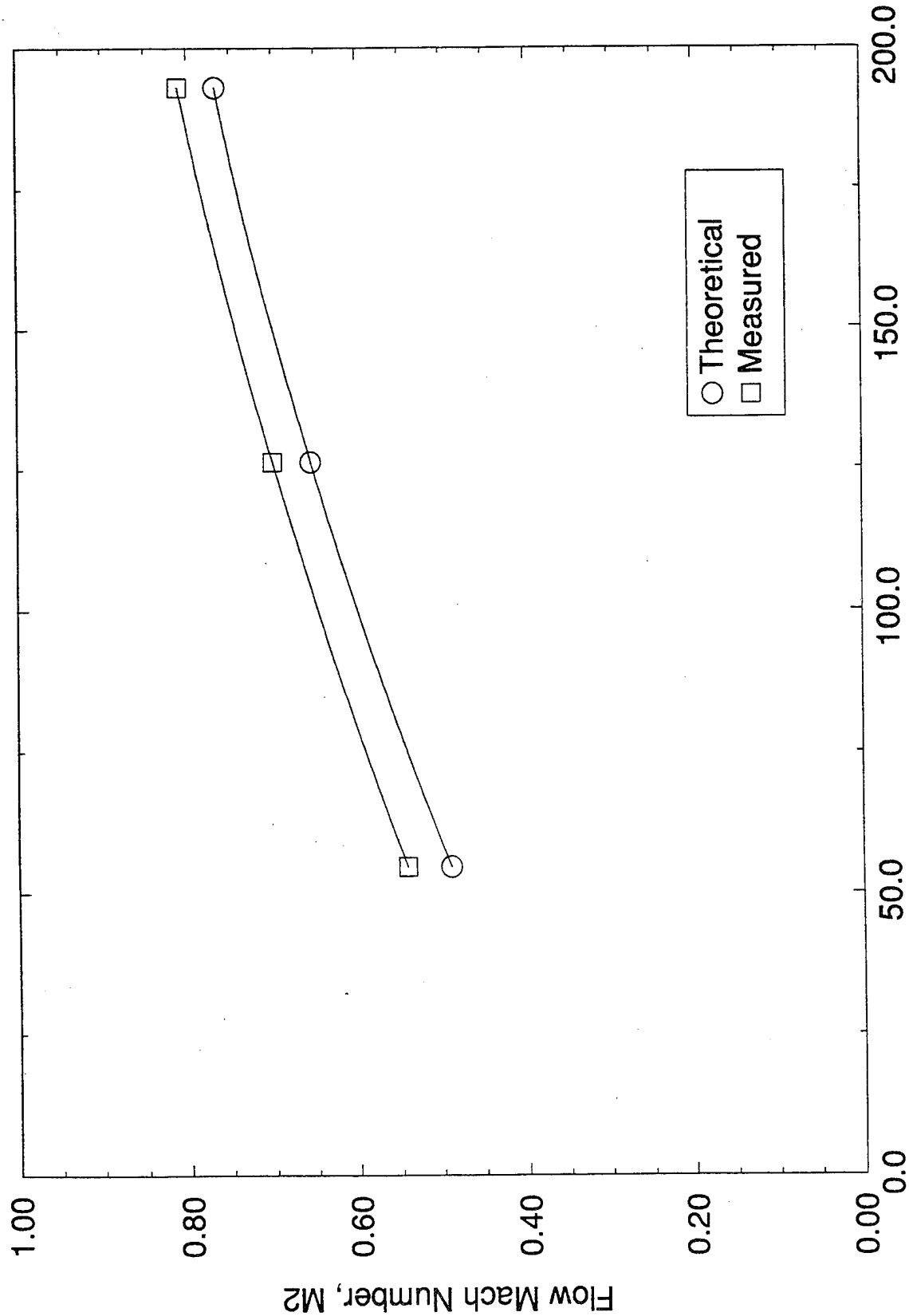

Figure 22. Center line Mach number at the muzzle during discharge tests.

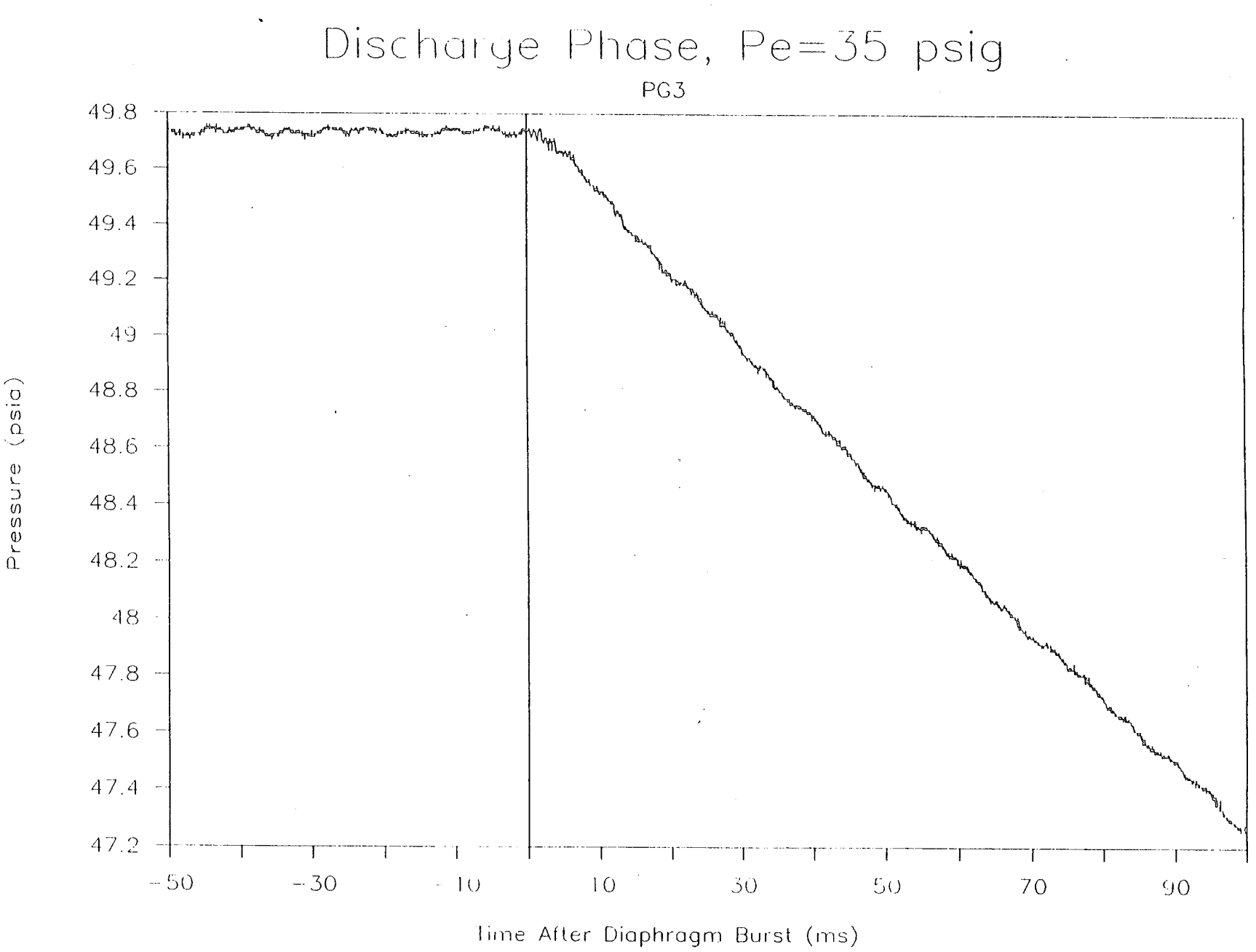

Figure 23. Typical pressure trace recorded from PG3 during the discharge phase tests showing the time history of the evacuator pressure.

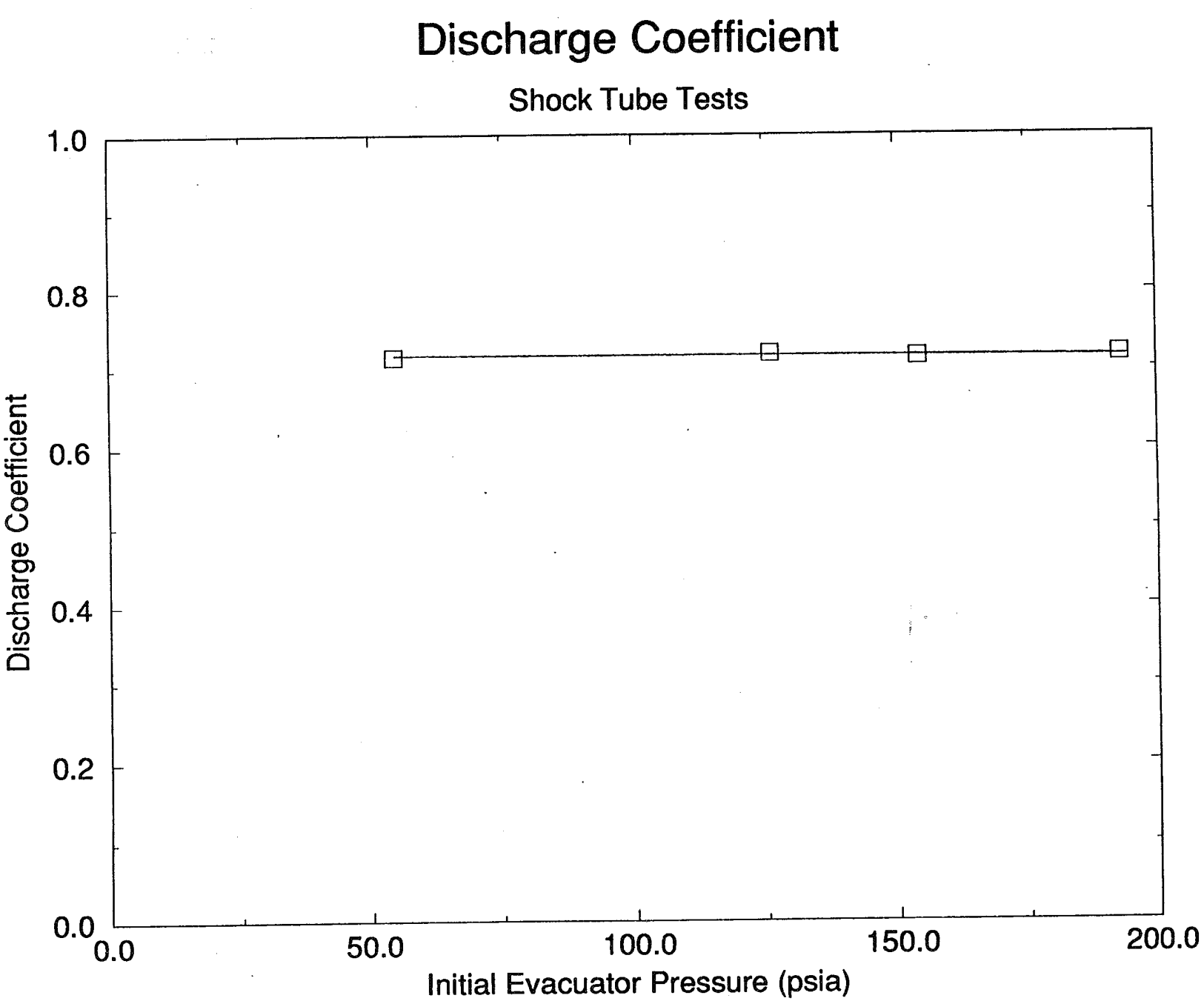

Figure 24. Variation of discharge coefficient with evacuator pressure.

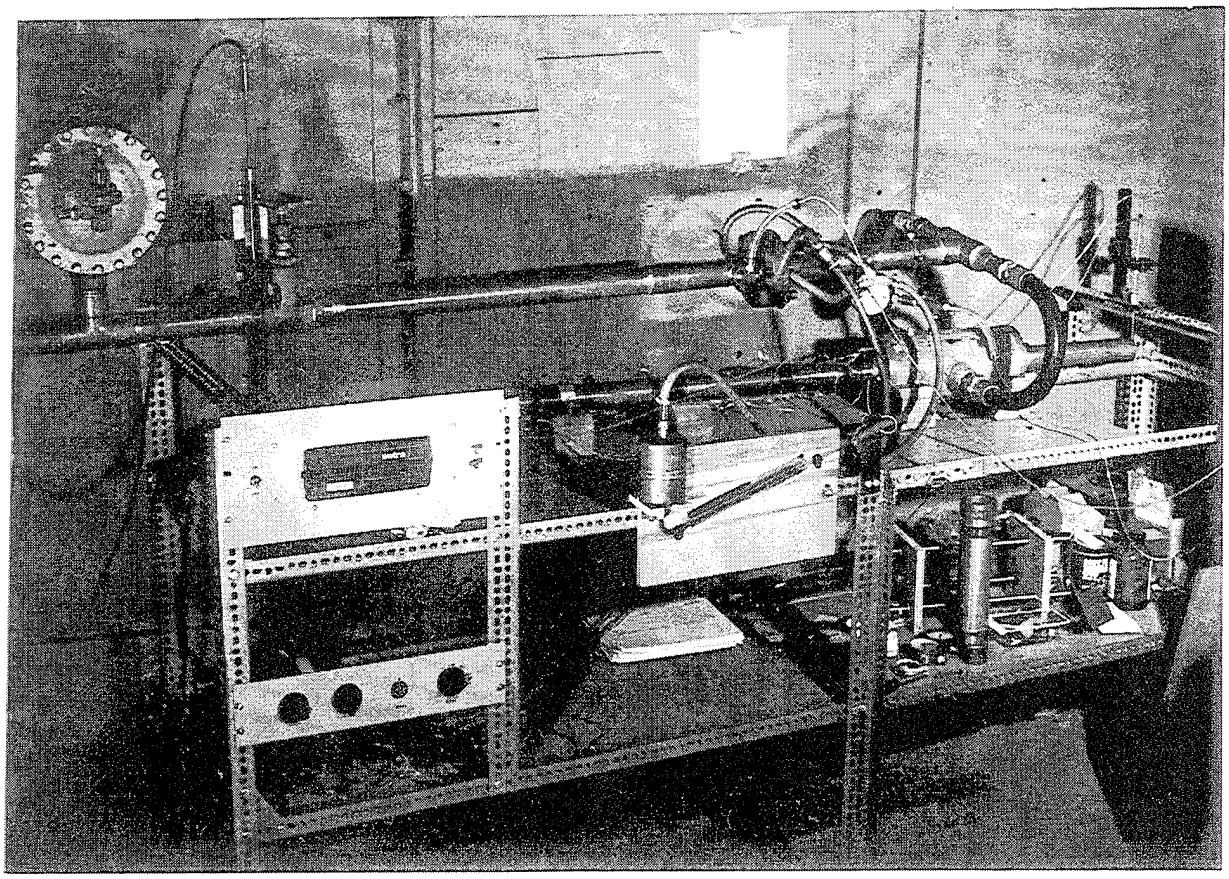

Figure 25a. Photograph of the RPI Steady-State Flow Facility showing bore evacuator model and inclined manometer.

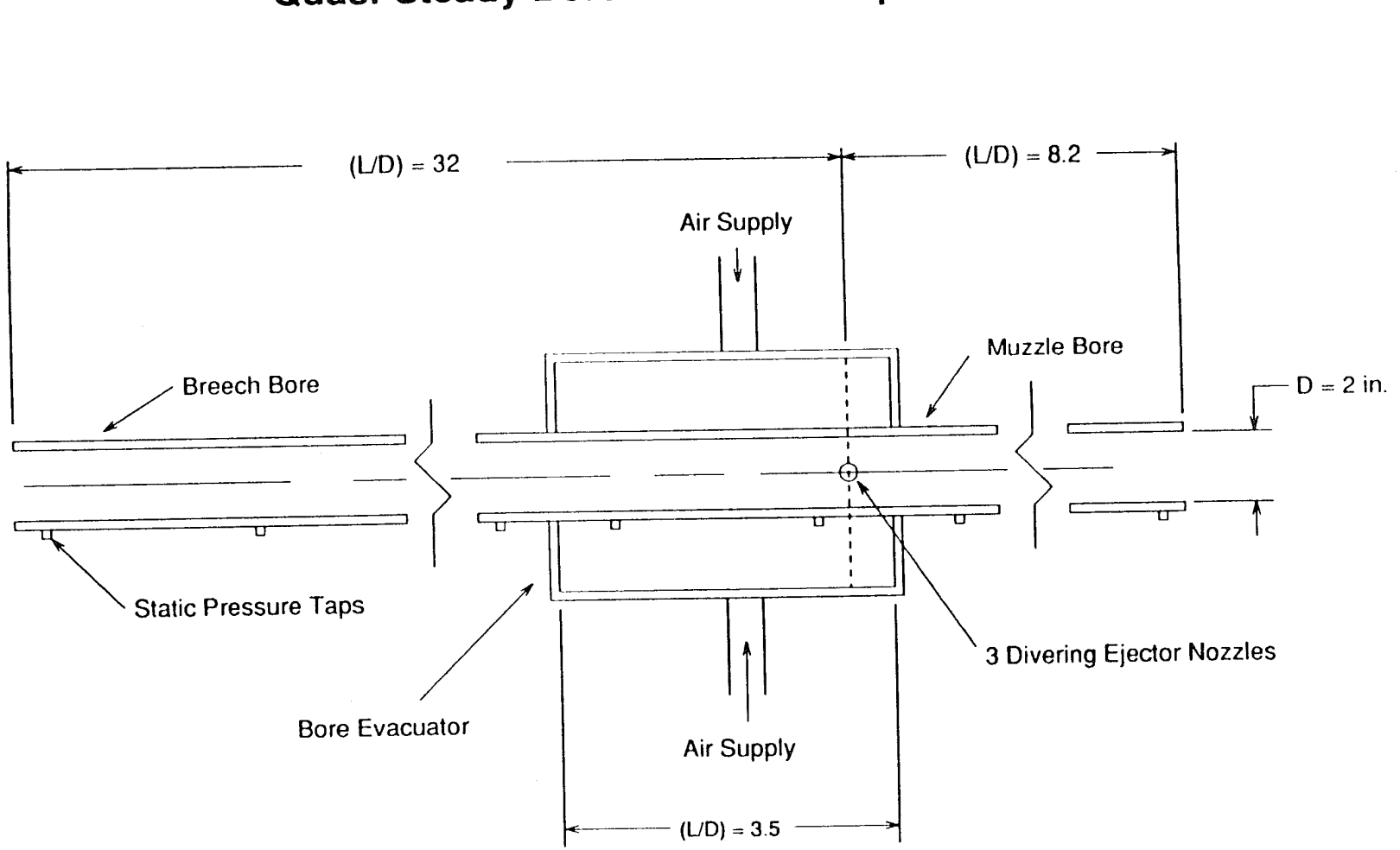

Figure 25b. Schematic of the baseline bore evacuator model configuration for the quasi-steady tests.

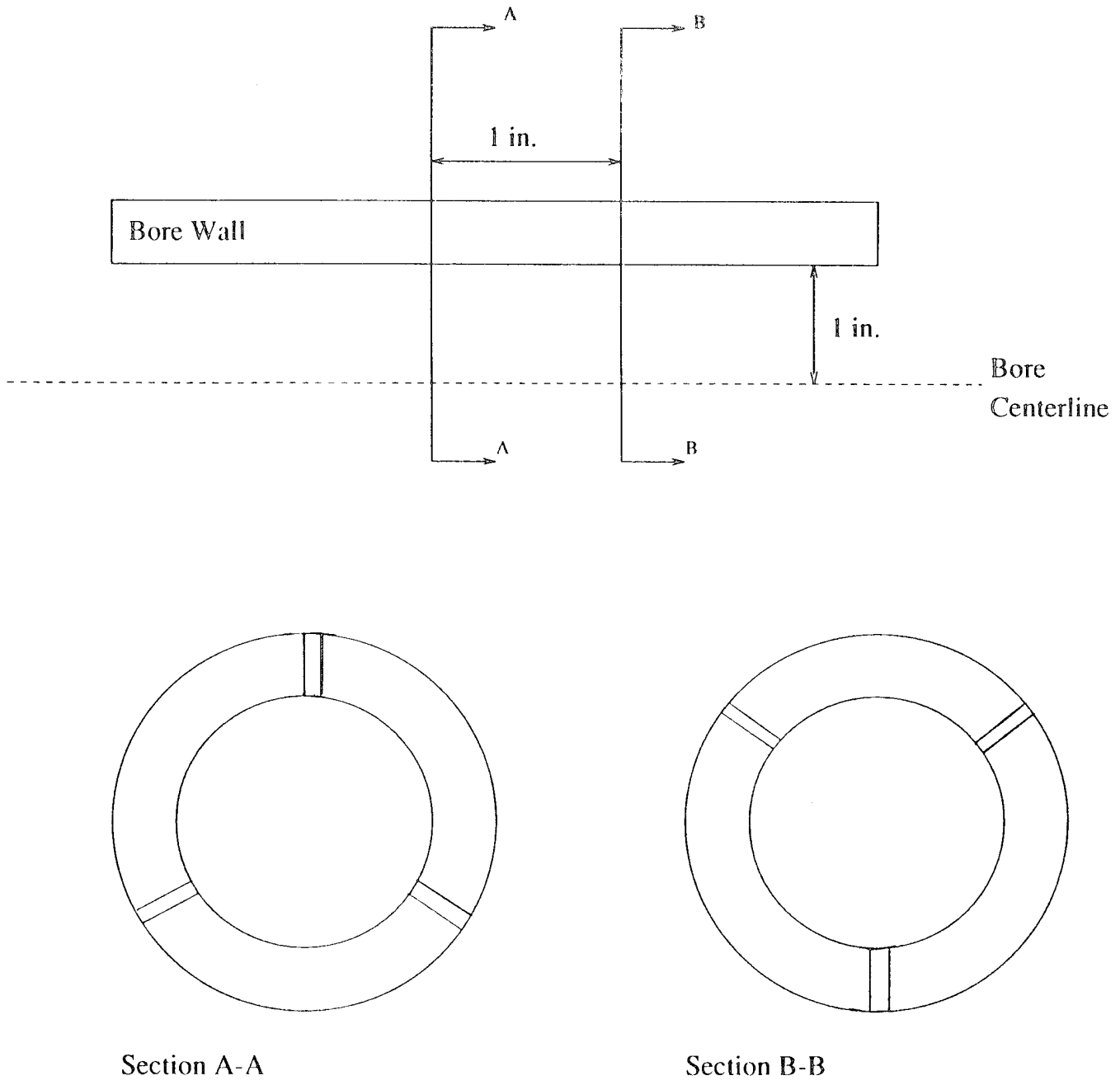

Figure 26. Schematic of the bore evacuator model with staggered discharge ports.

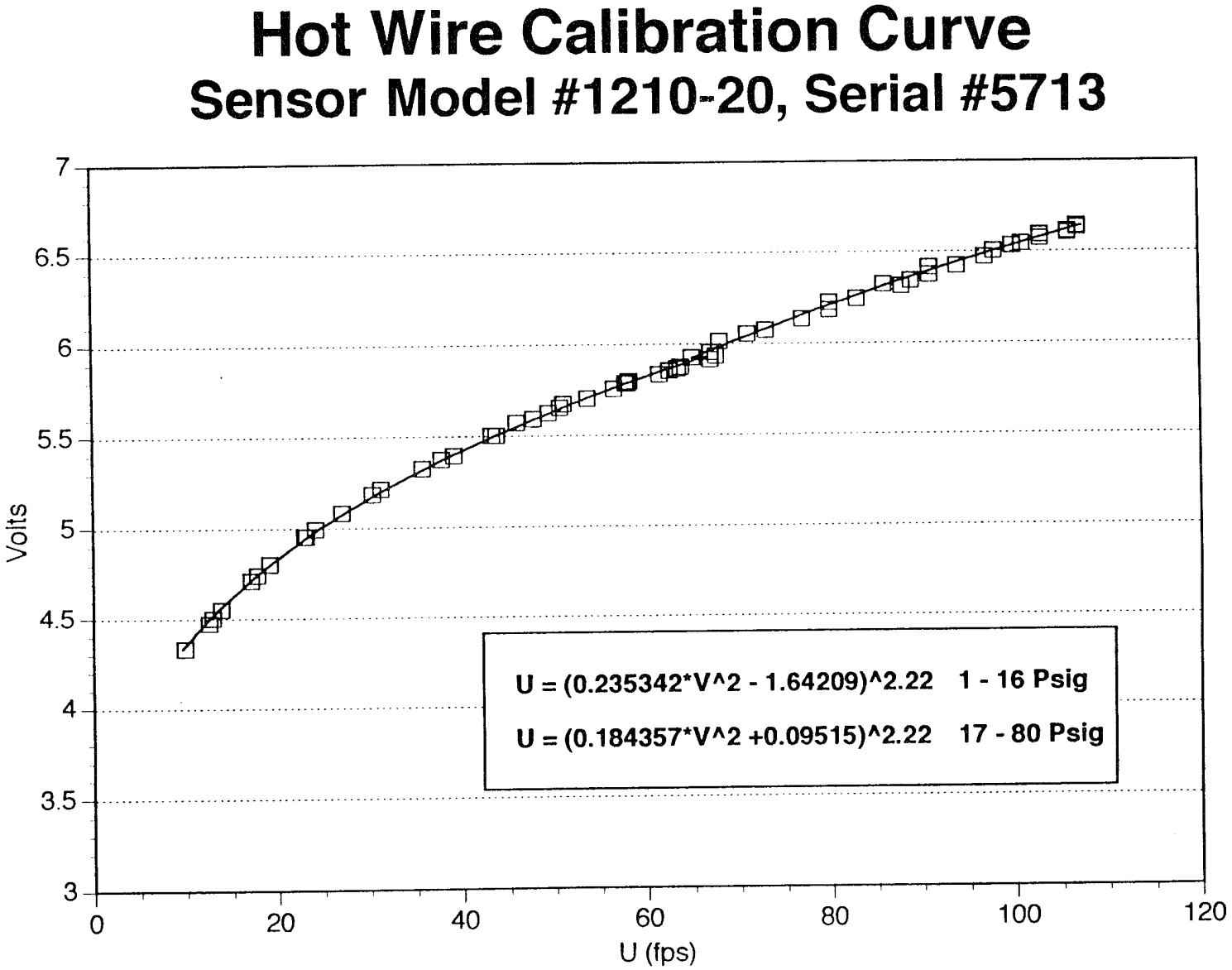

Figure 27. Typical calibration curve for hot film sensor.

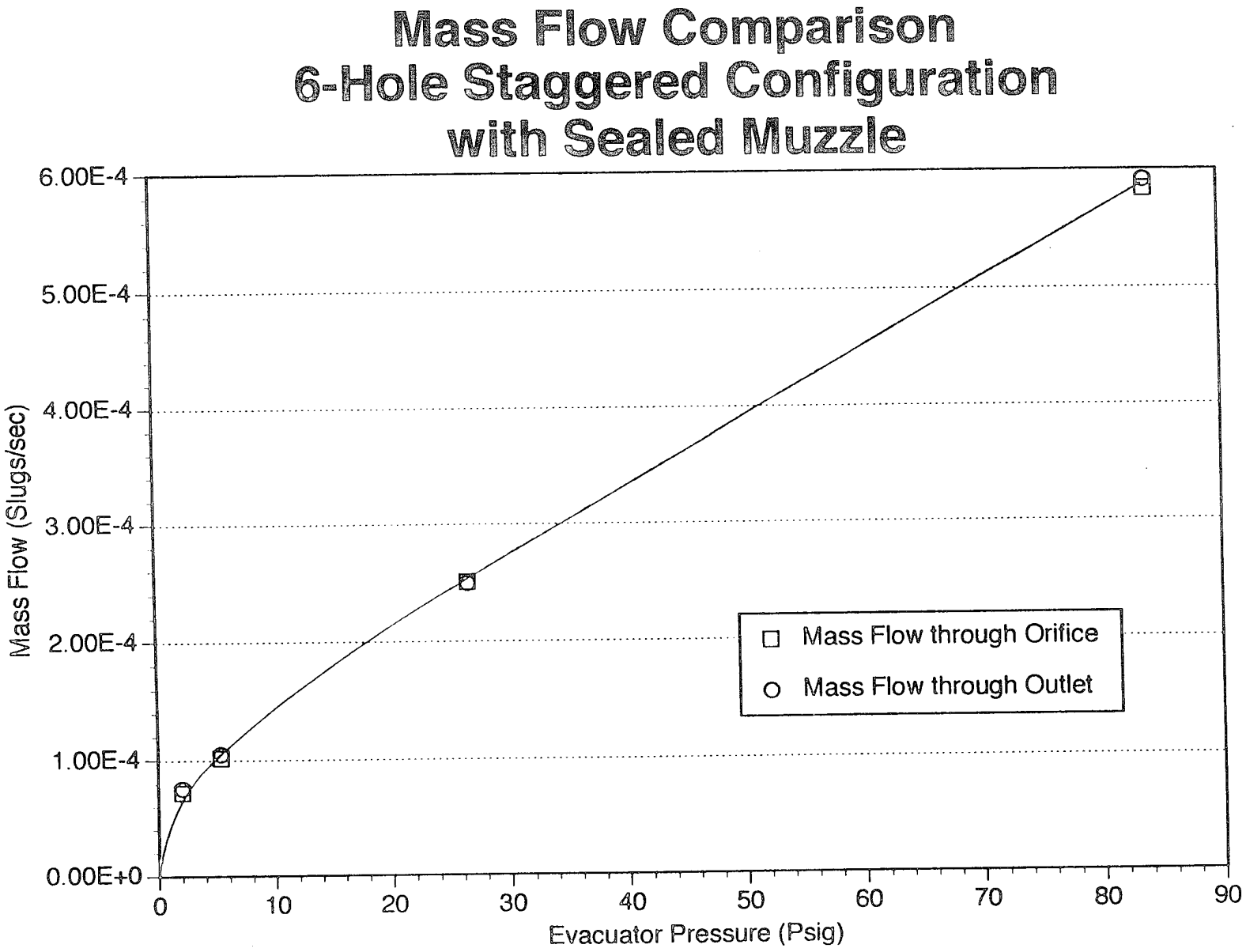

Figure 28. Comparison of the mass flow measured by the orifice meter and the mass flow calculated from integrating the breech velocity profile.

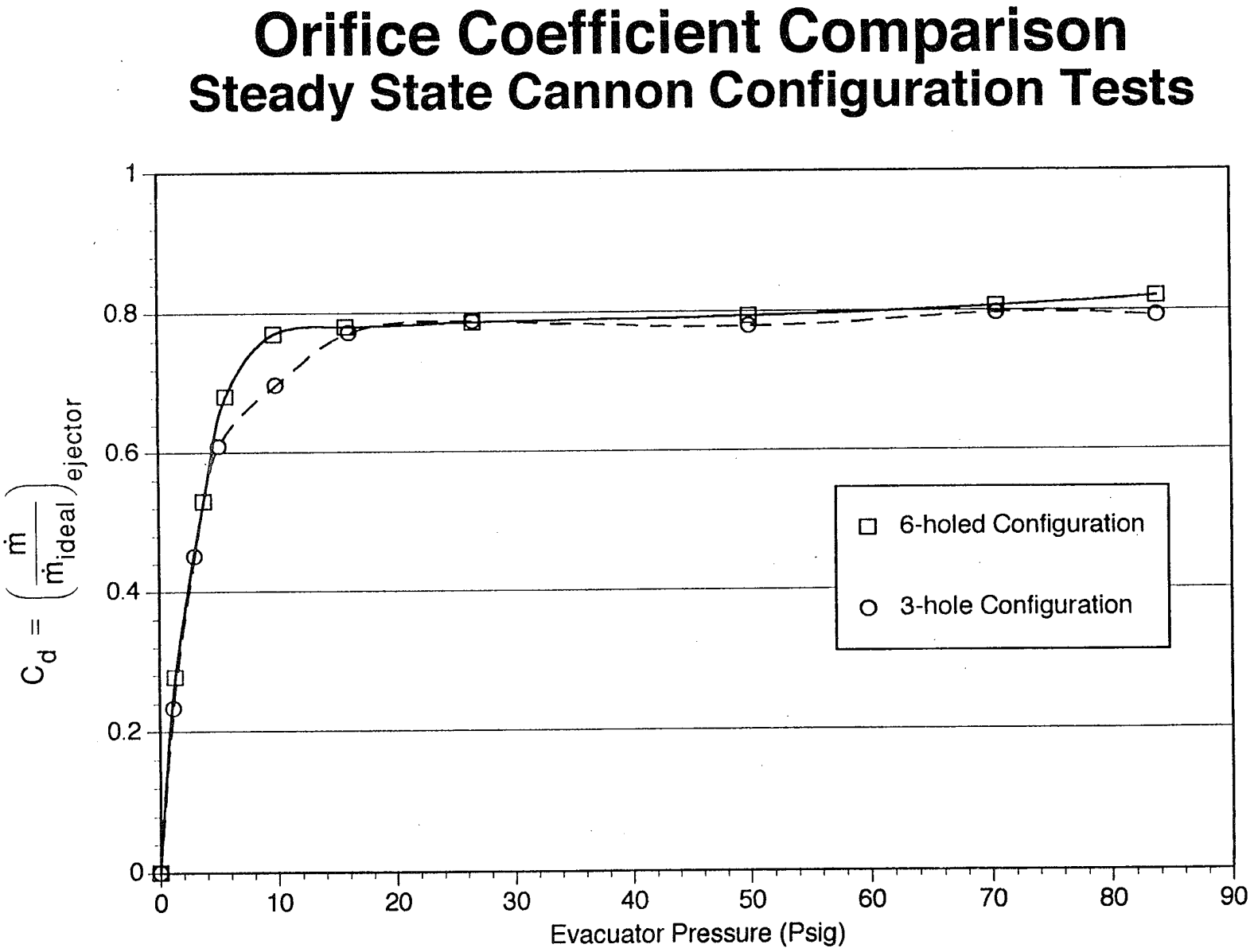

Figure 29. Orifice coefficient for baseline and staggered configurations.

Bore Pressures
Low Evacuator Pressure

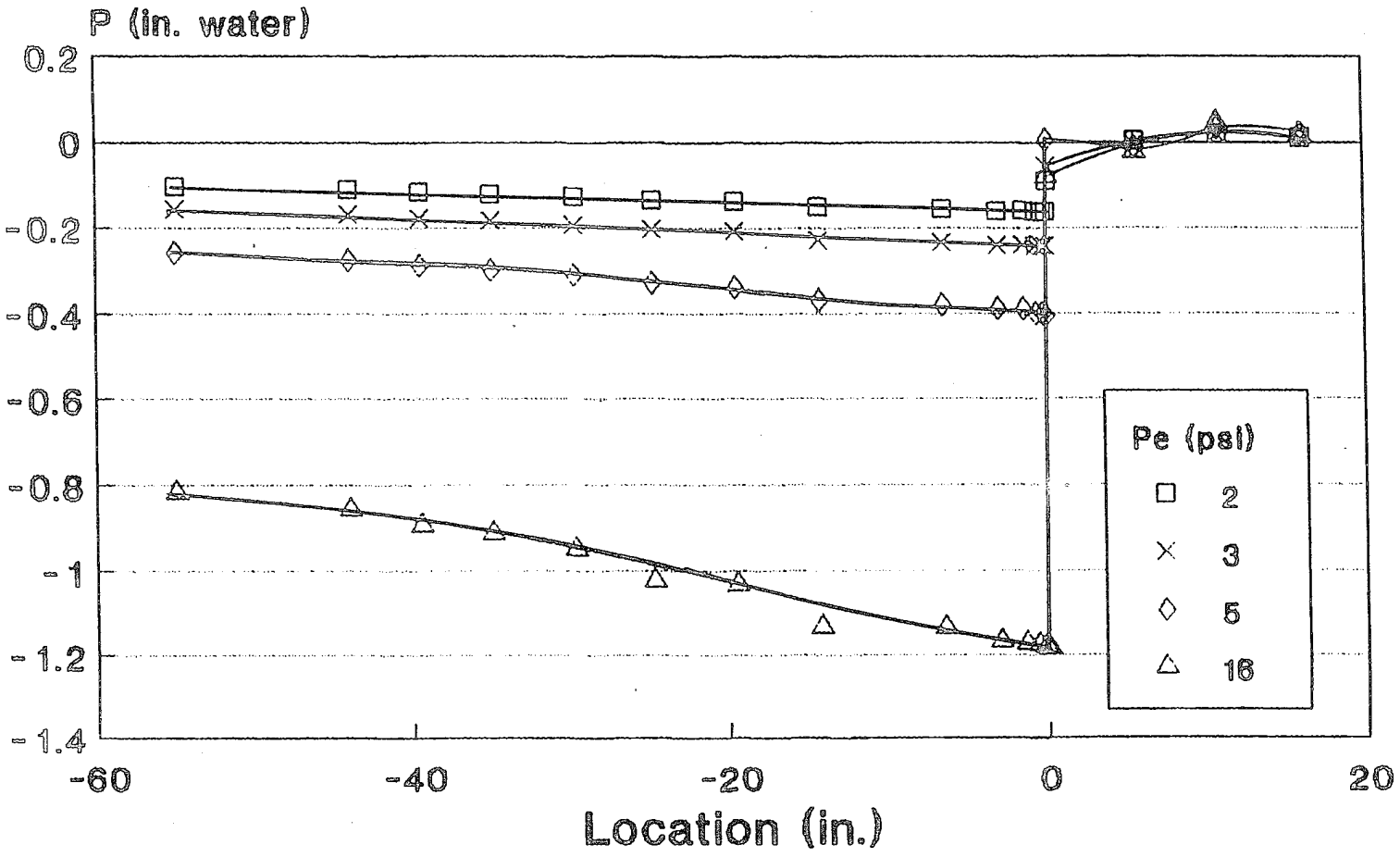

Figure 30a. Baseline barrel pressure distribution at low evacuator pressures.

Bore Pressures
High Evacuator Pressure

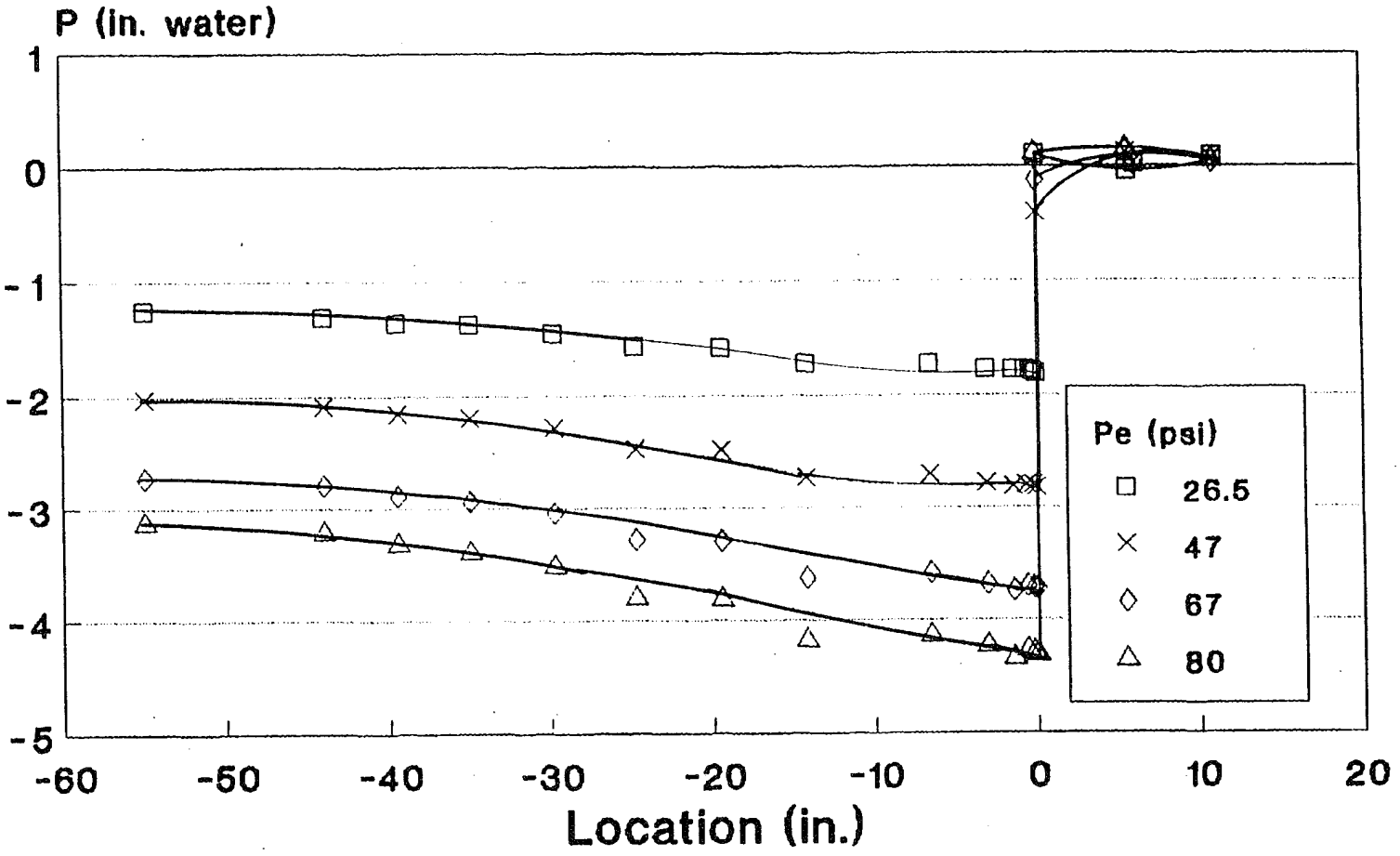

Figure 30b. Baseline barrel pressure distribution at high evacuator pressures.

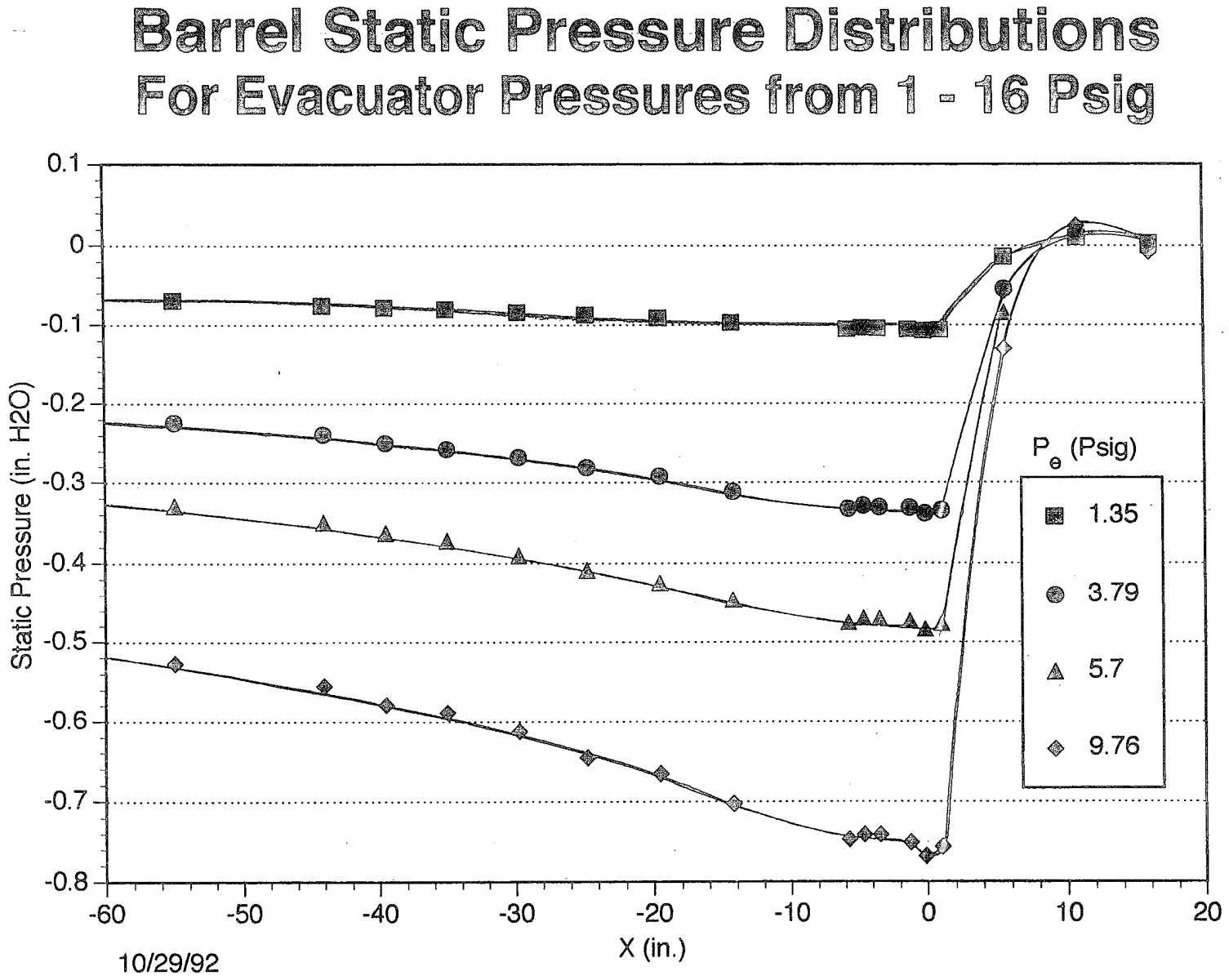

Figure 30c. Barrel pressure distribution for staggered configuration at low evacuator pressures.

Barrel Static Pressure Distributions
For Evacuator Pressures from 26 - 84 Psig

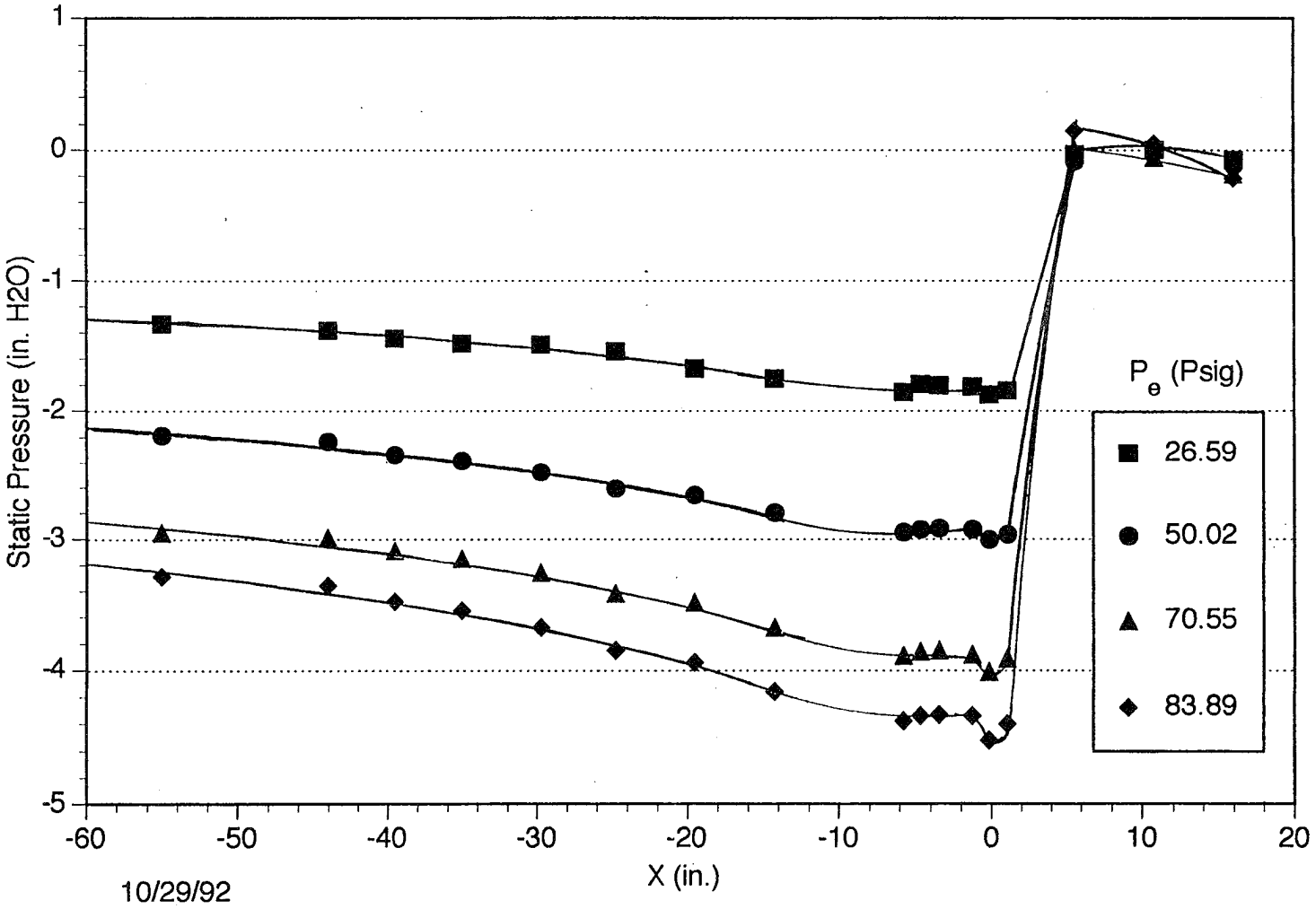

Figure 30d. Barrel pressure distribution for staggered configuration at high evacuator pressures.

Breech Velocity Profiles
Steady State Cannon Configuration

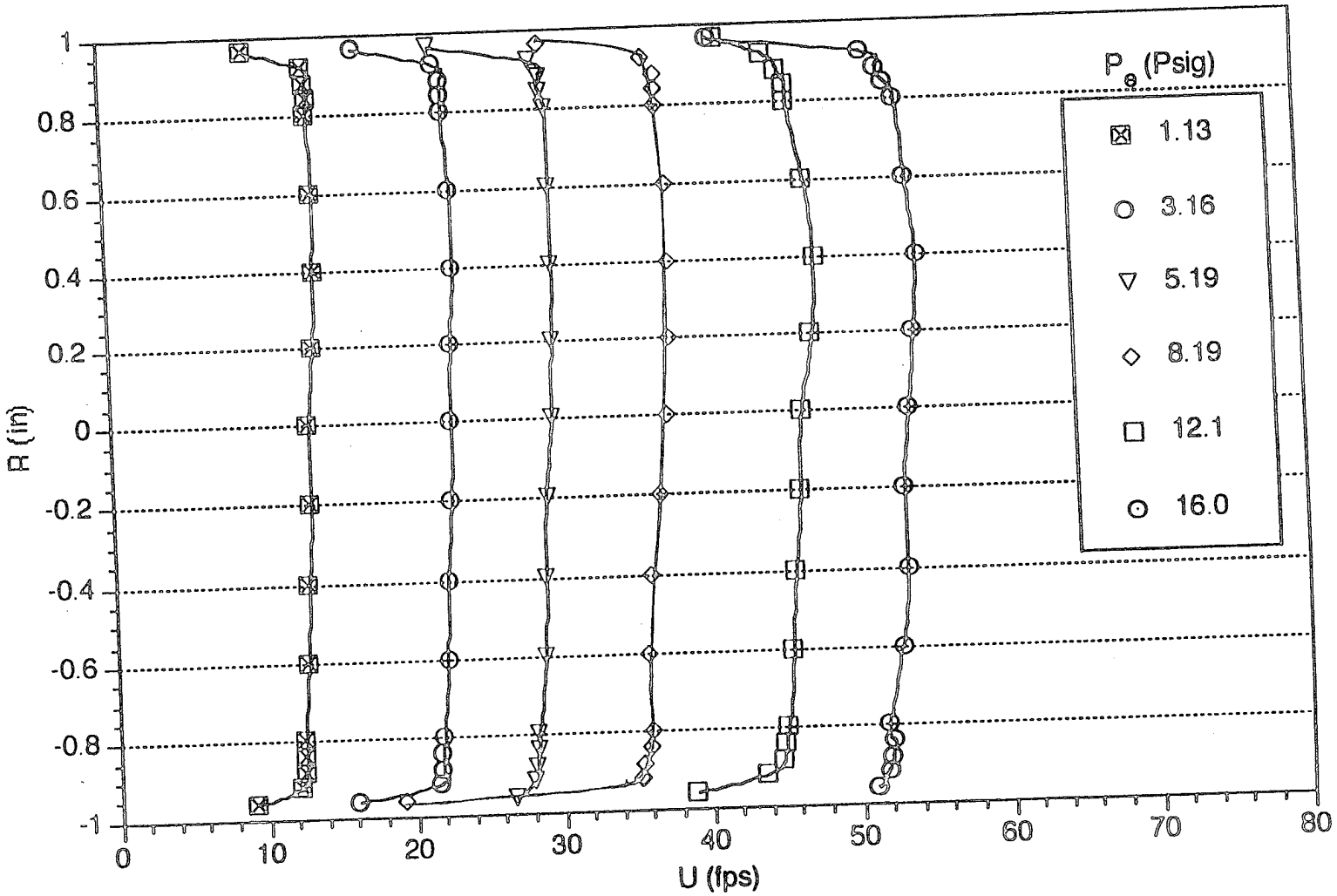

Figure 31a. Baseline breech velocity distribution at low evacuator pressures.

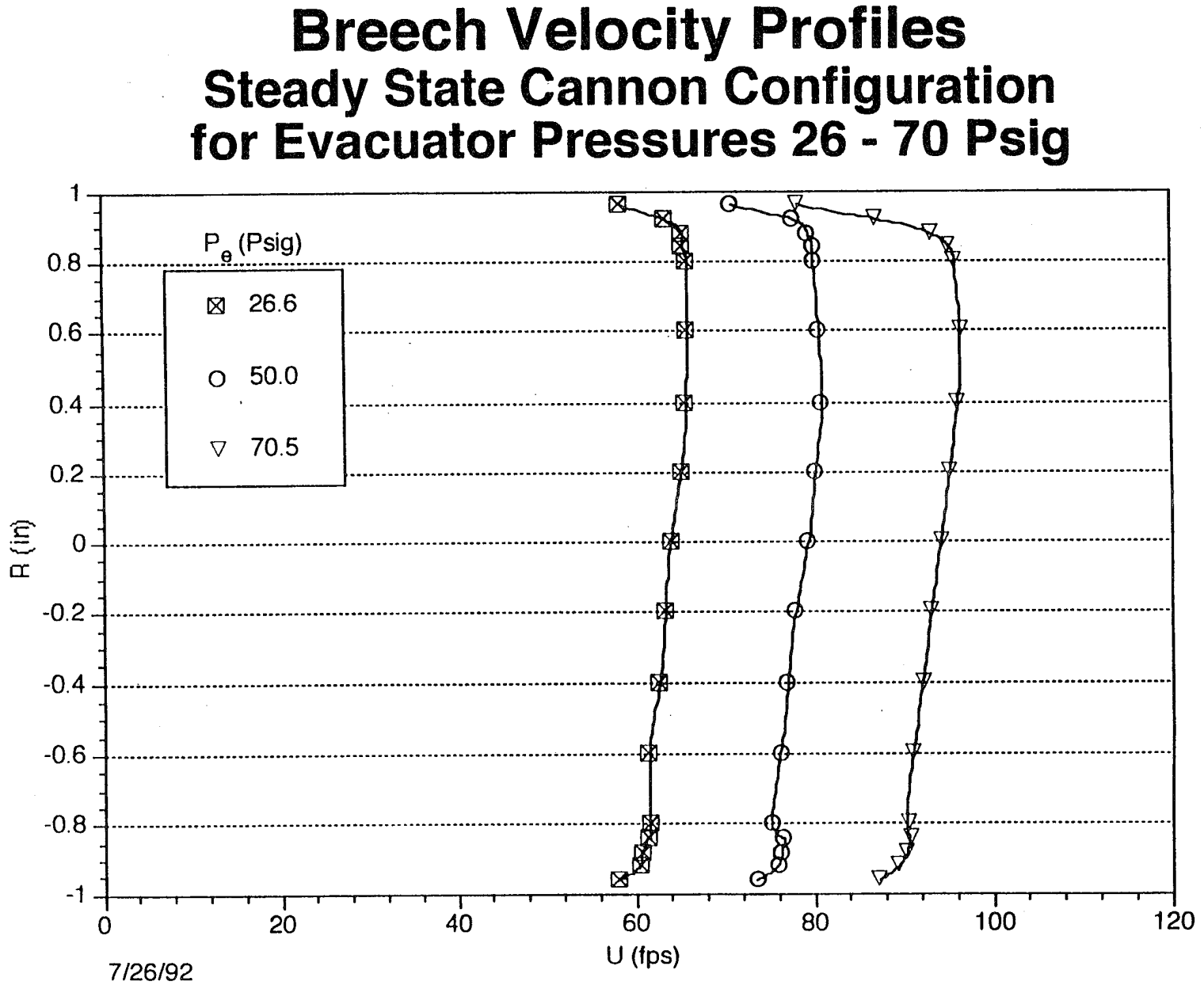

Figure 31b. Baseline breech velocity distribution at high evacuator pressures.

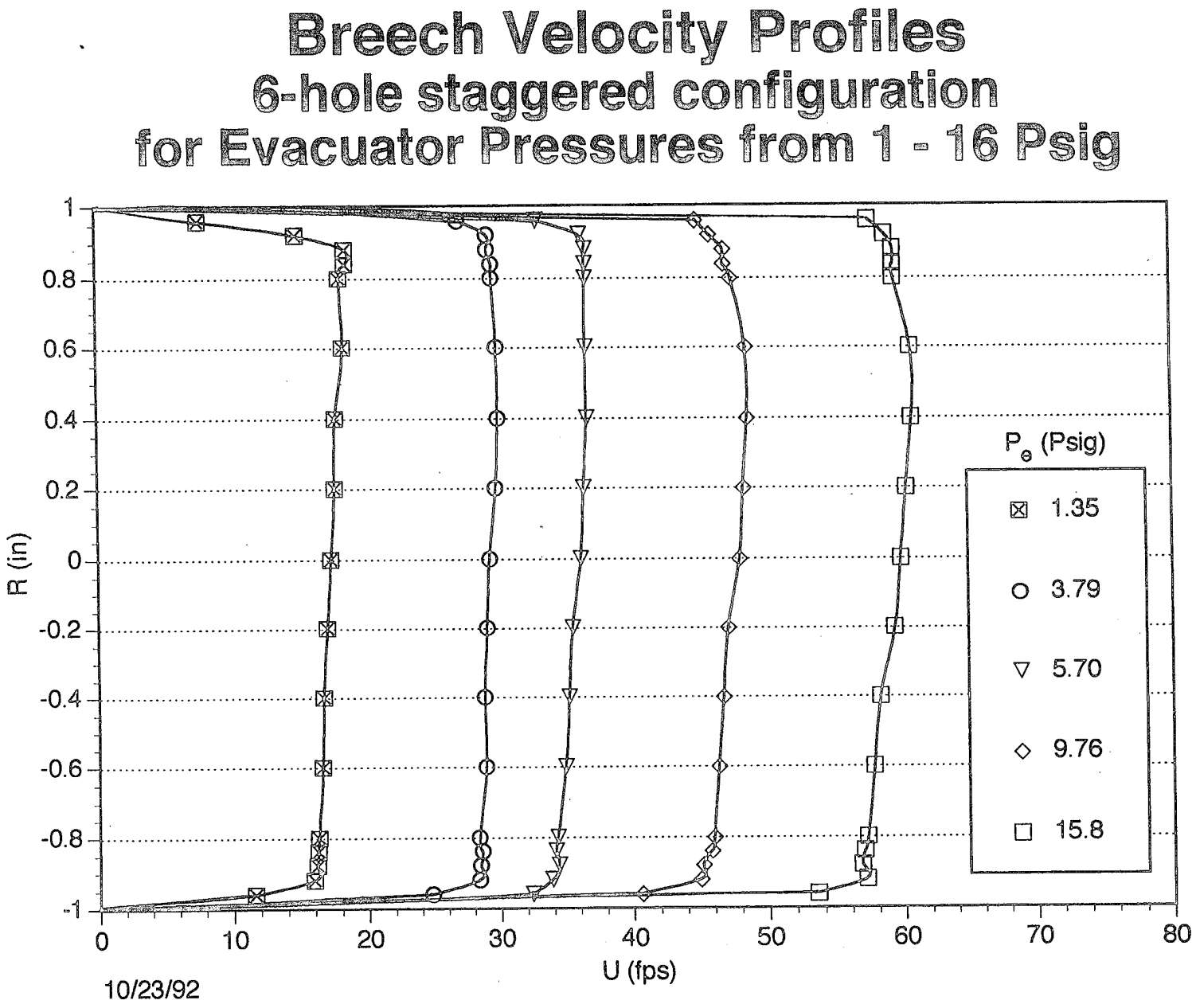

Figure 31c. Breech velocity distribution for staggered configuration at low evacuator pressures.

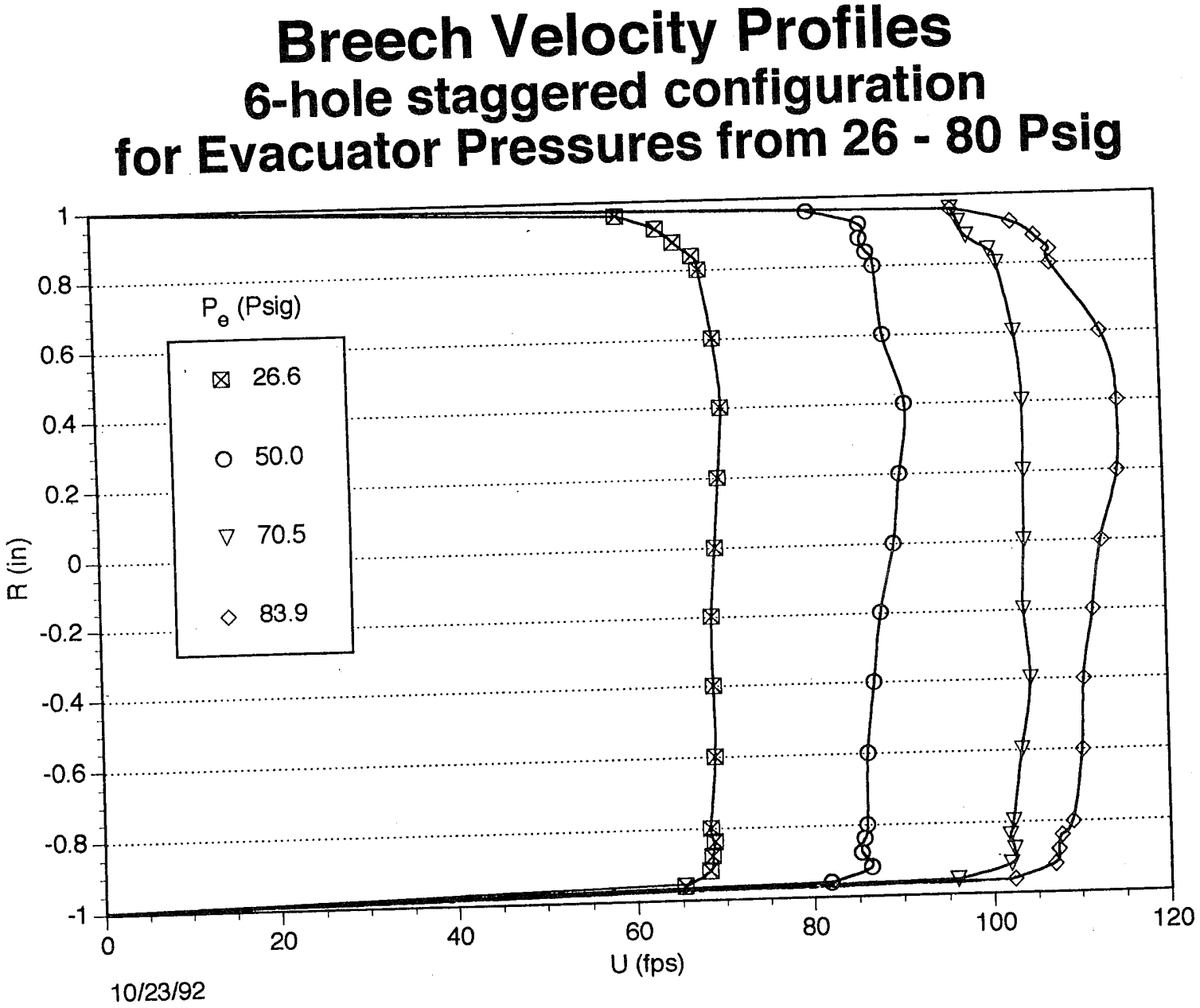

Figure 31d. Breech velocity distribution for staggered configuration at high evacuator pressures.

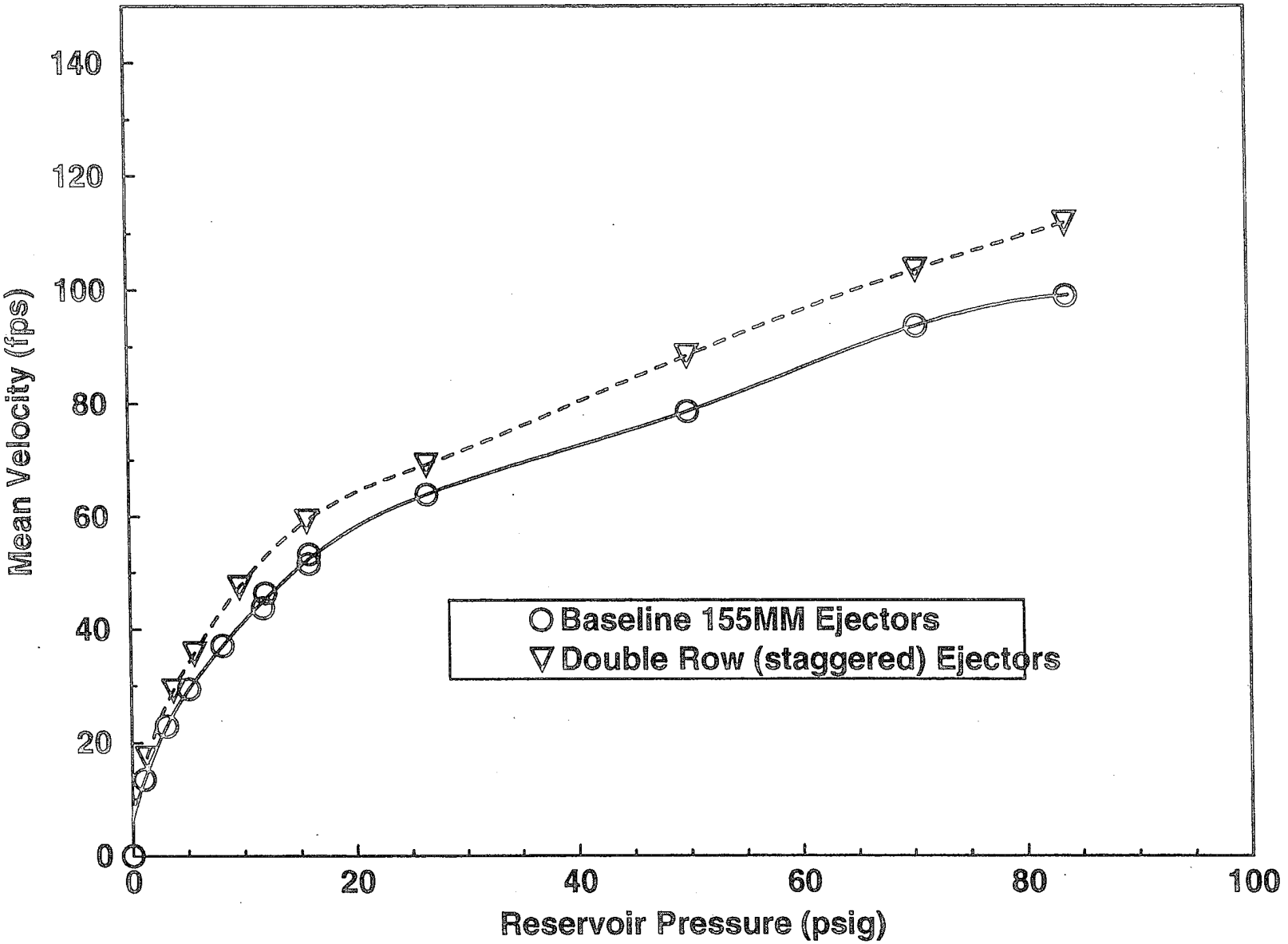

Figure 32. Mean breech velocities for baseline and staggered configurations.

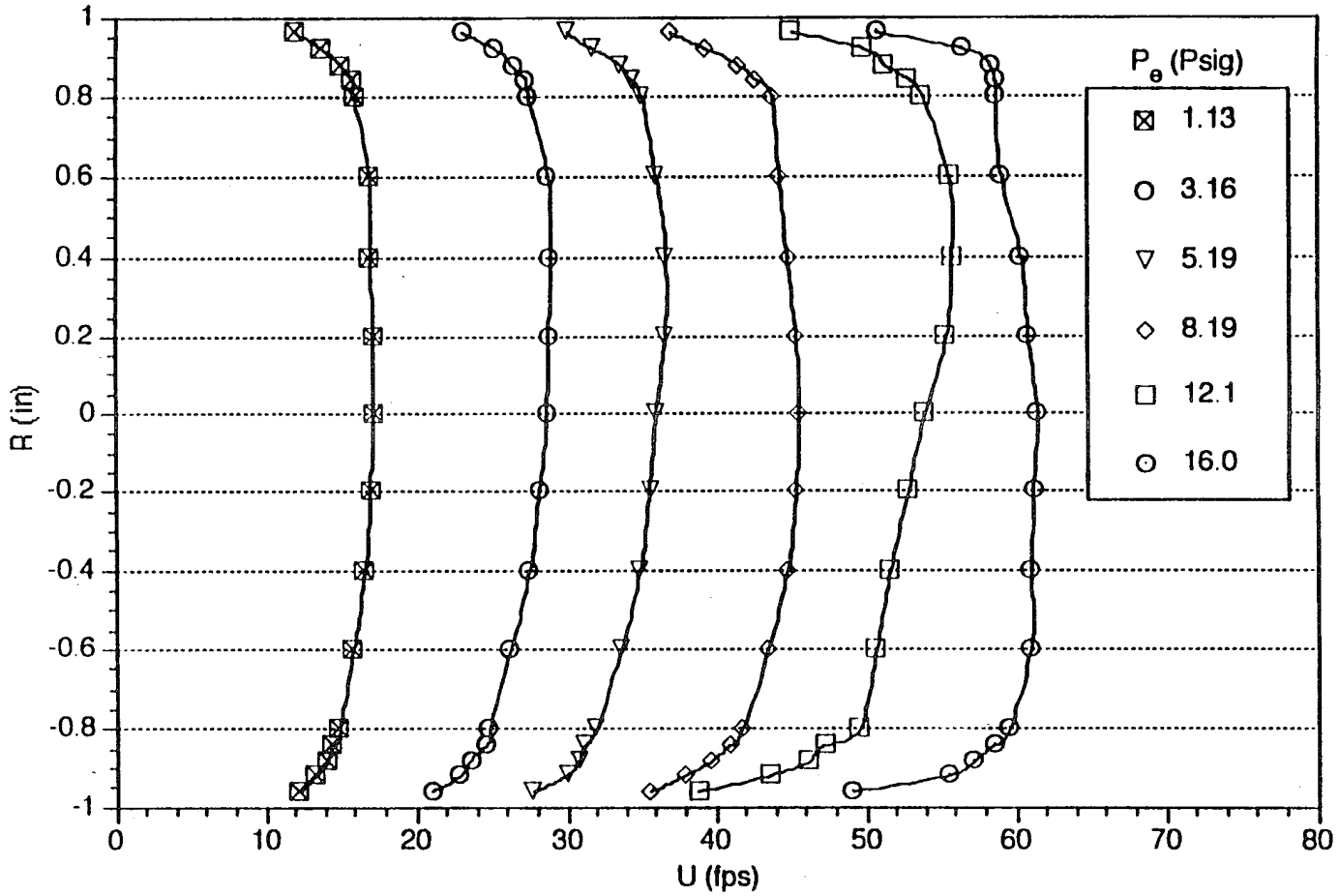

Figure 33a. Baseline muzzle velocity distribution at low evacuator pressures.

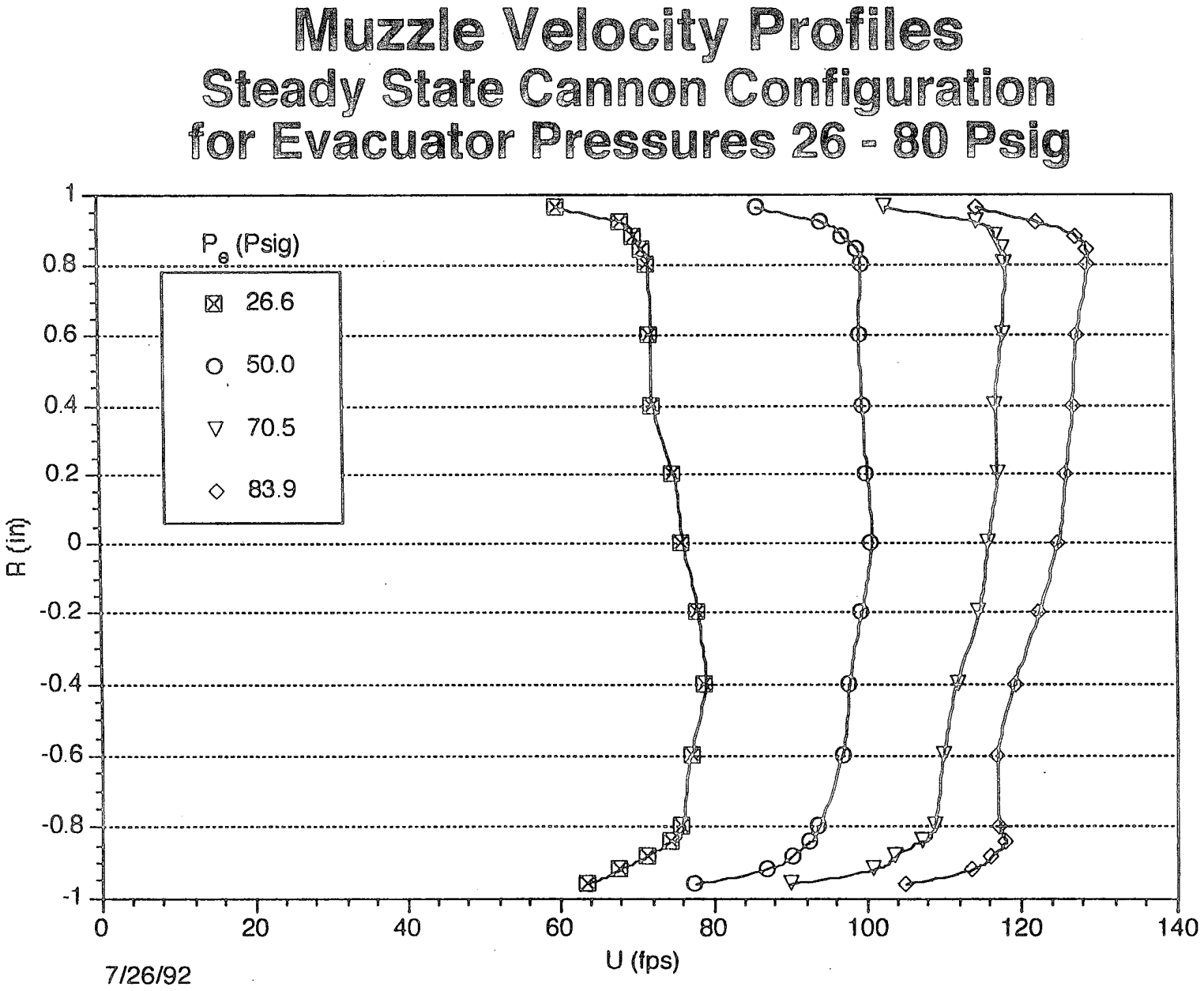

Figure 33b. Baseline muzzle velocity distribution at high evacuator pressures.

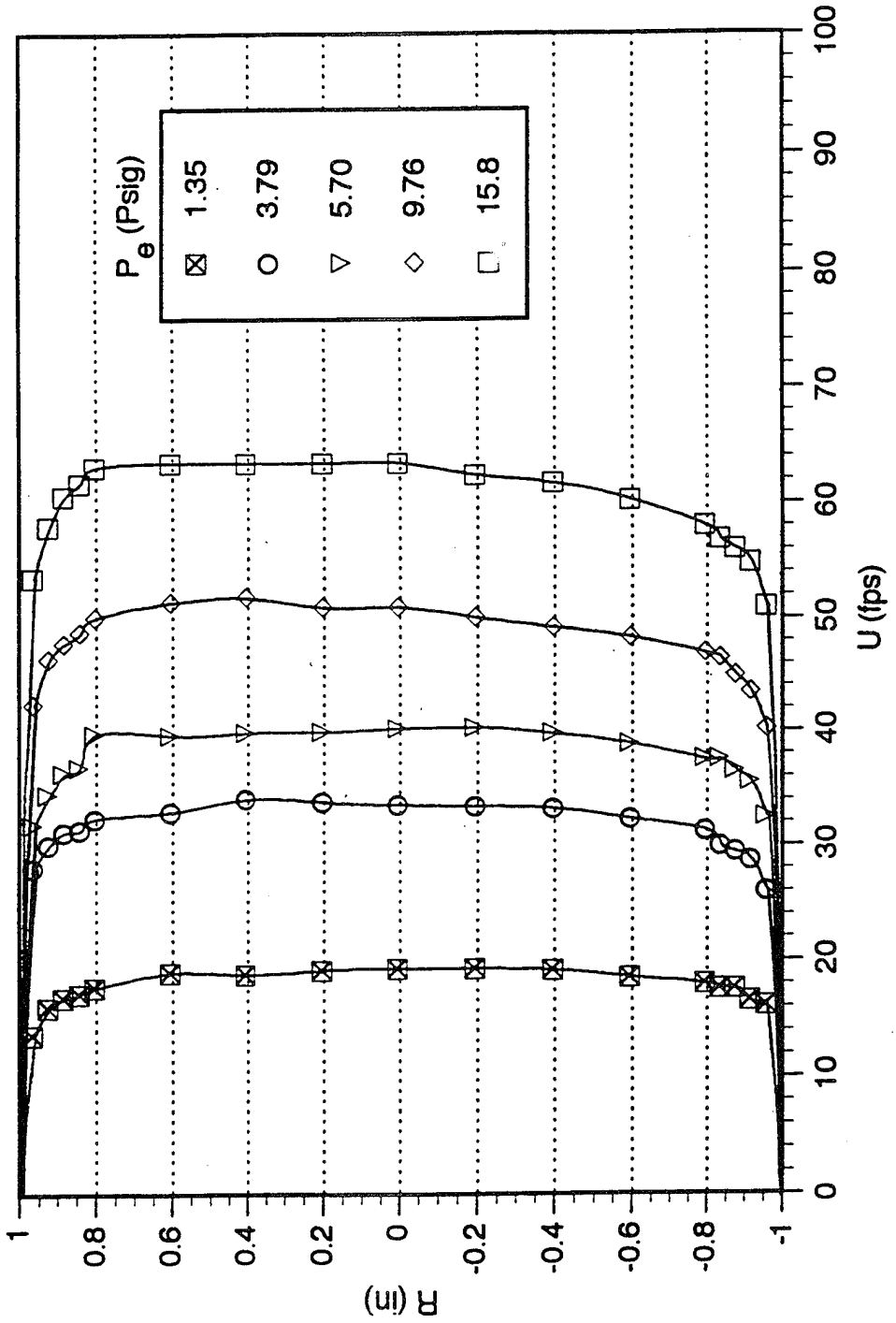

Figure 33c. Muzzle velocity distribution for staggered configuration at low evacuator pressures.

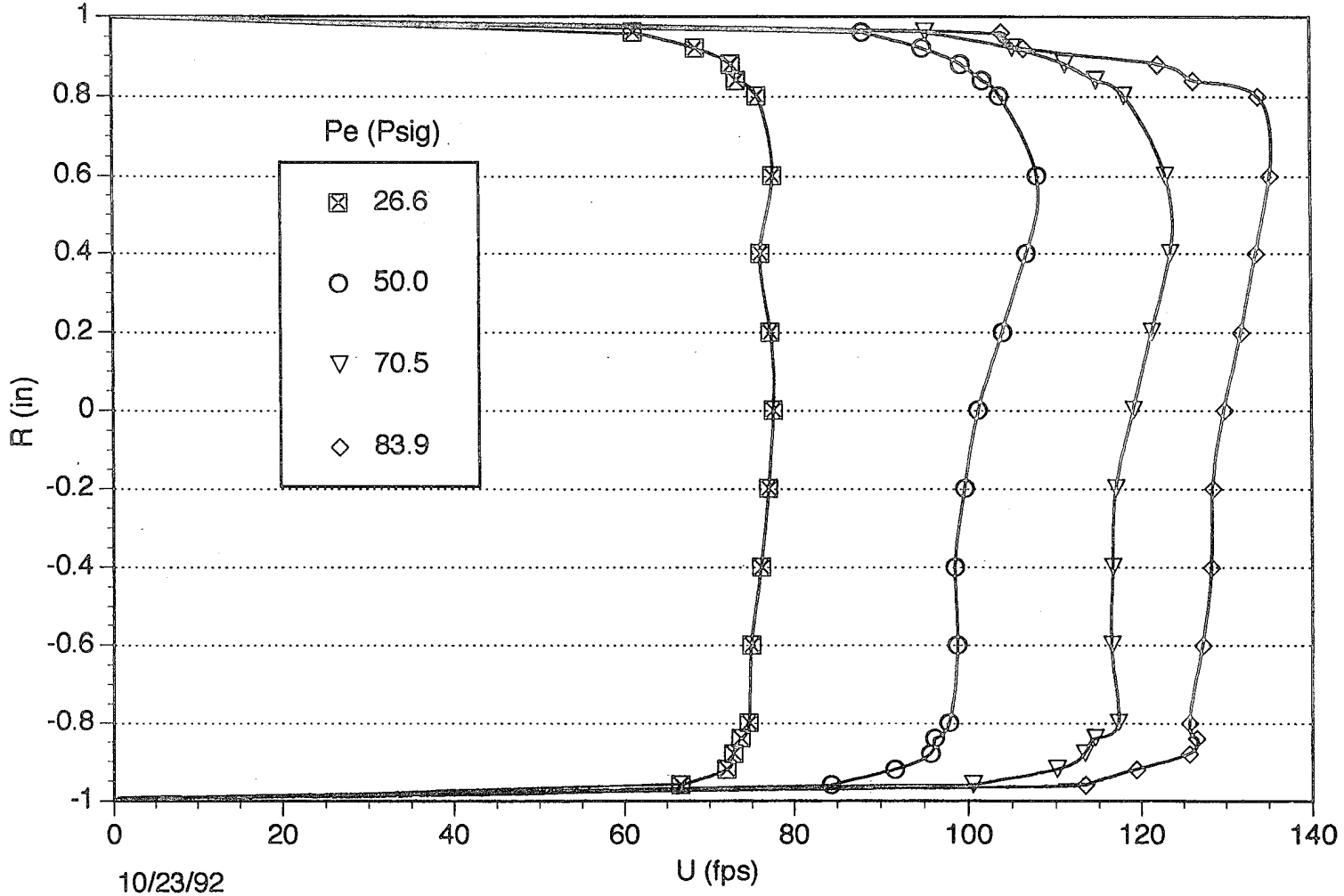

Figure 33d. Muzzle velocity distribution for staggered configuration at high evacuator pressures.

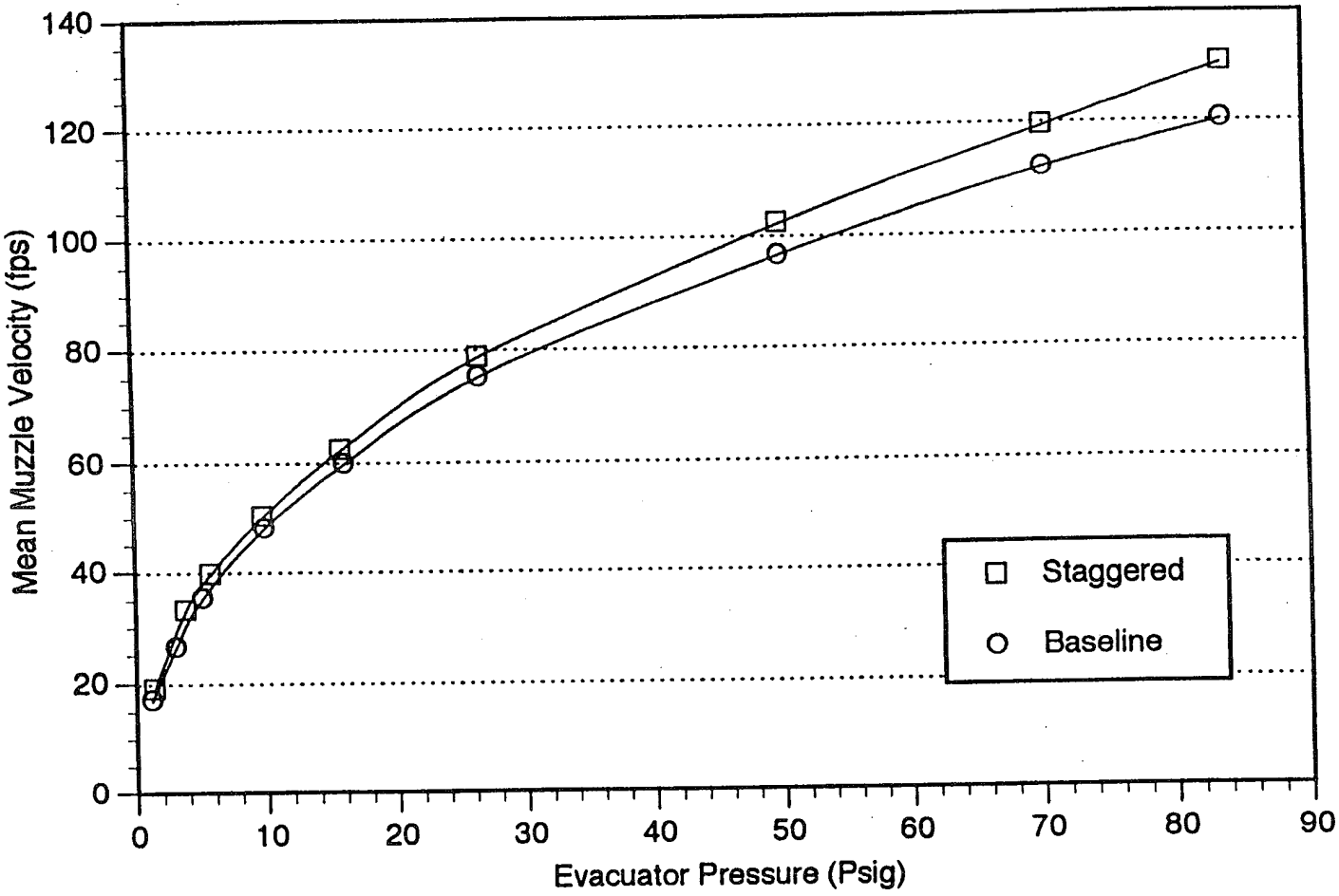

Figure 34. Mean muzzle velocities for baseline and staggered configurations.

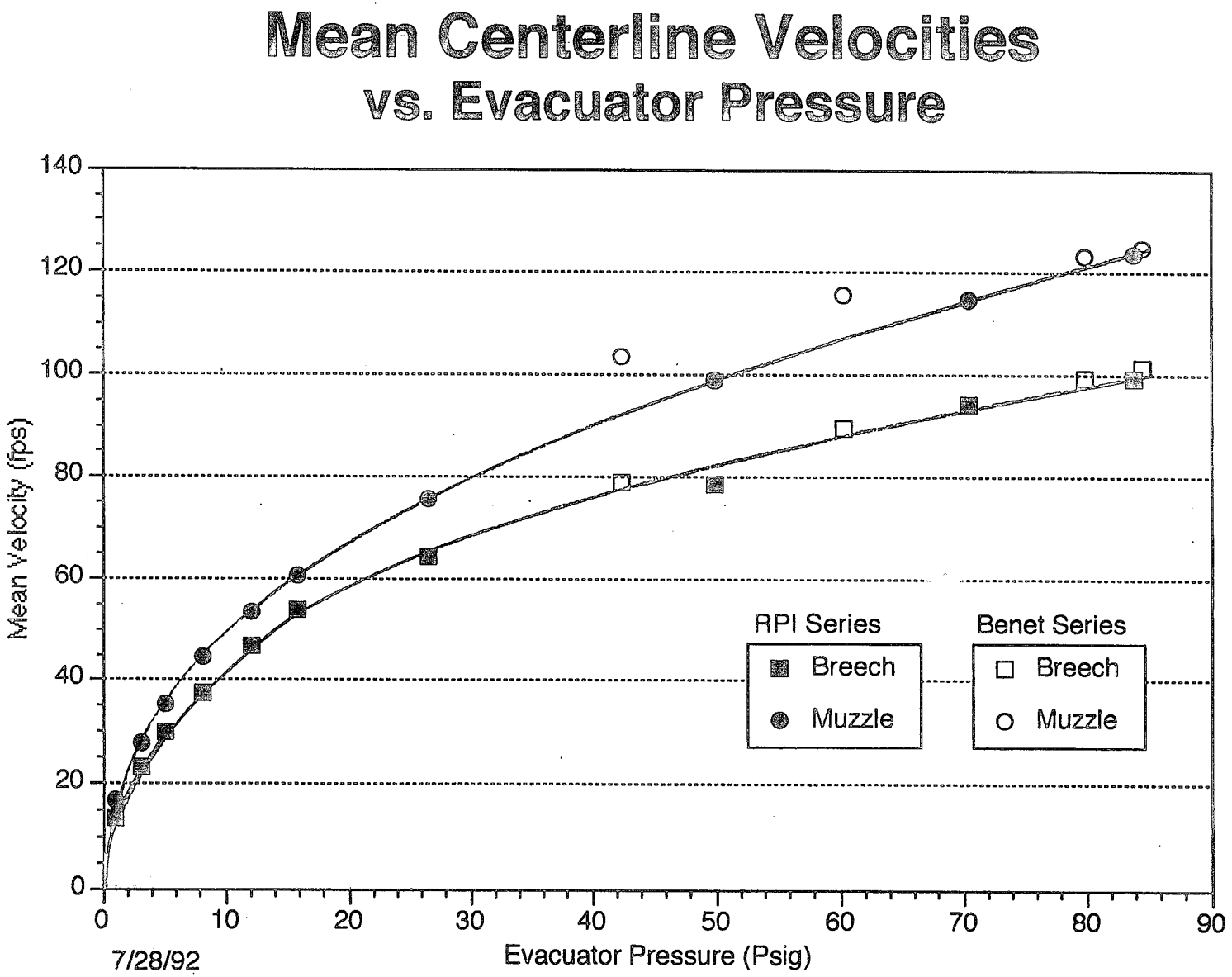

Figure 35. Comparison of full-scale and 33 percent breech and muzzle center line velocities.

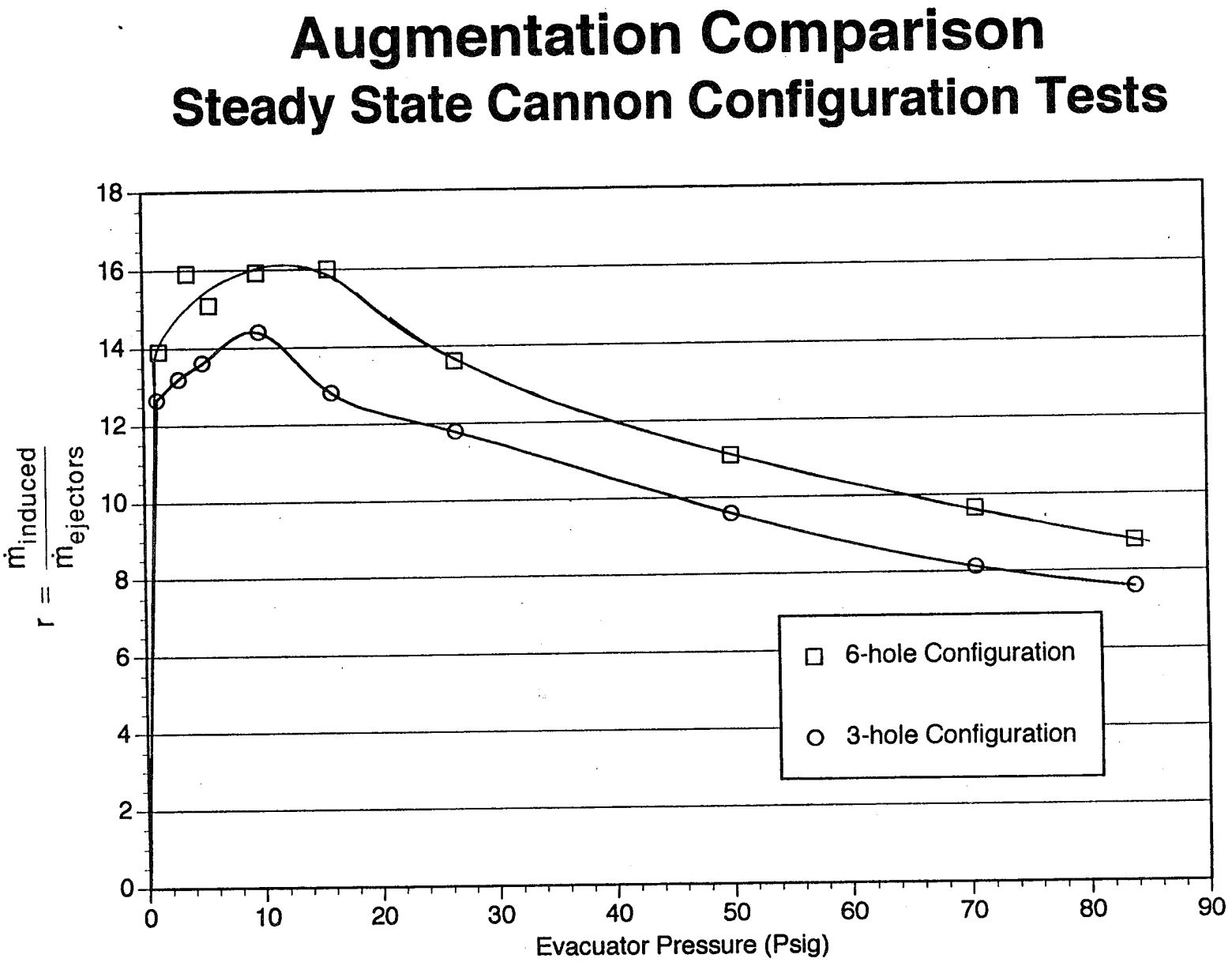

Figure 36. Mass flow augmentation ratio for baseline and staggered configurations.

Muzzle Velocity Profile Comparison
with and without Screen at Breech

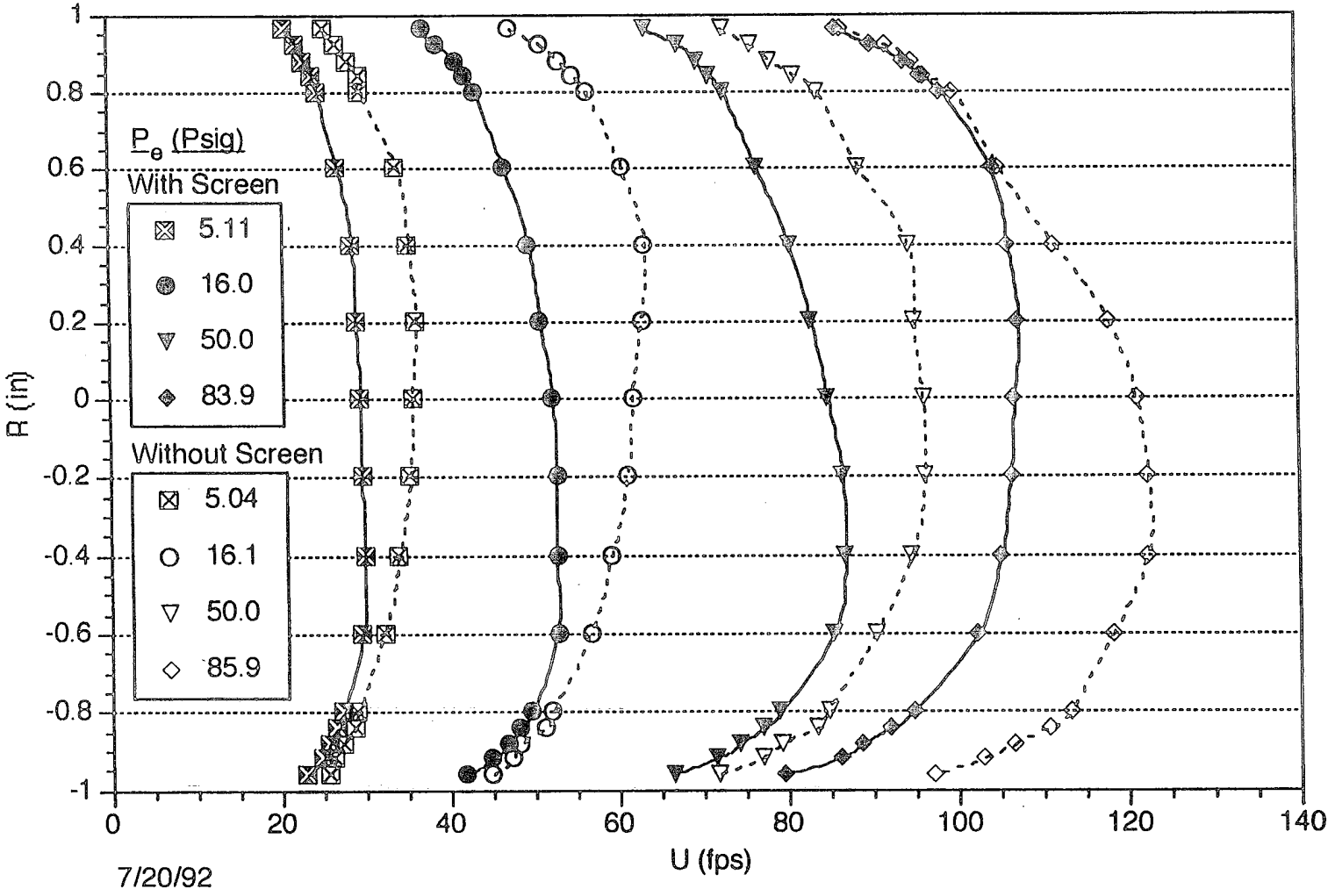

Figure 37. Comparison of muzzle velocity profiles with and without screen at breech.

TECHNICAL REPORT INTERNAL DISTRIBUTION LIST

	NO. OF COPIES
CHIEF, DEVELOPMENT ENGINEERING DIVISION	
ATTN: AMSTA-AR-CCB-DA	1
-DB	1
-DC	1
-DD	1
-DE	1
CHIEF, ENGINEERING DIVISION	
ATTN: AMSTA-AR-CCB-E	1
-EA	1
-EB	1
-EC	
CHIEF, TECHNOLOGY DIVISION	
ATTN: AMSTA-AR-CCB-T	2
-TA	1
-TB	1
-TC	1
TECHNICAL LIBRARY	
ATTN: AMSTA-AR-CCB-O	5
TECHNICAL PUBLICATIONS & EDITING SECTION	
ATTN: AMSTA-AR-CCB-O	3
OPERATIONS DIRECTORATE	
ATTN: SMCWV-ODP-P	1
DIRECTOR, PROCUREMENT & CONTRACTING DIRECTORATE	
ATTN: SMCWV-PP	1
DIRECTOR, PRODUCT ASSURANCE & TEST DIRECTORATE	
ATTN: SMCWV-QA	1

NOTE: PLEASE NOTIFY DIRECTOR, BENÉT LABORATORIES, ATTN: AMSTA-AR-CCB-O OF ADDRESS CHANGES.

TECHNICAL REPORT EXTERNAL DISTRIBUTION LIST

	NO. OF COPIES
ASST SEC OF THE ARMY RESEARCH AND DEVELOPMENT ATTN: DEPT FOR SCI AND TECH THE PENTAGON WASHINGTON, D.C. 20310-0103	1
ADMINISTRATOR DEFENSE TECHNICAL INFO CENTER ATTN: DTIC-OCP (ACQUISITION GROUP) BLDG. 5, CAMERON STATION ALEXANDRIA, VA 22304-6145	2
COMMANDER U.S. ARMY ARDEC ATTN: SMCAR-AEE	1
SMCAR-AES, BLDG. 321	1
SMCAR-AET-O, BLDG. 351N	1
SMCAR-FSA	1
SMCAR-FSM-E	1
SMCAR-FSS-D, BLDG. 94	1
SMCAR-IMI-I, (STINFO) BLDG. 59 PICATINNY ARSENAL, NJ 07806-5000	2
DIRECTOR U.S. ARMY RESEARCH LABORATORY ATTN: AMSRL-DD-T, BLDG. 305 ABERDEEN PROVING GROUND, MD 21005-5066	1
DIRECTOR U.S. ARMY RESEARCH LABORATORY ATTN: AMSRL-WT-PD (DR. B. BURNS) ABERDEEN PROVING GROUND, MD 21005-5066	1
DIRECTOR U.S. MATERIEL SYSTEMS ANALYSIS ACTV ATTN: AMXSY-MP ABERDEEN PROVING GROUND, MD 21005-5071	1
COMMANDER ROCK ISLAND ARSENAL ATTN: SMCRI-ENM ROCK ISLAND, IL 61299-5000	1
MIAC/CINDAS PURDUE UNIVERSITY P.O. BOX 2634 WEST LAFAYETTE, IN 47906	1
COMMANDER U.S. ARMY TANK-AUTMV R&D COMMAND ATTN: AMSTA-DDL (TECH LIBRARY) WARREN, MI 48397-5000	1
COMMANDER U.S. MILITARY ACADEMY ATTN: DEPARTMENT OF MECHANICS WEST POINT, NY 10966-1792	1
U.S. ARMY MISSILE COMMAND REDSTONE SCIENTIFIC INFO CENTER ATTN: DOCUMENTS SECTION, BLDG. 4484 REDSTONE ARSENAL, AL 35898-5241	2
COMMANDER U.S. ARMY FOREIGN SCI & TECH CENTER ATTN: DRXST-SD 220 7TH STREET, N.E. CHARLOTTESVILLE, VA 22901	1
COMMANDER U.S. ARMY LABCOM MATERIALS TECHNOLOGY LABORATORY ATTN: SLCMT-IML (TECH LIBRARY) WATERTOWN, MA 02172-0001	2
COMMANDER U.S. ARMY LABCOM, ISA ATTN: SLCIS-IM-TL 2800 POWER MILL ROAD ADELPHI, MD 20783-1145	1

NOTE: PLEASE NOTIFY COMMANDER, ARMAMENT RESEARCH, DEVELOPMENT, AND ENGINEERING CENTER, BENÉT LABORATORIES, CCAC, U.S. ARMY TANK-AUTOMOTIVE AND ARMAMENTS COMMAND, AMSTA-AR-CCB-O, WATERVLIET, NY 12189-4050 OF ADDRESS CHANGES.

TECHNICAL REPORT EXTERNAL DISTRIBUTION LIST (CONT'D)

	NO. OF COPIES
COMMANDER U.S. ARMY RESEARCH OFFICE ATTN: CHIEF, IPO P.O. BOX 12211 RESEARCH TRIANGLE PARK, NC 27709-2211	1
DIRECTOR U.S. NAVAL RESEARCH LABORATORY ATTN: MATERIALS SCI & TECH DIV CODE 26-27 (DOC LIBRARY) WASHINGTON, D.C. 20375	1 1
WRIGHT LABORATORY ARMAMENT DIRECTORATE ATTN: WL/MNM EGLIN AFB, FL 32542-6810	1
WRIGHT LABORATORY ARMAMENT DIRECTORATE ATTN: WL/MNMF EGLIN AFB, FL 32542-6810	1

NOTE: PLEASE NOTIFY COMMANDER, ARMAMENT RESEARCH, DEVELOPMENT, AND ENGINEERING CENTER, BENÉT LABORATORIES, CCAC, U.S. ARMY TANK-AUTOMOTIVE AND ARMAMENTS COMMAND, AMSTA-AR-CCB-O, WATERVLIET, NY 12189-4050 OF ADDRESS CHANGES.

DEPARTMENT OF THE ARMY
ARMAMENT RESEARCH, DEVELOPMENT AND ENGINEERING CENTER
BENÉT LABORATORIES, CCAC
US ARMY TANK-AUTOMOTIVE AND ARMAMENTS COMMAND
WATERVLIET, N.Y. 12189-4050

OFFICIAL BUSINESS
AMSTA-AR-CCB-O
TECHNICAL LIBRARY

DEPARTMENT OF THE ARMY

DA Label 18-1, Sep 83
Edition of Oct 74 will be used until exhausted.

OFFICIAL BUSINESS

ADMINISTRATOR
DEFENSE TECHNICAL INFO CENTER
ATTN: DTIC-OCP (ACQUISITION GROUP)
BLDG. 5, CAMERON STATION
ALEXANDRIA, VA 22304-6145